UNIVERSIDADE FEDERAL DO PAMPA

MARCELO ROMANSSINI

DEVELOPMENT OF AN IoT SENSOR NODE WITH EDGE COMPUTING FOR VIBRATION MONITORING OF INDUSTRIAL MOTORS

ALEGRETE

2025

MARCELO ROMANSSINI

DEVELOPMENT OF AN IoT SENSOR NODE WITH EDGE COMPUTING FOR VIBRATION MONITORING OF INDUSTRIAL MOTORS

Thesis presented to the Graduate Program in Electrical Engineering at the Federal University of Pampa, as a partial requirement for obtaining the Master's Degree in Electrical Engineering.

Supervisor: Alessandro G. Girardi
Co-supervisor: Paulo César C. de Aguirre

FEDERAL UNIVERSITY OF PAMPA
Master Degree in Electrical Engineering
Graduate Program in Electrical Engineering

ALEGRETE
2025

Ficha catalográfica elaborada automaticamente com os dados fornecidos
pelo(a) autor(a) através do Módulo de Biblioteca do
Sistema GURI (Gestão Unificada de Recursos Institucionais) .

R758d Romanssini, Marcelo
DEVELOPMENT OF AN IoT SENSOR NODE WITH EDGE COMPUTING FOR VIBRATION MONITORING OF INDUSTRIAL MOTORS / Marcelo Romanssini.
96 p.

Dissertação(Mestrado)-- Universidade Federal do Pampa, MESTRADO EM ENGENHARIA ELÉTRICA, 2025.
"Orientação: Alessandro Gonçalves Girardi".

1. Failure analysis of induction motors. 2. Vibration monitoring. 3. Edge and cloud processing. I. Título.

MARCELO ROMANSSINI

DEVELOPMENT OF AN IoT SENSOR NODE WITH EDGE COMPUTING FOR VIBRATION MONITORING OF INDUSTRIAL MOTORS

Dissertação apresentada ao Programa de Pós-Graduação em Engenharia Elétrica da Universidade Federal do Pampa, como requisito parcial para obtenção do Título de Mestre em Engenharia Elétrica.

Dissertação defendida e aprovada em: 24/04/2025

Banca examinadora:

_____

Prof. Dr. Alessandro Gonçalves Girardi

(Unipampa)

_____

Prof. Dr. Tiago Oliveira Weber

(UFRGS)

_____

Prof. Dr. Felipe Bovolini Grigoletto

(Unipampa)

Prof. Dr. Giovani Guarianti Pozzebon

(Unipampa)

Assinado eletronicamente por **ALESSANDRO GONCALVES GIRARDI**, **PROFESSOR DO MAGISTERIO SUPERIOR**, em 24/04/2025, às 11:45, conforme horário oficial de Brasília, de acordo com as normativas legais aplicáveis.

Assinado eletronicamente por **Tiago Oliveira Weber**, **Usuário Externo**, em 24/04/2025, às 11:51, conforme horário oficial de Brasília, de acordo com as normativas legais aplicáveis.

Assinado eletronicamente por **FELIPE BOVOLINI GRIGOLETTO**, **PROFESSOR DO MAGISTERIO SUPERIOR**, em 24/04/2025, às 15:04, conforme horário oficial de Brasília, de acordo com as normativas legais aplicáveis.

Assinado eletronicamente por **GIOVANI GUARIENTI POZZEBON**, **PROFESSOR DO MAGISTERIO SUPERIOR**, em 24/04/2025, às 16:44, conforme horário oficial de Brasília, de acordo com as normativas legais aplicáveis.

A autenticidade deste documento pode ser conferida no site https://sei.unipampa.edu.br/sei/controlador_externo.php?acao=documento_conferir&id_orgao_acesso_externo=0, informando o código verificador **1713106** e o código CRC **0F21C53E**.

ABSTRACT

Rotating machinery such as motors, pumps, generators, and compressors, plays a key role in many industries, ensuring productivity, efficiency, and operational safety. However, these machines are subject to wear and tear due to continuous operation and cyclic loads, leading to unexpected downtime and increased maintenance costs. Predictive maintenance (PdM), especially when based on vibration analysis, has proven to be one of the most effective strategies for detecting early signs of mechanical failures. Recent advances in Micro-Electro Mechanical Systems (MEMS) sensors and Internet of Things (IoT) technologies have enabled the development of compact, low-power devices capable of real-time data acquisition and transmission. This work presents a detailed review of faults in rotating electrical machinery, the main methods for fault identification, such as vibration monitoring, as well as methods for collecting and processing vibration data. This work also describes the implementation of an IoT sensor, based on MEMS accelerometers. The sensor is basically composed of a microcontroller, a temperature sensor and a triaxial accelerometer able of measuring acceleration on the X, Y and Z axes. The implemented IoT sensor is battery-powered, collects accelerated data every five minutes and transmits the data to the cloud via Wi-Fi using the MQTT protocol. After the sensor was implemented, two data processing strategies were evaluated: edge computing (data processing and features extraction at the sensor) and cloud computing (raw data sent directly to the cloud for processing). Through a series of performance and power consumption tests, it was demonstrated that the edge processing approach reduced the total processing time by up to 4.5 times and decreased the data transmission volume by a factor of 100 compared to cloud processing. This reduction resulted in 34.2 % less power consumption, making it highly suitable for battery-powered devices. Additionally, energy consumption estimates showed that the sensor operating with edge processing could reach a battery life of approximately 686 days, compared to only 198 days with cloud-based processing an improvement exceeding 70 %. Edge processing also provided greater stability and predictability at runtime, which is essential for real-time industrial monitoring applications. The extracted parameters showed high local precision, with deviations below 0.03 % for RMS acceleration and peak values. The deviations for the velocity parameters were less than 2 % when compared to the data processed in the cloud. This confirms the feasibility of embedded signal processing for reliable vibration analysis, reducing the need for transmitting large volumes of raw data. Furthermore, when compared to commercial systems such as the Minipa MVA-400 vibration meter and the WEG Motor Scan sensor, the developed sensor demonstrated good agreement in vibration measurements, particularly in the axial axis, with minor deviations attributed to differing internal algorithms and sensor orientations. Overall, the proposed system proves to be an efficient, scalable, and sustainable solution for predictive maintenance, enabling continuous condition monitoring of industrial rotating machinery, reducing maintenance costs, and minimizing unplanned downtime.

Keywords: Faults, induction motor, predictive maintenance, edge Computing, cloud computing, IoT, accelerometer, vibration, vibration monitoring.

RESUMO

Máquinas rotativas como motores, bombas, geradores e compressores, desempenham um papel fundamental em muitas indústrias, garantindo produtividade, eficiência e segurança operacional. No entanto, essas máquinas são propensas a desgaste devido à operação contínua e cargas cíclicas, levando a paradas inesperadas e aumento dos custos de manutenção. A manutenção preditiva (PdM), especialmente quando baseada em análise de vibração, provou ser uma das estratégias mais eficazes para detectar sinais precoces de falhas mecânicas. Avanços recentes em sensores do tipo Micro-Electro Mechanical Systems (MEMS) e tecnologias de Internet das Coisas (IoT) permitirMicro-Electro Mechanical Systemsam o desenvolvimento de dispositivos compactos e de baixo consumo de energia, capazes de aquisição e transmissão de dados em tempo real. Este trabalho apresenta uma revisão detalhada de falhas em máquinas elétricas rotativas, os principais métodos para identificação de falhas, como monitoramento de vibração, bem como métodos para coleta e processamento de dados de vibração. Este trabalho também descreve a implementação de um sensor IoT, baseado em acelerômetros MEMS. O sensor é basicamente composto por um microcontrolador, um sensor de temperatura e um acelerômetro triaxial capaz de medir a aceleração nos eixos X, Y e Z. O sensor de IoT implementado é alimentado por bateria, coleta dados acelerados a cada cinco minutos e os transmite para a nuvem via Wi-Fi usando o protocolo MQTT. Após a implementação do sensor, duas estratégias de processamento de dados foram avaliadas: computação de borda (processamento de dados e extração de recursos no sensor) e computação em nuvem (dados brutos enviados diretamente para a nuvem para processamento). Por meio de uma série de testes de desempenho e consumo de energia, foi demonstrado que a abordagem de processamento de borda reduziu o tempo total de processamento em até 4,5 vezes e diminuiu o volume de transmissão de dados em um fator de 100 em comparação com o processamento em nuvem. Essa redução resultou em um consumo de energia 34,2 % menor, tornando-o altamente adequado para dispositivos alimentados por bateria. Além disso, as estimativas de consumo de energia mostraram que o sensor operando com processamento de borda pode atingir uma vida útil de bateria de aproximadamente 686 dias, em comparação com apenas 198 dias com o processamento baseado em nuvem, uma melhoria superior a 70 %. O processamento de borda também proporcionou maior estabilidade e previsibilidade em tempo de execução, o que é essencial para aplicações de monitoramento industrial em tempo real. Os parâmetros extraídos apresentaram alta precisão local, com desvios abaixo de 0,03 % para aceleração RMS e valores de pico. Para os parâmetros de vibrações os erros foram menores de 2 % quando comparados aos dados processados em nuvem. Isso confirma a viabilidade do processamento de sinais embarcado para análises de vibração confiáveis, reduzindo a necessidade de transmissão de grandes volumes de dados brutos. Além disso, quando comparado a sistemas comerciais como o medidor de vibração Minipa MVA-400 e o sensor WEG Motor Scan, o sensor desenvolvido demonstrou boa concordância nas

medições de vibração, particularmente no eixo axial, com pequenos desvios atribuídos a diferentes algoritmos internos e orientações do sensor. No geral, o sistema proposto demonstra ser uma solução eficiente, escalável e sustentável para manutenção preditiva, permitindo o monitoramento contínuo das condições de máquinas rotativas industriais, reduzindo os custos de manutenção e minimizando o tempo de inatividade não planejado.
Palavras-chave: Falhas, motor de indução, manutenção preditiva, Processamento na borda, Processamento na nuvem, Vibração, Monitoramento de vibração.

LIST OF FIGURES

LIST OF TABLES

LIST OF ABBREVIATIONS AND ACRONYMS

PdM	Predictive maintenance
MEMS	Micro-Electro Mechanical Systems
IoT	Internet of Things
AI	Artificial Intelligence
ML	Machine Learning
RMS	Root-mean-square
CRF	Crest Factor
KUR	Kurtosis
FFT	Fast Fourier Transform
DFT	Fourier transform
PSD	Power Spectral Density
STFT	Short-Time Fourier Transform
WT	Wavelet Transform
HHT	Hilbert-Huang Transform
WVD	Wigner-Ville Distribution
EMD	Empirical Mode Decomposition
IMFs	Intrinsic Mode Functions
UART	Universal Asynchronous Receiver/Transmitter
I2S	Inter-Integrated Circuit Sound
EMI	Electromagnetic Interference
SoC	System on Chip
SPI	Serial Peripheral Interface
IDFT	Inverse Fourier Transform
OTA	Over-the-air
MQTT	Message Queuing Telemetry Transport

CONTENTS

1 INTRODUCTION

Rotating machinery is used in a variety of industries. They include equipment such as motors, pumps, fans, generators, compressors, and more. Motors and generators are essential to the operation of an industrial facility to maintain productivity, efficiency, and safety of operations. However, the increasing integration of mechanical and electrical components not only increases the efficiency and the power density, but also the complexity and susceptibility to failure of this machines(FU et al., 2023).

Research on the reliability of electrical machines has identified that failures can occur in all engine components (LEE et al., 2020). Machine failures often occur due to continuous operation and various cyclic loading situations. This process leads to gradual wear of components, which increases the risk of failure (MADHUKAR et al., 2023). This wear of machine components can be considered normal and is a consequence of machine operation. The operation these components under critical conditions, however, can lead to reduced machine life, compromising the integrity of healthy components, and exposing the machine to total failure.

Machine failure results in significant costs to the industry, including line production losses and increased maintenance costs (ROMANSSINI et al., 2023). Maintenance costs account for between 15 % and 60 % of the manufacturing cost of the final product, and in heavy industry these costs can be as high as 50 % of the total production cost (SHUKLA; NEFTI-MEZIANI; DAVIS, 2022). These costs can be reduced by choosing an efficient maintenance strategy, which allows detecting and correcting problems in machines in advance, avoiding greater wear of machine components or, in the worst case machine downtime.The main objective of the maintenance techniques strategy is to increase the availability of the machines with lower maintenance costs (KUMAR; SATHUJODA; BHALLA, 2022).

Predictive maintenance (PdM) has proven to be the most efficient technique for equipment maintenance in industrial environments (KUMAR; SATHUJODA; BHALLA, 2022). PdM is based on the analysis of data collected through monitoring or inspections (VILLARROEL; ZURITA; VELARDE, 2019), enabling the assessment of machine health and the definition of maintenance strategies. Various techniques are available for monitoring machine health, including acoustic emission, vibration monitoring, temperature monitoring, noise monitoring, current monitoring, oil and debris analysis, and corrosion monitoring, each with its specific application and use (MADHUKAR et al., 2023).

To minimize unexpected machine downtime, condition-based monitoring and early fault diagnosis have become essential practices (AN et al., 2023). A network of sensors is installed on machines to continuously monitor their operating condition, ensuring performance protection while reducing the risk of costly breakdowns and potential losses (QIAN et al., 2019). Among the various techniques employed in PdM, vibration analysis stands out as a particularly valuable tool for fault detection (WANG et al., 2021). By

analyzing the vibration patterns of machine, it becomes possible to detect abnormalities and early signs of faults. Vibration monitoring has proven to be an effective method for locating faults in machines components (SHUKLA; NEFTI-MEZIANI; DAVIS, 2022).

Vibrations are oscillatory movements of equipment around its equilibrium position. Any change in signal amplitude or frequency may indicate impaired machine performance (NASCIMENTO et al., 2022). Vibration analysis is a powerful diagnostic tool for detecting faults such as looseness, eccentricity, imbalance, blade defects, misalignment, defective bearings, damaged gears and cracked or bent shafts (ALTHUBAITI; ELASHA; TEIXEIRA, 2022; TIBONI et al.,). Consequently, this technique has become a well-established and widely adopted PdM approach for monitoring rotating machines (RANJAN; GHOSH; KUMAR, 2020).

Compared to other PdM techniques, vibration analysis offers several advantages, including high accuracy, sensitivity to a wide range of defect types, and it is a noninvasive and nondestructive method (LI et al., 2021; CHENG et al., 2021). However, it also has some limitations, such as difficulty in detecting faults in low-speed machines (POPESCU; AIORDACHIOAIE; CULEA-FLORESCU, 2021), the need for continuous monitoring, and reliance on high-quality sensors for accurate data collection.

Vibration data acquisition can be performed using many vibration measurement devices available on the market. These devices can use different types of transducers to perform a measurement. Among these, accelerometer are the most commonly used for capturing vibration signals (PEDOTTI; ZAGO; FRUETT, 2016)

Advancements in manufacturing technologies have significantly improve the accuracy and cost-effective microelectromechanical systems (MEMS) accelerometers compared to traditional piezoelectric accelerometers (Guru Manikandan et al., 2021; ROSSI et al., 2023). Their affordability, ease of integration, and compatibility with the Internet of Things (IoT) technologies have made them an ideal solution for continuous vibration monitoring in industrial environments. As sensor technology continues to advance, the cost of individual sensors has been steadily decreasing, enabling the installation of thousands of sensors on industrial machines in moderns plants. These sensors generate vast amount of data during operation, allowing for real-time monitoring and analysis (LU et al., 2023).

With the increasing use of sensors for industrial machine monitoring, the amount of data has grown exponentially. Cloud computing is a widely used approach for processing large amounts of datasets, offering scalable storage and high computational power. It has proven its worth in machine condition monitoring and fault diagnosis (LU et al., 2023), particularly in applications where AI-powered fault detection is required. By leveraging powerful cloud-based servers, machine learning algorithms can analyze large datasets to identify potential failures. However, as the number of sensors increases, so do the challenges associated with data transmission bandwidth, power consumption storage requirements, and processing resources (QIAN et al., 2019). Transmitting raw vibration data to the cloud

can be inefficient, requiring significant network bandwidth and higher power consumption, particularly for battery-powered IoT devices.

An alternative approach to overcome these difficulties is edge computing (SATYANARAYANAN, 2017). In this paradigm, data processing occurs directly at the edge of the network, close to the data source. Edge computing reduces the load on cloud servers, optimizes bandwidth usage, and improves data processing efficiency (QIAN et al., 2019). A key feature of edge computing is that sensor data is processed directly on edge devices, such as portable devices, IoT nodes, mobile phones, smartwatches, etc. This approach offers several advantages for machine signal processing and fault diagnosis in industrial machines, such as reduced latency by enabling real-time data processing and fault diagnosis, lower energy consumption since only relevant information is transmitted to the cloud, improved data privacy by keeping raw data within the local network, and scalability by allowing the creation of flexible and customized sensor networks (LU et al., 2023). Although cloud computing offers superior processing power, relying entirely on the cloud can introduce infrastructure bottlenecks and limit efficiency.

A critical issue in vibration-based fault diagnosis is the balance between computational accuracy and energy efficiency when opting for cloud computing or edge computing. The main trade-off between these approaches lies in the way data is processed: cloud computing allows the use of advanced artificial intelligence (AI) models with high accuracy, but requires the continuous transmission of large volumes of data, significantly increasing energy consumption. On the other hand, edge data processing, such as processing and feature extraction from vibration data at the sensor, reduces the size of the data packet, facilitating transmission and decreasing power consumption, although it may limit the complexity of algorithms and analytical accuracy due to hardware constraints.

Early fault detection in rotating electrical machines are widely used across various industrial sectors and is crucial for ensuring operational efficiency, reducing downtime,and preventing costly failures. To address this need, the present work proposes the designs and implementation of an IoT sensor node capable of monitoring vibration and temperature. The sensor is designed to meet key industry requirements, including robustness for operation in harsh environments, low power consumption to extend battery life, and ease of installation.

Given the importance of early fault detection in industrial environments and the increasing adoption of edge computing (HE et al., 2023), we implemented an IoT sensor node for vibration monitoring, specially in induction electric motors commonly used in industrial applications. The proposed sensor node was designed to collet, processing, extracting features and transiting the relevant information to the cloud for further analysis. The system architecture allowing both cloud-based and edge-based processing, enabling direct comparison between the two approaches. The concept of the proposed IoT sensor node and its data flow for fault detection are shown in Fig. 1.

Figure 1 – Predictive maintenance of industrial machines.

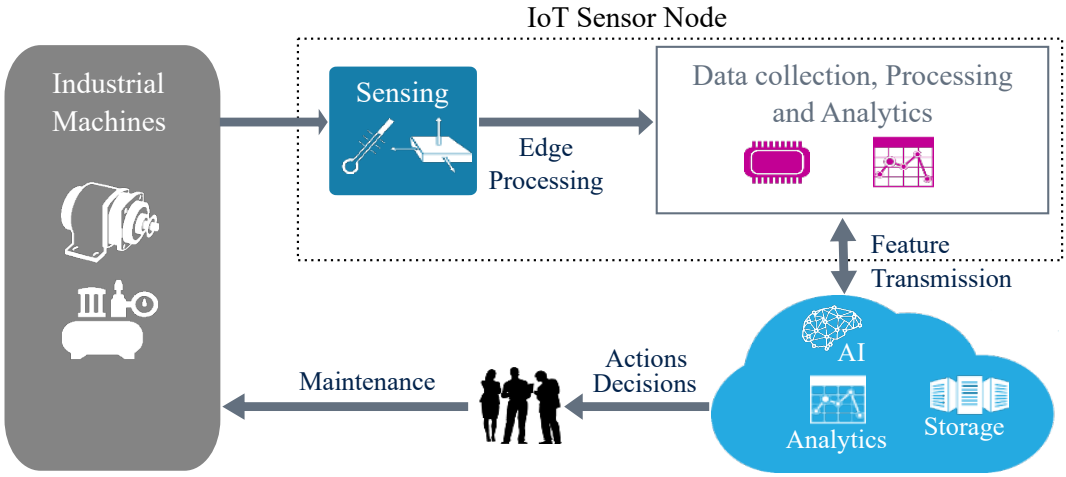

The implemented IoT sensor node consists primarily of a microcontroller, responsible for system control, data acquisition, and processing, along with an accelerometer. It transmits the extracted vibration signal information to the cloud via Wi-Fi using the MQTT messaging protocol.

The hardware must be robust and capable of withstanding harsh industrial conditions, including exposure to dust, moisture, electrical noise, and electromagnetic interference. Additionally, it must be easy to install and integrate into existing industrial setups, ensuring that the system simplifies maintenance tasks rather than adding complexity. To achieve this, the proposed data collection system features wireless data transmission via Wi-Fi, eliminating the need for physical cable connections and enabling greater flexibility in sensor placement. Moreover, the system is designed to operate with low power consumption, maximizing battery life and ensuring reliable long-term operation in industrial environments.

1.1 OBJECTIVES

This dissertation aims to propose a robust, easy-to-install, low-power IoT sensor for monitoring vibrations in rotating electrical machines in industry. In addition, it analyzes the energy consumption of two distinct approaches: the transmission of raw vibration data to the cloud (cloud processing) and the processing and extraction of vibration signal features at the edge (edge computing).

1.1.1 SPECIFIC OBJECTIVES

- Development, hardware design of an IoT sensor for vibration and temperature measurement;
- Development, design of firmware for acquisition, processing and sending of vibration and temperature data to the cloud;

- Evaluate the main vibration data processing techniques to extract relevant parameters for fault diagnosis;
- Compare cloud computing and edge computing approaches in terms of energy consumption, processing time and accuracy of results.

This analysis will allow us to understand the advantages and limitations of each approach, contributing to the choice of the most efficient strategy for fault monitoring in industrial machines.

1.2 ORGANIZATION OF THE WORK

This work is organized into five chapters. Initially, an overview of the main types of failures that occur in induction motors is presented, addressing the fundamental concepts of vibration and the ways of diagnosing failures through vibration analysis. Then, the main sensor models used in vibration data collection, the most common methods of wireless data transmission, the main processing techniques applied to failure detection are discussed, in addition to a conceptual review of edge computing and cloud computing.

Chapter 3 presents the entire development of the proposed IoT sensor for vibration monitoring in induction electric motors. Chapter 4 presents the methodology used to evaluate the developed sensor as well as the results of the evaluations performed. Finally, Chapter 5 presents the final considerations of the work and some suggestions for future work.

2 THEORETICAL AND CONCEPTUAL FOUNDATIONS

This chapter covers the main concepts related to vibration monitoring applied to the predictive maintenance of rotating machinery. The most common types of electrical machine failures are presented, along with the evaluation criteria based on ISO 10816, the types of transducers used to acquire vibration signals, and the technologies available for transmitting, processing, and analyzing the collected data. The advantages and limitations of each approach for more efficient, real-time diagnostics are also discussed. The concepts presented in this chapter will serve as a reference for the development of the work.

2.1 FAULTS IN INDUCTION MOTORS

Industrial electric motors play a vital role in various manufacturing and industrial processes, but they are not immune to problems and failures. Understanding the main causes of these issues is crucial for maintaining productivity and reducing downtime (DINEVA et al., 2019). Electric motor failures can lead to safety issues and higher operating costs, affecting productivity and efficiency, while increasing energy consumption and reducing motor life. As we can see in the Figure 2, around 41 % of problems in induction motors are related to bearings, 38 % of problems are related to the stator/armature and others faults types less than 21 % (CIPRIANI et al., 2021). In Figure 3 we can see the three main components and those that fail most in an induction electric motor.

Figure 2 – Main failures that occur in electric induction motors.

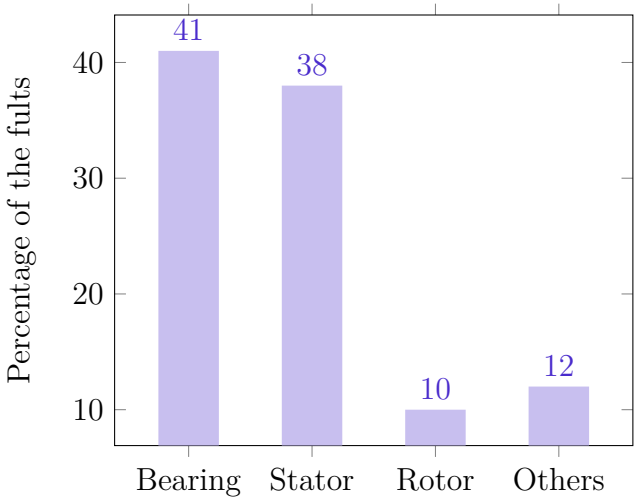

Source: (GAEID; PING, 2011)

One of the leading contributors to electric motor problems is overheating, which can result from factors such as excessive loads, insufficient ventilation, or worn-out bearings (CIPRIANI et al., 2021). Elevated temperatures can lead to insulation breakdown and winding damage, ultimately causing motor failure.

Another common factor behind motor failures is electrical imbalances. These imbalances can lead to uneven wear on motor components, reduced efficiency, and increased

Figure 3 – Three fundamental components of an induction motor: rotor, stator and rolling bearings.

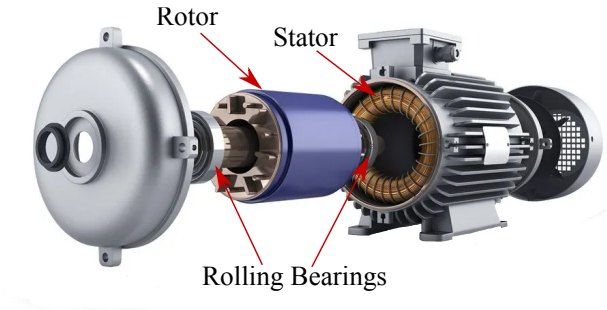

Source: Adapted from (Electric Motor Engineering, 2025)

energy consumption (PREETHI; SURYAPRAKASH; MATHANKUMAR, 2021). Mechanical problems, including misalignment, unbalanced loads, and excessive vibration, can also contribute to motor issues. Misalignment between the motor and the driven equipment can create excessive stress on bearings and shafts, accelerating wear and tear. Unbalanced loads can cause uneven wear on motor components, reducing their lifespan. Uncontrolled vibration can lead to structural damage and adversely affect motor performance (LIPUS et al., 2016).

The most effective way to mitigate the problems presented in Figure 2 is through continuous monitoring of the machine, which allows early identification of problems that cause failures, such as unbalance, misalignment and excessive vibration. The use of monitoring systems to identify the operating status of induction motors makes it possible to limit loss of performance and component failures through early diagnosis of anomalous working conditions (CIPRIANI et al., 2021). These anomalies often manifest as distinct vibration patterns, allowing for early detection and preventative maintenance.

Vibration analysis is a highly effective method for identifying faults in electric motors due to its ability to provide valuable information about the mechanical condition of the motor and associated components. By monitoring vibrations generated during engine operation, irregularities such as misalignments, unbalanced loads, worn bearings and other mechanical problems can be detected using statistical data analysis, artificial intelligence or even combining both methods (MALLA; PANIGRAHI, 2019; LI et al., 2018). Moreover, vibration analysis is non-invasive, making it a cost-effective and efficient diagnostic tool that can extend the lifespan of electric motors, enhance operational efficiency, and reduce unexpected downtime in industrial settings.

2.2 VIBRATIONS IN ROTATING ELECTRICAL MACHINES

Machine health monitoring systems are essential, especially considering that downtime in industry and manufacturing can generate average losses of approximately $ 260,000 per hour (SANGEETHA et al., 2024). Therefore, fault detection and diagnosis

Figure 4 – Vibration severity levels defined by ISO 10816.

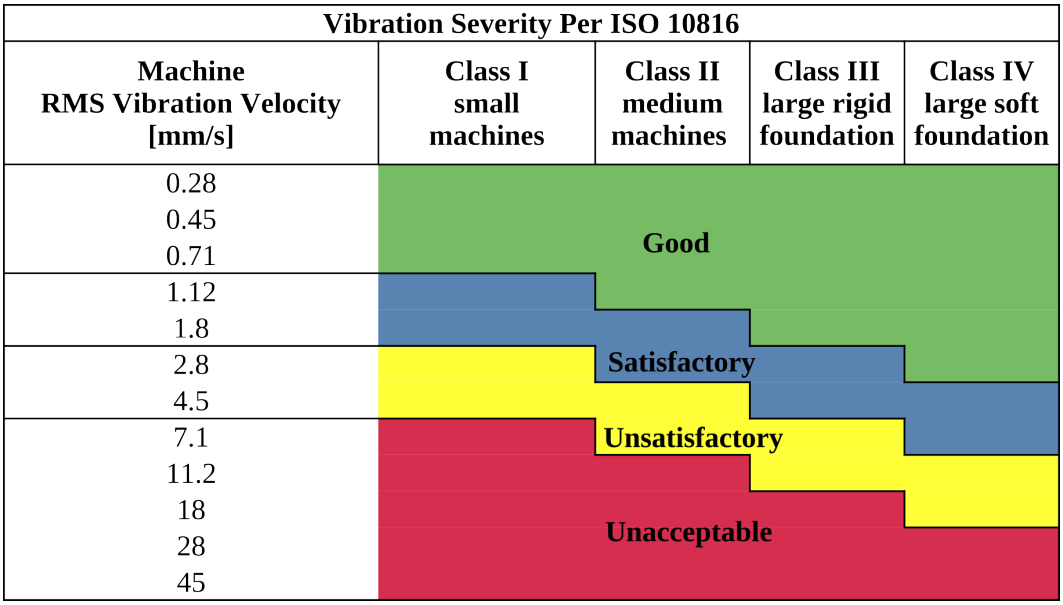

Fonte: Adapted from ISO 10816

in electrical machines and drive systems are extremely important to avoid or reduce the machine downtime. Among the most commonly used techniques for this purpose is vibration analysis, widely used in predictive maintenance programs. Vibration in industrial equipment can both indicate proper operation and signal imminent failures.

Rotating machines, when operating normally, exhibit a specific and relatively constant vibrational behavior known as a spectral signature. This signature corresponds to the characteristic waveform of the machine's vibration in its ideal operating state (SILVESTRE, 2012). By periodically monitoring these vibrations, it is possible to detect changes that indicate anomalies, allowing for the planning of corrective maintenance before a catastrophic failure occurs.

ISO 10816 is one of the oldest and most widely used standards for assessing vibration levels in rotating machinery. Based on statistical studies conducted by the ISO TC 108 committee, the standard establishes severity criteria, defining acceptable vibration limits and alert or intervention levels for different classes of machinery (SANGEETHA et al., 2024). ABNT NBR 10082:2011, based on ISO 10816-3:1995, is also a national reference that addresses vibration assessment criteria for rotating electrical machinery (PEDOTTI et al., 2019).

Variables such as acceleration, velocity, and displacement are widely used to quantify vibration levels in rotating machinery. Among these, vibration velocity is often used in conjunction with the limits established by ISO 10816 to monitor and assess the severity of equipment operating conditions (SANGEETHA et al., 2024). Figure 4 shows the severity levels defined by this standard for different classes of machinery.

The vibration study methodology can be divided into three main stages, as illustrated in Figure 5:

Figure 5 – Basic steps for carrying out a vibration study.

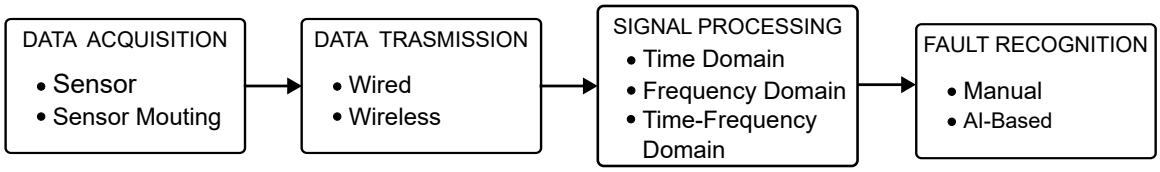

Signal processing involves manipulating, filtering, digitizing, and analyzing raw data to extract the main and most significant parameters for artificial intelligence analysis or training. This step is essential in vibration analysis, as it enables the identification of patterns and insights inside within a large mass of data, which would otherwise be difficult to interpret (AMEZQUITA-SANCHEZ; ADELI, 2016; LU, 2010). Fault detection is the final stage of the vibration analysis process. At this point, the vibration signal is recorded in either the time or frequency domain and subsequently analyzed by an expert to diagnose the type and location of the fault (ZHAO et al., 2021).

It's important to note that, despite its effectiveness, vibration analysis isn't completely accurate. However, it's a powerful tool for monitoring the health of industrial machinery. When combined with technical standards, such as ISO 10816, and a reliable measurement process, it becomes possible to predict failures and extend equipment life, reducing costs and increasing operational safety and reliability.

2.3 TECHNIQUES TO COLLECT VIBRATION DATA

To measure machinery vibration, a transducer or a vibration pickup is used. A transducer is a device that converts changes in mechanical quantities into changes in other physical quantities, usually an electrical signal proportional to a parameter of the experienced motion. There are three commonly used transducers for vibration measurement: displacement sensors, velocity sensors and accelerometers (SCHEFFER; GIRDHAR, 2004). Each sensor has some advantages and disadvantages, depending of the application. The type of sensor used is basically determined by the frequency range, sensitivity and operating limits.

New approaches have been proposed, such as the use of vision data from the event-based camera (LI et al., 2023). However, accelerometers are most commonly used because of their greater accuracy, measurement range, ease of mounting, and cost. Moreover, it is relatively simple to numerically integrate the acceleration signal and obtain the velocity and displacement (CORREA; GUZMAN, 2020; PEDOTTI; ZAGO; FRUETT, 2017). Next subsections discuss the main characteristics of these three types of sensors.

2.4 DISPLACEMENT TRANSDUCERS

Displacement transducers use capacitive, optical or ultrasonic principles to measure vibration displacement. They are suitable for measuring vibration frequencies below 10 Hz (GOYAL; PABLA, 2016). There are several types of displacement transducers, some of which are based on variable resistance and others on induced currents. The most used for predictive maintenance in rotating machines are those based on induced currents (CORREA; GUZMAN, 2020). These transducers, also called eddy current sensors or gap current sensors, are installed in a short distance from the surface whose vibrations are to be measured. The eddy current sensor uses a high-frequency current in a coil inside sensor head to generate a high-frequency magnetic field. When this magnetic field achieve a conductor in the measuring object, an eddy current is generated on the surface of the measuring object and the impedance of the sensor coil changes. This change in impedance is proportional to the gap between the transducer and the vibrating surface (DOWELL; SYLVESTER, 1999). The main advantage of this type of sensor over others is its application in low frequency measurements and its great temperature stability (CORREA; GUZMAN, 2020). Also, it requires a simple processing circuit. This sensor can easily identify problems like imbalance and misalignment in electrical motors or generators. On the other hand, the disadvantages are that this type of sensor is difficult to install, it is susceptible to shocks and the calibration depends on the type of surface material (GHAZALI; RAHIMAN, 2021).

2.5 VELOCITY TRANSDUCER

Velocity transducers are electromechanical sensors designed to directly measure vibratory movement. The velocity sensor is basically composed of three parts: a permanent magnet, a coil of wire and springs supports. The schematic of velocity sensor is shown in Fig. 6. This type of sensor is based on the principle of electromagnetic induction. The movement of a coil within a magnetic field results in the generation of an induced voltage across the end wires of the coil. This voltage is produced by the transfer of energy from the magnetic field of the magnet to the wire coil. When the coil is subjected to vibration, it experiences relative movement with respect to the magnet, which leads to the induction of a voltage signal. This voltage signal is directly proportional to the speed of vibration applied to the sensor. An advantage is that this sensor does not need any external power supply for its operation. The sensitivity of the velocity is constant over a specified frequency range, usually between 10 Hz and 1000 Hz. The sensitivity decreases at low vibration frequencies, which causes inaccurate readings at vibration frequencies below 10 Hz (SCHEFFER; GIRDHAR, 2004) (GOYAL; PABLA, 2016).

Another advantages of velocity sensors are the ease of installation, strong signal in the mid-frequency range and low cost when compared to piezoelectric accelerometers. The

Figure 6 – Velocity sensor schematic with the indication of main components.

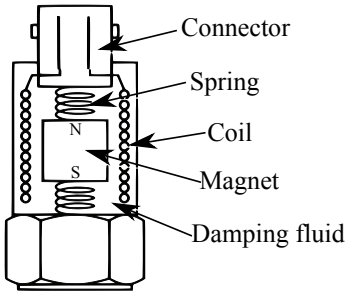

disadvantages include the relative large size, weight, variable sensitivity to input frequencies, narrow frequency response, moving parts, and sensitivity to magnetic interference (SCHEFFER; GIRDHAR, 2004; CORREA; GUZMAN, 2020).

2.6 ACCELEROMETERS

Accelerometers are electromechanical transducers designed for measuring linear acceleration and are the most popular transducers used for rotating machinery applications (SCHEFFER; GIRDHAR, 2004). There are many types of accelerometers, however, for measurement of vibration of rotating machines the most used are the piezoelectric and the MEMS accelerometers. These sensors can be uniaxial - when detects acceleration in only one axis -, or triaxial - when the accelerometer can identify movements in three dimensions. Compared to the uniaxial accelerometer, the triaxial accelerometer demands a larger memory capacity, resulting in a higher cost (GHAZALI; RAHIMAN, 2021).

2.6.1 PIEZOELECTRIC ACCELEROMETER

The piezoelectric accelerometer produces an electrical signal in the output proportional to the incident acceleration. The working mechanism is based on the piezoelectric effect that converts mechanical motion to a voltage signal. When the piezoelectric crystal

Figure 7 – Schematic of a piezoelectric accelerometer.

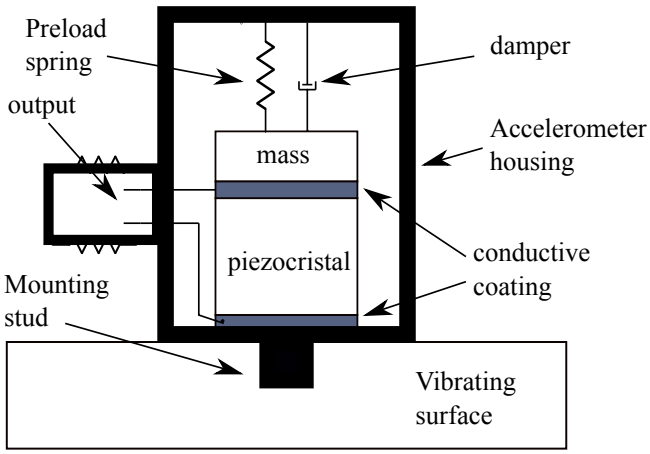

of the sensor is deformed by an external force (acceleration), it generates a certain potential difference between its terminals that is proportional to the force to which it is subjected (CORREA; GUZMAN, 2020; DZHUDZHEV et al., 2013). A representation of the piezoelectric sensor and its components can be seen in Fig. 7. This type of accelerometer is one of the most used transducers for measuring vibrations, as it presents the best general characteristics when compared to the other transducers. It has a wide frequency range and presents dynamic range with good linearity. It is relatively robust and stable so that its characteristics remain stable for a long period of time. Piezoelectric accelerometers have greater reliability when compared to other types of sensors, being able to operate in a frequency range of 1 Hz to 30 kHz, therefore suitable for measuring high frequency vibrations (SCHEFFER; GIRDHAR, 2004; PEDOTTI; ZAGO; FRUETT, 2017).

2.6.2 MEMS ACCELEROMETER

The rapid development of semiconductor micro-fabrication techniques made possible the creation of devices composed of mechanical parts with dimensions of up to a few micrometers (Guru Manikandan et al., 2021). It led to the development of Micro-Electro Mechanical Systems (MEMS) accelerometers. These devices are characterized by their small size and low cost compared with the piezoelectric accelerometers (VARANIS et al., 2018). As a result, MEMS accelerometers are particularly attractive for vibration monitoring in rotating structures (ROSSI et al., 2023).

MEMS accelerometers can be implemented based on piezoresistive or capacitive principles. Capacitive MEMS accelerometers are less sensitive to thermal excitation, which enables capacitance sensing to provide a wider operating temperature range (VARANIS et al., 2018). They present three fundamental structures for their operation: the mobile test mass, the spring region and the fixed structures or capacitive fingers. Figure 8 depicts these elements. The capacitive fingers are placed on both sides of the accelerometer. The accelerometer design allows for lateral movement of test mass. When the sensor is at rest, the capacitance is equal on both sides of the test mass. When the device is under the effect of an acceleration in a given direction, the mass moves to the opposite direction, so the capacitance's formed between the fingers and the fixed structure in both sides are different. The acceleration is measured by reading the changes in the differential capacitance (TEZ; AKIN, 2013).

Most of the MEMS accelerometers available in the market are capable of measuring accelerations in three perpendicular directions simultaneously. Furthermore, MEMS accelerometers allow the easy acquisition of analog or digital signals, even with cheap micro-controllers. This can be considered the biggest advantage over traditional accelerometers which are more accurate and reliable but require wires to transmit the collected data and still need a more robust signal conditioning circuit (ROSSI et al., 2023).

MEMS accelerometers have been implemented and tested for vibration measure-

Figure 8 – Diagram of an integrated MEMS accelerometer.

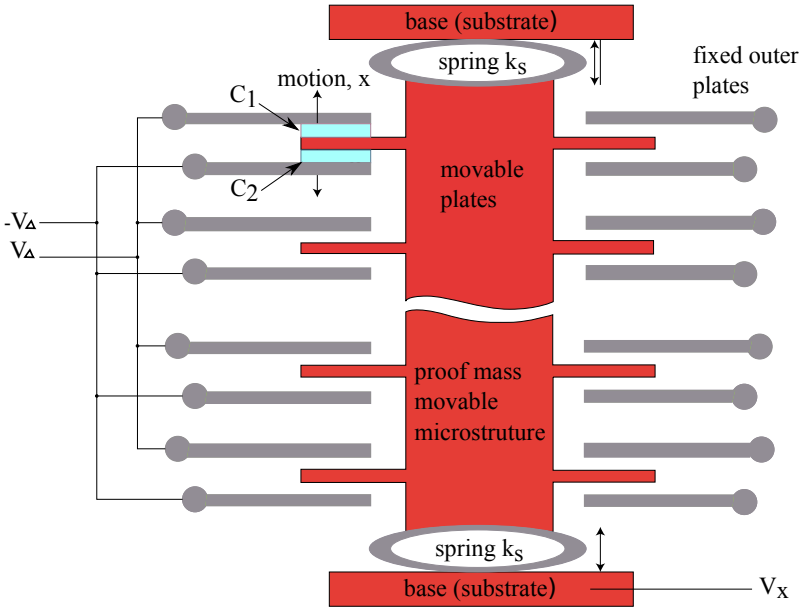

ment in a wide variety of machines, primarily because of their ease of integration into IoT systems. In the study by Rossi, a comparison was made between a piezoelectric accelerometer (PCB 352A56), considered the reference due to its higher sensitivity, and a MEMS accelerometer (ADXL356C) connected to a Raspberry Pi. Both accelerometer were mounted in the same position on a rotating machine, and the results showed a difference of less than 5 % between the signals measured (ROSSI et al., 2023). This low discrepancy, considering the superior metrological characteristics of the reference system, demonstrates the viability of using MEMS accelerometers in a wide range of applications that previously required only piezoelectric accelerometer. The growing adoption of MEMS accelerometers in recent years is largely due to advances in manufacturing technologies that have improved their accuracy, expanded their frequency range, and reduced costs compared to traditional piezoelectric sensors.

2.6.3 SENSOR MOUNTING

Effective acquisition of vibration data is highly dependent on the proper technique of sensor mounting on the machine. In continuous or online machine condition monitoring, vibration sensors are usually mounted at a specific location on the machine (GHAZALI; RAHIMAN, 2021). The mounting methods depend largely on the sensor to be used. However, there are four main methods that can be used for both velocity and acceleration sensors: stud bolt mount, adhesive mount, magnetic mount, and unmounted (SCHEFFER; GIRDHAR, 2004).

In stud mounting, the sensor is screwed into a stud to attach it to the machine. This technique is extremely reliable and secure, making it ideal for permanently mounted applications. It also provides the best frequency response compared to other methods.

Figure 9 – Magnetic mounting of two MEMS accelerometers on an electrical motor.

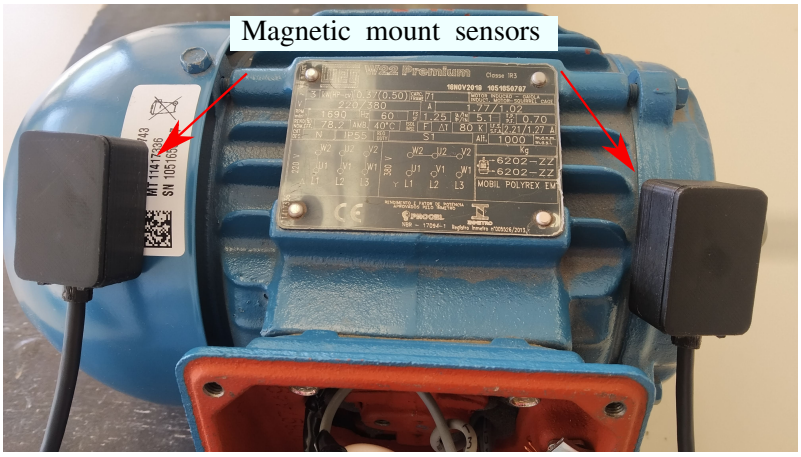

It is important to ensure that the mounting surface is clean and free of paint to avoid irregularities that could cause incorrect readings or damage to the sensor (SCHEFFER; GIRDHAR, 2004).

If the machine cannot be drilled for stud mounting, adhesive mounting is a good alternative. This method involves applying epoxy, glue or wax to the mounting surface. It is easy to apply, but the dampening effect of the adhesive reduces measurement accuracy. In addition, sensors mounted with adhesive are more difficult to remove compared to other mounting methods (SCHEFFER; GIRDHAR, 2004).

The magnetic mount is typically used for temporary vibration measurements with portable analyzers. It is not recommended for permanent monitoring because the sensor can be inadvertently moved and the multiple surfaces and materials of the magnet can interfere with the high-frequency vibrations (SCHEFFER; GIRDHAR, 2004). This can be mitigated by using neodymium magnets, the strongest type of permanent magnets commercially available. The magnetic mount is the most flexible mounting method, as the sensor can be attached and removed countless times without damaging the device or machine. Figure 9 illustrates magnetic mounting in an electric motor.

Finally, the unmounted method uses a probe tip with no external mechanism. It is often used in hard-to-reach places. However, the length of the probe tip can affect measurement accuracy, with longer probes leading to greater inaccuracies (GHAZALI; RAHIMAN, 2021). It is also used in manual vibration measurements, where the probe tip is placed on the machine surface at the point of interest for a few seconds and then removed.

In addition to the four methods described, there are other techniques for mounting vibration sensors using clamps, brackets, and flexible cables. These methods provide additional flexibility for mounting sensors on rotating machinery, but may introduce harmonics into the measured signal.

Choosing the right method for mounting vibration sensors on rotating machinery is critical to obtaining accurate and reliable data. Each method has its advantages and

limitations, and selection should be based on the application and the equipment to be used. Proper installation and placement of the sensors is also critical for accurate measurements.

2.7 DATA TRANSMISSION

Permanent or long-term measurement of vibration in rotating machinery requires a reliable means of storing and transmitting measurement data. There are several ways to establish communication between measuring devices to transmit vibration data. Communication can be direct from the device/sensor to the Internet, where the data is stored for later analysis, or communication can be from sensor to sensor to the end device, which must have access to the Internet. The fourth industry revolution (Industry 4.0) is based on automation and digitalization. This includes the introduction of the Internet of Things (IoT), machine-to-machine communication, improved data transmission and communication, and condition monitoring (WU et al., 2017; SICARD et al., 2022; SWAMY; KOTA, 2020).

With the evolution of technology and the insertion of IoT in industries, various forms of communication and data transmission are available. Among them, the most widespread are: wired, Bluetooth, Wi-Fi and LoRa/LoraWAN (WU et al., 2017; RIZZI et al., 2017; LEONARDI et al., 2018; CHEIKH et al., 2022).

Wired data transmission is a stable and secure method for connecting sensors to the monitoring system (SINHA, 2014; HOU; BERGMANN, 2012; SOFI et al., 2022).The main advantage of data transmission via cables is the high data transfer rates that can be achieved. Additionally, cables can transmit data over long distances and provide a high level of security. Unlike wireless communication methods, wired communication is less susceptible to interference or hacking, making it a secure and reliable choice for transmitting sensitive data. However, there are some disadvantages. This method involves high costs, complicated cable installation and maintenance, and is still not scalable (BAL, 2014; WU et al., 2017). In summary, wired connections provide a stable and reliable means of data transmission that is less susceptible to interference than wireless connections. However, wired connections are less practical in terms of mobility and may require additional hardware and setup.

Bluetooth is a widely used wireless communication technology for short-distance data transmission and can be used to transmit vibration data from rotating machinery (SEFERAGIĆ et al., 2020). It is a simple and easy-to-use technology with low power consumption and relatively low cost (RONDÓN et al., 2019). However, Bluetooth has some limitations, such as limited range and the potential for interference from other wireless technologies operating on the same frequency band (CHANG, 2014; RONDÓN et al., 2019). To overcome these limitations, Bluetooth Mesh technology emerged. It is a mesh networking protocol that allows large-scale networks of Bluetooth devices to be built, providing greater coverage and flexibility. Bluetooth Mesh is more reliable than traditional

Bluetooth, with built-in error correction and redundancy features. However, the use of multiple devices can create security vulnerabilities (MARTÍNEZ; ERAS; DOMÍNGUEZ, 2018). Despite these advantages and disadvantages, Bluetooth and Bluetooth Mesh remain a popular choice for many applications that require wireless data transmission, such as vibration monitoring of rotating machinery. Using Bluetooth Mesh in large-scale networks can provide better coverage and flexibility, while traditional Bluetooth can be a more cost-effective solution for small-scale applications with limited range.

Wi-Fi is also widely used for wireless communication in IoT applications, including vibration monitoring of rotating machinery in industry (JABER; BICKER, 2016; SICARD et al., 2022). Wi-Fi is a widely used wireless communication technology that can transmit data over longer distances than Bluetooth (FELLAN et al., 2018). Wi-Fi Mesh offers the advantage of scalability, allowing large networks of Wi-Fi devices to be built to cover larger areas and support more devices because devices can communicate with each other and create multiple paths for data transmission (BRUNO; CONTI; GREGORI, 2005). Wi-Fi devices can be easily connected to other Wi-Fi enabled devices such as computers and smartphones, making it easier to access and analyze vibration data (ZHANG et al., 2021). However, there are also some limitations to using Wi-Fi and Wi-Fi Mesh for vibration monitoring, such as high power consumption, possible interference, and security concerns. The use of Wi-Fi and Wi-Fi Mesh may also require additional infrastructure and installation costs depending on the size and complexity of the network (SICARD et al., 2022; FELLAN et al., 2018).

LoRa/LoraWAN technologies are wireless communication methods used to transmit vibration data from rotating machinery (IKPEHAI et al., 2019; JOSHITHA et al., 2021). These technologies offer long range, low power consumption, and high network capacity (ZHOU et al., 2019). LoRa technology, developed by Semtech Corporation, is a physical layer technology, while LoRaWAN is a network protocol built on top of LoRa (WIXTED et al., 2016). They are suitable for monitoring machines in remote locations, offering a large network capacity and interoperability between different devices and networks (MIKHAYLOV et al., 2018). However, their relatively low data rates make them suitable for low-to-moderate data rate applications, such as vibration monitoring. Overall, LoRa/LoraWAN technologies offer reliable and cost-effective methods for wireless transmission of vibration data, especially for monitoring rotating machinery in remote and hard-to-reach locations (ERTÜRK et al., 2019).

In summary, several methods are available for transmitting vibration data acquired from rotating machinery, ranging from wired to wireless communication technologies. A summary of the characteristics of the main communication and data transmission methods can be found in Table 1. Wired communications provide stable and reliable data transmission with high security, but can be less convenient and more expensive. Bluetooth and Wi-Fi offer wireless communication options with varying range, scalability, and

potential security concerns. LoRa/LoraWAN offers long range and high network capacity, but with lower data transfer rates. The choice of communication method depends on specific application requirements, such as the distance between sensors and the monitoring system, the amount of data to be transmitted, and the level of security required. Overall, the development of IoT and digitalization has greatly expanded the options for transmitting vibration data and offers more efficient and cost-effective solutions for monitoring rotating machinery in various industries.

Table 1 – Comparison between common communication methods

	Wired	**Bluetooth**	**Wi-Fi**	**LoRa**
Frequency band	-	2.4 GHz	2.4 GHz - 5 GHz	sub-GHz, 2.4 GHz
Typical range	-	1 - 50 m	100 m	3 km - 12 km
Range on factory floor	-	≈ 5 m	≈ 25 m - 50 m	-
Max Data rate		1 Mb/s	35 Mb/s - 1 Gb/s	00.18 - 37.5 kbps, 31.72-253.91 kbps
Latency	Lowest	Moderate	Low	High
Throughput	High	Low	Moderate	Low
Scalability	Difficult	Easy	Easy	Easy
Interference susceptibility	Low	High	High	
Power consumption	-	Moderate	High	Low

Source: (SICARD et al., 2022; DEREVIANCKINE et al., 2023; LYCZKOWSKI et al., 2019; LEE; SU; SHEN, 2007; CARVALHO; MIERS, 2023)

2.8 TECHNIQUES FOR SIGNAL PROCESSING

Obtaining information through signal processing is one of the key elements of machine vibration analysis. At the same time, signal processing can be considered complex, as it aims to highlight the characteristics of collected vibration signals, which are often noisy and complex. Therefore, the data must be processed so that the features of interest can be extracted.

There are several vibration signal processing methods that can be applied to rotating machinery monitoring to identify and diagnose defects or characteristic variations in the measured signal that indicate possible failures. These techniques can be divided into time-domain analysis, frequency-domain analysis, and time-frequency analysis. The choice of technique depends largely on the signal to be analyzed and the characteristics of the signal to be evaluated to identify possible defects. It is worth noting that, when discussing processing techniques for signal feature extraction, the focus here is on the theoretical foundation, not addressing specific practical aspects, such as the size of the data window used for feature extraction, which can vary depending on the technique used and the data sampling frequency.

2.8.1 TIME DOMAIN ANALYSIS

The technique of vibration analysis of rotating machinery in the time domain is the simplest analysis that can be performed. Many features such as the presence of amplitude modulation, shaft frequency components, shaft imbalance, transients, and higher frequency components can be identified visually by analyzing portions of the waveform in function of time (HOWARD, 1994). However, this is not sufficient to more effectively detect changes in the vibration signal caused by potential faults. More sophisticated parameters and approaches should be used for time domain analysis, such as statistical parameter trends in the time domain (GANGSAR; TIWARI, 2014). Several statistical parameters can be defined, such as root-mean-square (RMS), peak, crest factor, and kurtosis (KUMAR; SATHUJODA; BHALLA, 2022). These parameters are described hereafter.

- Peak: the maximum value of signal x(t) in the measured time interval and is defined as (JAIN; BHOSLE, 2022; HOWARD, 1994):

$$Peak = max(|x(t)|) \tag{2.1}$$

- Root-mean-square (RMS): Root-mean-square is related to the energy of the sampled signal, so it can contain useful information about signal construction (JAIN; BHOSLE, 2022; YADAV; PAHUJA, 2020). This parameter is defined as:

$$RMS = \sqrt{\frac{1}{N}\sum_{i=1}^{N}(x_i)^2} \tag{2.2}$$

  Here, N is the number of measured points and x_i is the value of i^{th} sensor output signal.

- Crest Factor (CRF): Crest factor is the ratio of peak and RMS value of the signal, which shows the spikiness of vibration signal. A CRF near 1 represents a lower spiky signal (JAIN; BHOSLE, 2022; YADAV; PAHUJA, 2020). Crest factor is defined as:

$$CRF = \frac{Peak}{RMS} \tag{2.3}$$

- Kurtosis(KUR): Kurtosis is the measure of the tailedness of the probability density function of a time series. This number is related to the tails of the distribution. A high kurtosis value corresponds to greater extremity of deviations (or outliers). The kurtosis is defined as the standardized fourth moment (JAIN; BHOSLE, 2022; YADAV; PAHUJA, 2020):

$$KUR = \mu_4 = \frac{\mu_4}{\sigma^4} \tag{2.4}$$

where μ_4 is the unstandardized central fourth moment and σ is the standard deviation.

A summary of the advantages and disadvantages of the time domain vibration analysis techniques can be seen in Table 2.

Table 2 – Advantages and disadvantages of time domain methods.

Time domain methods	**Advantages**	**Disadvantages**
Peak	Simple technique.	It considers only the maximum value of x(t), because this technique is sensitive to noise.
RMS	Easy technique, RMS values are not affected by isolated peaks in the signal.	It is not able to detect failures in the early operating stages.
CFR	Easy to estimate.	Reliable only in the presence of a spiky signal.
KUR	High performance in detecting faults; independent of the signal amplitude.	Its effectiveness depends on the presence of significant impulsivity in the signal.

2.8.2 FREQUENCY DOMAIN ANALYSIS

The characteristics of a signal in the frequency domain are often used for fault detection in rotating machinery through vibration analysis. Frequency domain analysis is

a powerful tool for analysing vibration signals in rotating machinery to diagnose faults. This method helps in identifying the frequency components present in a signal and their amplitudes (VISHWAKARMA et al., 2017). Many signal features that are not visible with time domain analysis can be observed with frequency domain analysis. However, frequency analysis is not suitable for signals whose frequency varies with time (GHAZALI; RAHIMAN, 2021). The main frequency domain methods for detecting faults in rotating machinery are described below.

- Fast Fourier Transform (FFT): The Fast Fourier Transform is a computer algorithm that computes the discrete Fourier transform (DFT) much faster than other algorithms (BRIGHAM; MORROW, 1967) (GOYAL; PABLA, 2016). Through the FFT, it is possible to convert a signal from the time domain to the frequency domain. Using this signal represented in the frequency domain, the intensity of the different frequency components (the power spectrum) of a signal can be checked in the time domain. Vibration analysis in rotating machinery benefits from this technique because each component of the machine contributes a specific frequency component to the vibration signal. Therefore, one of the ways to detect faults is to compare the frequency components and their amplitudes to a signal from the same machine operating under perfect conditions. FFTs are used in predictive maintenance to detect various types of faults in rotating machinery, such as misalignment, imbalance and bearing faults (PATIL; GAIKWAD, 2013; KHADERSAB; SHIVAKUMAR, 2018; LIN et al., 2016; KUMAR; DIWAKAR; SATYNARAYANA, 2012; SALEEM; DIWAKAR; SATYANARAYANA, 2012; MARTINS et al., 2021).

- Cepstrum Analysis: Cepstrum analysis is the inverse Fourier transform of the logarithmic spectrum of the signal and is defined as (LAKIS, 2007):

$$C(x(t)) = \mathcal{F}^{-1}(log(X(\omega))) \tag{2.5}$$

  Here, $\mathcal{F}$ is the inverse of the Fourier Transform, $x(t)$ is the signal in the time domain and $X(\omega)$ is the signal in the frequency domain. Cepstrum analysis involves analyzing the logarithm of the power spectrum to detect any periodic structure in the spectrum, such as harmonics, side bands, or echoes (GOYAL; PABLA, 2016). It is useful in detecting faults such as bearing and localized tooth faults that produce low harmonically related frequencies. There are four types of cepstrum, with power cepstrum being the most commonly used in machine diagnostics and monitoring. Cepstrum analysis has been used in gearbox diagnosis and monitoring, detection of friction in sliding bearings, and diagnosis of faults in a universal lathe machine (SATYAM; RAO; DEVY, 1994; LI; AI, 2008; RANDALL; SMITH, 2016; LIU et al.,

2020; RANDALL, 2017). The Cepstrum analysis can be sensitive to noise present in the vibration signals. This can lead to inaccurate or distorted results, especially at lower frequencies.

- Envelope Analysis: Envelope analysis is a technique used to separate low-frequency signals from background noise in rolling element bearings and in low-speed machine diagnostics (RANDALL; ANTONI, 2011). The technique involves band-pass filtering and demodulation to extract the signal envelope, which can contain diagnostic information. Envelope analysis has the advantage of early detection of bearing problems, but determining the best frequency band for this technique is a challenge (GOYAL; PABLA, 2016). The introduction of quadratic envelope analysis solved the problem of noise components in the signal. Envelope analysis has been applied in several studies to detect faults in bearings and induction motors (CHEN et al., 2022; CHENG et al., 2018; ABBOUD et al., 2017; RANGEL-MAGDALENO et al., 2017), but it has shown poor performance compared to other techniques, such as acoustic emission analysis (GOYAL; PABLA, 2016).

- Power Spectral Density (PSD): PSD represents the power of a signal at different frequencies. The PSD is calculated by taking the Fourier Transform of a signal and

Table 3 – Summary of main advantages and disadvantages of frequency domain analysis.

Frequency Domain Analysis	**Advantages**	**Disadvantages**
FFT	Easy to implement.	It is not efficient for detecting failures if the frequency and amplitude signals of the machine in normal operation are unknown.
Cepstrum Analysis	Easy technique, useful to detect harmonics, side bands or echoes.	Sensitive to noise present in the vibration signals.
Envelope Analysis	Early detection of bearing problems.	Determining the best frequency band for this technique is a challenge.
PSD	Clear frequency domain of the signal, which allows identification of specific frequency components associated with faults or anomalies in rotating machinery.	Specialist is required for graphical interpretation of the signal.

squaring the magnitude spectrum (SCHEFFER; GIRDHAR, 2004). The PSD is a powerful tool for analysing the strength of signal fluctuations as a function of frequency. It allows the detection and measurement of oscillatory signals in time series data and indicates the frequencies at which the oscillations are strong or weak. The PSD is a graphical representation of the energy distribution of the signal over different frequencies and is commonly used for fault diagnosis in induction machines (GOYAL; PABLA, 2016). Vibration analysis using PSD offers several advantages, such as a clear frequency domain of the signal, which allows identification of specific frequency components associated with faults or anomalies in rotating machinery. Also, it enables quantitative comparisons between different signals or different operating conditions, facilitating trend analysis and condition monitoring (MEHRJOU et al., 2011; GOYAL; PABLA, 2016). However, it is important to consider some limitations of PSD analysis. Often the assumption of stationarity is made, which means that the statistical properties of the signal are assumed to be constant over time (RADI; AL., 2019).

All presented vibration analysis methods in the frequency domain have advantages and disadvantages, which are summarized in Table 3.

2.8.3 TIME-FREQUENCY DOMAIN ANALYSIS

In the real world, most signals are not stationary, i.e., the spectrum may change with time. In the case of vibration in machines, it can vary during operation. The vibration signal may contain different frequency components at different instants of time (GOYAL; PABLA, 2016). This variation is a problem for frequency domain analysis (GHAZALI; RAHIMAN, 2021). To overcome this challenge, time-frequency domain analysis techniques have been developed that can provide information about the time-varying frequency content of vibration signals. Time-frequency analysis allows not only the representation of the signal in three dimensions (time-frequency amplitude), but also the detection and tracking of the evolution of defects that produce weak vibration performance (LAKIS, 2007). Conventional vibration analysis methods rely on stationary assumptions that are unsuitable for analysing non-stationary signals. Therefore, time- frequency domain analysis methods such as the short-time Fourier transform (STFT), wavelet transform (WT), Hilbert-Huang transform (HHT), Wigner-Ville distribution (WVD), and power spectral density (PSD) are used to identify local features in the time and frequency domains (GHAZALI; RAHIMAN, 2021). These techniques are discussed in more detail below and the summary of the advantages and disadvantages can be seen in the Table 4.

- Short-time Fourier transform (STFT): This technique was developed to overcome the problems of FFT. It is basically an addition to the FFT's ability to analyze nonstationary or noisy signals. The STFT consists of a method that divides the

nonstationary vibration signal into many small segments that can be assumed to be locally stationary, and applies the conventional FFT to these segments (LAKIS, 2007). The STFT is defined as:

$$S_t(\omega) = \frac{1}{2\pi} \int_{-\infty}^{\infty} e^{-j\omega\tau} S(\tau) h(\tau - t) d\tau \tag{2.6}$$

Here, a signal $S_t(\tau\ )$ is obtained by multiplying the signal by a window function $h(\tau)$ centered on (τ) to produce a modified signal that emphasizes the signal around time τ. With that, the Fourier Transform reflects the frequency distribution at that time (LAKIS, 2007; GHAZALI; RAHIMAN, 2021). The main drawback of the STFT is the tradeoff between time and frequency. The resolution is determined by the size of the window. A large window gives good resolution in the frequency domain and poor resolution in the time domain and vice versa (LAKIS, 2007). Despite this drawback, the STFT method is more efficient than conventional analysis methods in the time and frequency domains and is widely used in the analysis of vibration signals to monitor machine conditions (HUANG et al., 2021; SANTHOSHI et al., 2021; JUNIOR et al., 2022; LEIBER et al., 2023; WANG et al., 2017).

- Wavelet Transform (WT): The Wavelet Transform is a linear transformation in which a time signal is decomposed into wavelets, i.e., local functions of time endowed with a predetermined frequency content (GHAZALI; RAHIMAN, 2021). Wavelet transforms are a powerful technique for analyzing vibration signals in rotating machinery (AL-BADOUR; SUNAR; CHEDED, 2011; TENG et al., 2019). By decomposing a non-stationary signal into its individual frequency components, WT can reveal time-varying features and identify transient events that may be missed by conventional Fourier transform-based methods. The wavelet scalogram provides a time-frequency representation that aids in visualization and analysis of the signal (LOPARO et al., 2000; LAKIS, 2007). The advantages of using WT for vibration analysis in rotating machinery include the ability to detect local changes in vibration signals and improved time resolution. However, there are limitations to its use, including careful selection of the wavelet function and the possibility of cross terms in the wavelet scalogram (GHAZALI; RAHIMAN, 2021; LAKIS, 2007). Despite these limitations, WT is a valuable tool that is becoming increasingly popular in industry and academia for the analysis of transient vibration signals (LI et al., 2016).

- Wigner–Ville distribution (WVD): The Wigner-Vielle distribution is based on the cross-correlation function between the signal and a time-lagged version of itself (LI et al., 2019). It decomposes the signal into a series of elementary waveforms, each of which has its own time and frequency characteristics. Thus, the time-frequency representation is independent of the windowing function, allowing simultaneous

analysis of the signal in the time and frequency domains (LAKIS, 2007). The advantages of WVD for vibration analysis include its high time-frequency resolution and the ability to detect and locate transient events with high accuracy (LIAO et al., 2021; GHAZALI; RAHIMAN, 2021). However, WVD has some limitations, such as the presence of interference terms, which can make interpretation of the results difficult (SUN; JIN; YANG, 2015). Despite its limitations, WVD is a valuable tool for analyzing non-stationary signals in rotating machinery, especially for detecting and diagnosing faults in bearings, broken rods in induction and gears (DING et al., 2022; LIU et al., 2022).

- Hilbert–Huang transform (HHT): The Hilbert-Huang Transform is a method for analyzing stationary, non-stationary, and transient signals. It combines empirical mode decomposition (EMD) and the Hilbert transform to obtain a Hilbert spectrum that can be used for fault diagnosis in machines (GHAZALI; RAHIMAN, 2021). The HHT consists of two main steps. First, the EMD method decomposes the signal into a series of intrinsic mode functions (IMFs), which are essentially vibration components with well-defined instantaneous frequencies. Each IMF represents a specific frequency component of the signal, which allows for a more detailed analysis

Table 4 – Main advantages and disadvantages of time-frequency domain analysis.

Time-Frequency Domain Analysis	**Advantages**	**Disadvantages**
STFT	More efficient than conventional analysis methods in the time and frequency domain; low computational complexity.	The resolution is determined by the size of the window.
WT	Ability to detect local changes in vibration signals; improved time resolution.	Need a careful selection of the wavelet function.
WVD	High time-frequency resolution; ability to detect and locate transient events with high accuracy.	The presence of interference can make it difficult to interpret the results.
HHT	Suitable for analyzing stationary, non-stationary and transient signals; high time-frequency resolution; ability to capture transient phenomena; low computation time.	Sensitivity to noise; generation of undesirable IMFs in the low-frequency range; difficulty in separating low-frequency components.

of the time-varying features. After obtaining the IMFs, the Hilbert transform is applied to each IMF to calculate the instantaneous frequency as a function of time. In this way, a time-varying frequency representation of the signal is obtained, which allows the detection of transient events and the analysis of frequency fluctuations (PAI et al., 2008; SUSANTO et al., 2018).

The advantages of HHT for vibration analysis in rotating machinery include its adaptability to nonstationary and nonlinear signals, its high time-frequency resolution, its ability to capture transient phenomena, and its low computation time. It is particularly effective in identifying and analyzing fault signatures associated with bearings, gears, and other rotating components. However, the HHT has certain limitations, such as sensitivity to noise, generation of undesirable IMFs in the low-frequency range, and difficulty in separating low-frequency components (GOYAL; PABLA, 2016; GHAZALI; RAHIMAN, 2021).

In summary, HHT is a valuable technique for vibration analysis in rotating machinery, providing a detailed time-frequency representation of non-stationary signals and enabling the detection and diagnosis of faults and transient events. Its application in conjunction with other analysis methods can improve the understanding of vibration behavior and contribute to effective condition monitoring and maintenance strategies (BIN et al., 2012; LIU et al., 2018; ZHANG; FENG, 2022).

2.9 EDGE VERSUS CLOUD COMPUTING FOR DATA PROCESSING ON IOT SYSTEMS

With the continuous advancement of sensor technology, the cost of individual sensors has steadily declined. Consequently, modern industrial plants now deploy thousands of sensors on motors and transmission systems, generating vast amounts of operational data. In this context, cloud computing is a suitable paradigm for processing large amounts of data, offering fast and secure storage and computing services. It has proven its worth in machine condition monitoring and fault diagnosis (ROMANSSINI; AGUIRRE; GIRARDI, 2025).

Cloud computing excels in AI-powered fault diagnosis by leveraging powerful servers to process vast amounts of sensor data. By leveraging cloud resources, machine condition data can be transmitted over wired or wireless networks to centralized servers, where signal processing, feature extraction, fault recognition, and prognosis are performed using vast computational and storage resources (LU et al., 2023). Furthermore, cloud-based fault diagnosis models can be iteratively refined using newly collected data, improving accuracy over time. However, as the number of sensors increases, so does the volume of data, leading to greater demands on transmission bandwidth, power consumption, storage, and computing resources (QIAN et al., 2019). While cloud computing remains a dominant

paradigm, valued for its agility and competitive advantage, the rapid expansion of IoT devices exposes the limitations of a centralized approach, challenging the scalability and efficiency of cloud-based systems (KÜNAS et al., 2022).

While cloud computing offers significant processing power (LU et al., 2023), relying solely on the cloud for all data processing can overload the infrastructure and reduce efficiency. One promising solution to mitigate these challenges is edge computing (SATYANARAYANAN, 2017), which decentralizes data processing by analyzing information directly at the edge of the network, closer to the data source. This approach reduces the load on cloud servers, optimizes bandwidth usage, and improves processing speed and efficiency (QIAN et al., 2019). By minimizing latency and increasing system autonomy, edge computing is particularly beneficial for data-intensive applications. In monitoring systems, for example, transmitting large volumes of raw sensor data to the cloud can be time-consuming and resource-intensive. Local processing at the edge mitigates transfer delays, reduces dependence on cloud infrastructure, and improves overall system responsiveness (KÜNAS et al., 2022). Table 5 shows the main characteristics of both cloud processing and edge processing.

A characteristic feature of edge computing is that sensor data is processed directly on local devices or gateways, such as IoT nodes, mobile devices and embedded systems (YU et al., 2018). This localized approach offers several advantages for machine signal processing and fault diagnosis. It enables real-time data processing and accelerates fault detection and response times. It also reduces the consumption of cloud resources by reducing data transfer overhead, preventing network congestion and improving data privacy by keeping sensitive information local. In addition, edge computing supports real-time control, allowing fault diagnosis and control algorithms to run on the same processor, improving efficiency and reliability. Its flexibility also facilitates scalable and customizable sensor networks, making it well-suited for industrial applications (LU et al., 2023).

Edge computing complements cloud computing by mitigating its limitations, such as high bandwidth consumption and scalability challenges in environments with many IoT devices. By processing data close to the source, this approach enables real-

Table 5 – Characteristics of edge and cloud computing.

Characteristic	**Edge Computing**	**Cloud Computing**
Deployment Model	Distributed	Centralized
Main Components	Edge Nodes	Virtualized Resources
Computational Power	Limited	Virtually Unlimited
Storage Capacity	Limited	Virtually Unlimited
Response Time	Low Latency	Higher Latency
Big Data Handling	Local Processing	Data Center Processing

Source: (YU et al., 2018)

Table 6 – Comparison between Cloud Computing and Edge Computing.

Aspect	**Cloud Computing**	**Edge Computing**
Latency	Higher latency due to data transmission to remote servers.	Low latency, as processing occurs close to the data source .
Bandwidth Consumption	High bandwidth usage, as large volumes of data need to be transmitted.	Reduces bandwidth consumption by processing data locally and transmitting only relevant information.
Processing Power	High processing power with scalable resources in remote servers.	Limited processing power, depending on the hardware of the edge node.
Privacy and Security	Greater risk of privacy breaches, as data is stored and processed remotely.	Enhanced security and privacy by keeping sensitive data at the source.
Cost	Can be expensive due to infrastructure requirements and recurring storage and processing costs.	Can reduce operational costs by minimizing the need for cloud bandwidth and processing.
Scalability	Highly scalable, allowing for dynamic expansion of computing resources.	Limited scalability due to the capacity of local devices and edge infrastructure.
Reliability	May suffer from connection instability and dependency on remote servers	Higher reliability for critical applications by reducing reliance on external connections.

time monitoring and faster diagnostics, reducing dependence on the cloud. In addition to improving efficiency, data decentralization increases system reliability and resilience, which is essential for mission-critical applications that require low latency and continuous operation (WANG et al., 2019).

IoT devices have different connectivity, power, and processing capacity constraints. To maximize their lifetime, it is essential to decide when to process data locally and when to send it to the cloud. Edge computing enables flexible task allocation, considering the energy availability of the devices. Several studies propose schemes to optimize energy consumption and distribution of the computational load, resulting in lower costs, better quality of service, and reduction of energy consumption by up to 80% (YU et al., 2018).

Table 6 shows a summary of the main differences between edge and cloud processing.

2.10 CONCLUSION

This chapter presented a comprehensive theoretical and conceptual review of the main failures in rotating machinery and vibration monitoring techniques applied to predictive maintenance. The most common types of failures in rotating electrical machinery, the acceptable vibration limits established by the ISO 10816 standard, and the main types of transducers used to acquire vibration signals were explored. Transmission technologies, processing strategies, and data analysis methods were also discussed, with an emphasis on cloud and edge applications. Furthermore, the characteristics, advantages, and limitations of each transducer were described. Proper selection of each component, from data acquisition and transmission to processing, whether in the cloud or at the edge, is essential to ensure accurate assessment and anticipate potential failures before they compromise machine operation.

In summary, vibration monitoring for predictive maintenance of rotating machinery is a constantly evolving field, driven by technological advances and the growing demand for greater operational reliability. As highlighted, selecting the most appropriate monitoring technique is essential for effectively assessing machine health. Future research should focus on improving these techniques and exploring innovative approaches, such as integrating IoT and cloud platforms for real-time monitoring and analysis. Furthermore, the ability to process data at the edge can optimize the power consumption of IoT sensors and reduce the overhead on transmission channels, minimizing the transmission of large volumes of raw data.

3 IOT SENSOR NODE FOR VIBRATION AND TEMPERATURE MONITORING

This chapter presents, in detail, the design and development of an IoT sensor for monitoring rotating electrical machinery in industry. The sensor's functional and operational requirements are described, as well as the main hardware components and embedded firmware responsible for acquiring, pre-processing, and transmitting vibration data. Furthermore, the design decisions that ensure the sensor's energy autonomy are discussed, targeting applications in industrial environments with limited access to conventional power sources.

3.1 HARDWARE DESIGN

The IoT sensor developed for vibration and temperature measurement consists of a microcontroller - which is responsible for controlling, acquiring, processing and transmitting data-, a MEMS accelerometer and a temperature sensor, both of which are integrated on the same circuit board. The two sensors together are referred as the sensor unit. The system is designed to be efficient and reliable, ensuring accurate data collection with low power consumption. In addition, the sensor has wireless connectivity that facilitates its installation and integration with cloud systems or local servers, as well as non-volatile memory for data storage in case the sensor loses communication with the server. Figure 10 shows the modules that compose the system and the simplified connection diagram between them.

Four main requirements were taken into account when developing the sensor: the first is low power consumption, aiming to maximize battery life and reduce the need for frequent maintenance; the second is ease of installation, avoiding structural modifications to the equipment, such as drilling or routing cables; the third requirement is compact dimensions, which allow the sensor to be installed in confined spaces without

Figure 10 – Schematic of the proposed system for monitoring and identifying faults.

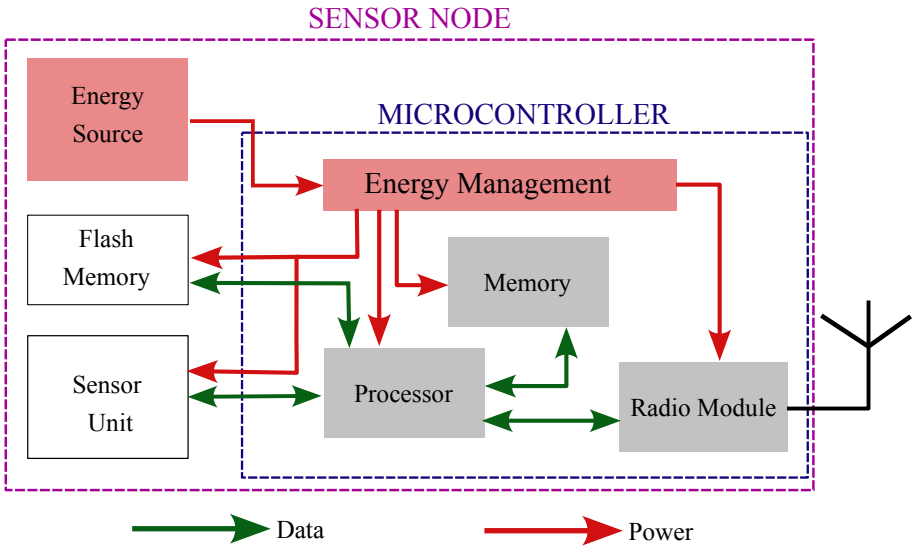

Table 7 – IoT sensor technical requirements

Parameters	Value	Observations
Operating voltage	3.0–3.7 V	Battery compatible
Wireless communication	Wi-Fi 2.4 GHz	MQTT support
Average consumption	< 50 mA (active mode)	Maximize battery life
Temperature sensor	125°C	
Battery life	> 365 days	Reduce sensor maintenance
Offline operation	7 days (offline)	Data loss reduction

interfering with machine operation; and finally, the ability to operate in high-temperature environments was considered, ensuring reliable system operation up to 125°C, a common condition in harsh industrial applications. The IoT sensor requirements are summarized in Table 7.

The implemented IoT sensor can operate with two distinct approaches: edge processing and cloud processing. In the first approach, we hypothesize that performing data processing at the edge, i.e., directly on the sensor, can significantly reduce the monitoring system's energy consumption compared to sending the entire data to the cloud for analysis. To investigate this hypothesis, the system was designed with two distinct data acquisition and processing approaches.

In the first approach, focusing on local processing, vibration and temperature signals are preprocessed within the sensor itself, allowing the extraction of relevant parameters (RMS acceleration, peak acceleration, RMS vibration, and peak vibration). Only this processed information is then transmitted to the server, significantly reducing the data volume and, consequently, the time and energy consumption associated with wireless communication.

In the second approach, with remote processing, all raw data is transmitted in its entirety to the cloud, where parameter extraction is performed later. In this case, for example, each acquisition involves sending 2,048 samples per axis, totaling 6,144 points for the vibration data alone, not counting the metadata and packet headers, which further expand the volume of transmitted data. We chose to take 2,048 samples due to the need for greater precision in spectral analysis via FFT, allowing for better frequency resolution. We configured the accelerometer sampling rate at 2 kSPS, this number of samples also corresponds to exactly 1 second of signal per axis.

Figure 11 illustrates a comparison between these two strategies, highlighting their differences in the operational flow of the developed IoT sensor. The main objective is to experimentally evaluate whether the edge processing approach is in fact more energy efficient and whether the accuracy of edge processing is affected when compared to cloud processing.

Figure 11 – Execution flow for edge and cloud processing approaches.

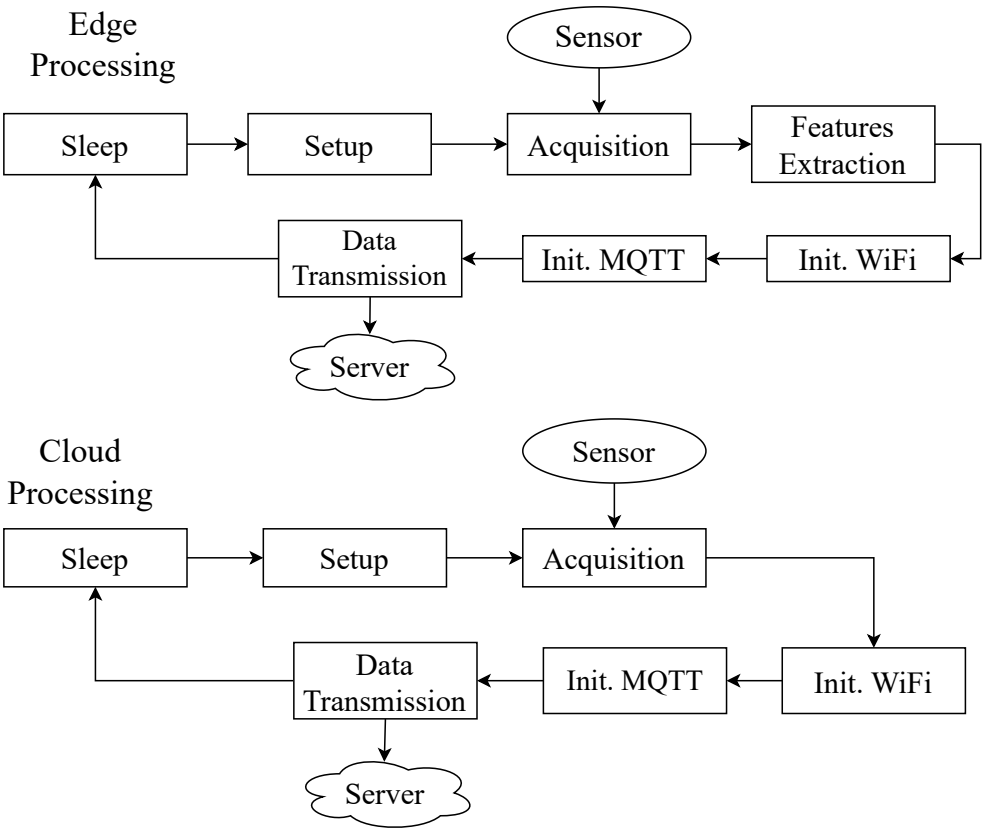

3.1.1 MICROCONTROLLER

The developed sensor is powered by a 3.6 V lithium-ion battery, and the ESP32-WROOM-32 microcontroller was chosen as the central processing unit. This choice was motivated not only by its immediate availability during the initial development phase, but also by its technical advantages in battery-powered IoT applications.

The ESP32 is fully compatible with 3.6 V systems, eliminating the need for additional regulation or power conditioning stages. Furthermore, it offers high processing capacity, enabling the local execution of complex computational routines, such as FFT, a fundamental requirement for processing vibration data and extracting parameters at the edge.

The integrated Wi-Fi module significantly optimizes communication and reduces development time by eliminating the need for external transceivers and simplifying firmware integration. The ESP32-WROOM-32 is a system-on-a-chip (SoC) that integrates a processing unit, memory, and Wi-Fi and Bluetooth connectivity, facilitating sensor implementation. These features make this microcontroller an efficient and cost-effective solution for the proposed IoT sensor.

The ESP32-D0WDQ6 chip, has two CPU cores with variable frequencies from 80

Figure 12 – ESP32 microcontroller accelerometer connection diagram.

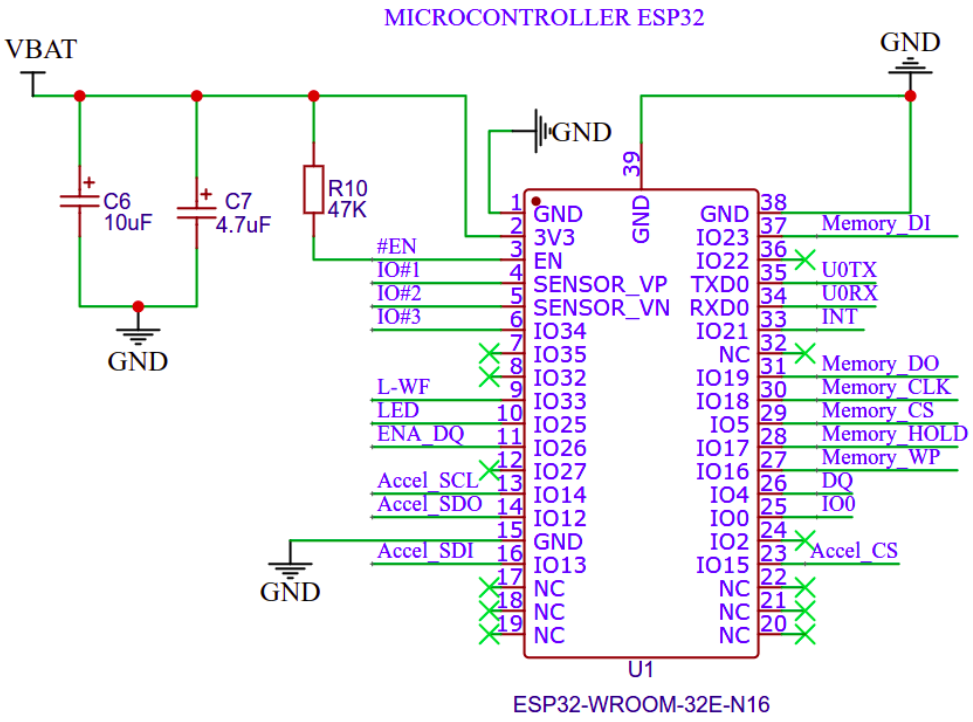

MHz to 240 MHz and a low-power coprocessor for simple tasks. Various peripherals such as touch sensors, SD, Ethernet, SPI, UART, I2S and I2C interfaces are also integrated. The module is designed to operate with extremely low power consumption (less than 5 μA) and offers data transmission rates of up to 150 Mbps. The Wi-Fi power is configurable, reaching up to 20 dBm. The operating system used by the module is FreeRTOS, which allows secure over-the-air (OTA) updates.

The ESP32 in the implemented sensor was configured to operate at a frequency of 80 MHz, to meet the power requirement. Among the available peripherals, the SPI interface was used to communicate with the sensor unit, and the Wi-Fi transmission power was set to 16 dBm. The electrical circuit diagram of the microcontroller is shown in Fig. 12.

The microcontroller reads acceleration data from the accelerometer and temperature information from the sensor via the SPI protocol. After acquisition and preprocessing, the data is transferred to the cloud or a local server via Wi-Fi using the MQTT protocol, eliminating the need for physical connections between the measurement and analysis devices.

The developed sensor also includes two LEDs that indicate power and Wi-Fi connection status, as well as a port for firmware uploading and debugging. This high level of integration accelerates development, simplifies operation, and reduces both the complexity and the overall size of the sensor.

Figure 13 – ICM-42352 accelerometer connection diagram.

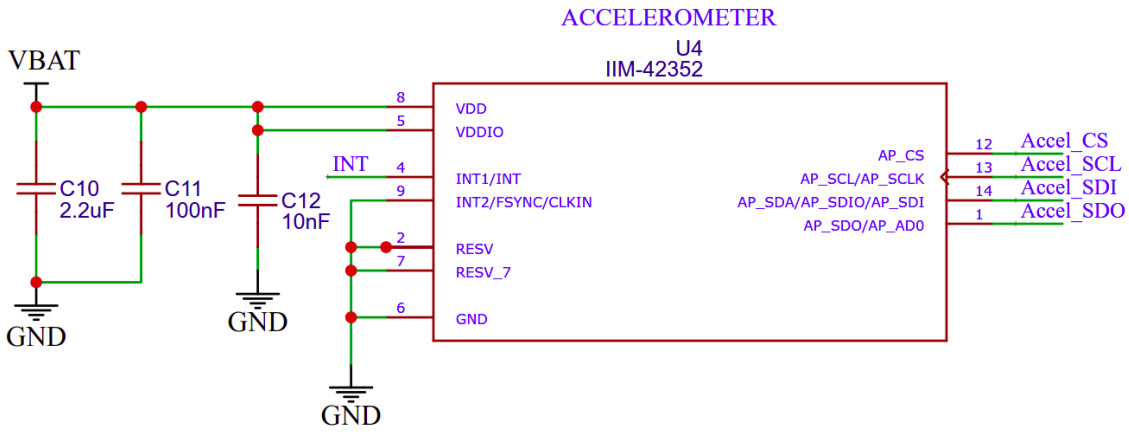

Table 8 – IIM-42352 accelerometer acceleration and sensitivity specifications.

Amplitude	Sensitivity
± 2g	16.384 LSB/g
± 4g	8.192 LSB/g
± 8g	4.906 LSB/g
± 16g	2.048 LSB/g

Source: (INVENSENSE, 2022)

3.1.2 MEMS ACCELEROMETER

To collect acceleration data, a triaxial MEMS accelerometer, model IIM-42352, was used. This accelerometer stands out for being robust, presenting low consumption, low noise (noise spectral density of 70 $\mu g/\sqrt{Hz}$), has a flat frequency response range from DC to 4 kHz (-3 dB point) and still offers a data output rate of up to 32 kHz. This device is designed for industrial applications such as vibration measurement, predictive maintenance, platform stabilization, and robotic applications. The IMM-42352 uses separate test masses for each axis and is capable of measuring linear acceleration in all three separate axes up to an amplitude of ±16 g (INVENSENSE, 2022). It also has four programmable amplitude and sensitivity ranges, as shown in Table 8.

Additionally, the IIM-42352 can withstand impacts with accelerations of up to 20 g. When placed on a flat surface, it registers 0 g on the x- and y-axes and +1 g on the z-axis. The scale factor is factory calibrated, independent of the sensor supply voltage, and optimized for low power consumption - it consumes only 0.28 mA in low-noise mode and only 7.5 μA in full-chip sleep mode (INVENSENSE, 2022).

All electrical connections between the accelerometer and ESP32, as well as the power connections, were made following the guidelines of the Chip Datasheet (INVENSENSE, 2022) and are illustrated in Figure 13. The accelerometer is powered by the battery voltage (VBAT), while the Accel-CS, Accel_SCK, Accel_SDI, Accel_SDO and INT connections are for communication via SPI protocol and are linked to the ESP32 microcontroller.

Figure 14 – DS18B20 temperature sensor connection diagram.

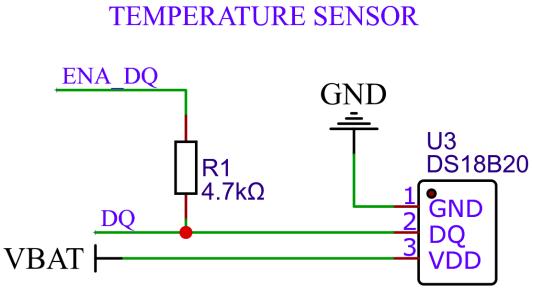

3.1.3 TEMPERATURE SENSOR

We use the DS18B20 digital sensor to measure the engine/machine temperature. This temperature sensor measures from -55 °C to +125 °C with an accuracy of ±0.5 °C between -10 °C and +85 °C and has a programmable resolution of 9 to 12 bits. It uses a 1-wire interface that requires only a data line and ground to communicate with a microprocessor. The sensor can be powered via the data line ("parasitic power" mode), eliminating the need for an external power source. Each device has a unique 64-bit serial code that allows multiple sensors to be used on the same bus. Applications include temperature control, industrial systems and consumer products. The electrical schematic for the temperature sensor connection is shown in Figure 14.

3.1.4 FLASH MEMORY

The IoT sensor, designed for temperature and vibration measurement, also incorporates non-volatile memory (W25N01GVZEIG flash memory) with a capacity of 1 Gb (approximately 128 MB). This choice ensures that the system operates reliably even under unstable connectivity conditions.

According to the Table 7, one of the design requirements is that the sensor be able to store locally, without loss of information, at least seven full days of data. Considering the worst-case scenario—in which the machine operates 24 hours a day, with data collected every five minutes—and the storage of 2,048 acceleration samples per axis (with 16 bits

Figure 15 – Non-volatile memory connection schematic.

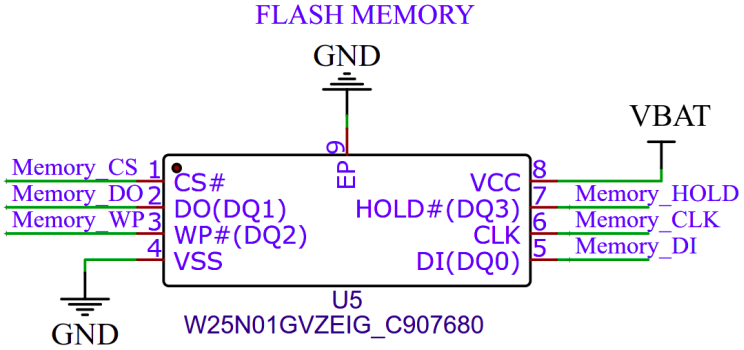

per sample), in addition to the date and time information, the volume of data generated per day is approximately 3.38 MB. Therefore, the chosen memory can store more than 37 days of continuous data, providing a wide margin of safety for offline operation. This ensures that collected data is not lost in the absence of an internet connection, being stored locally until it can be transmitted to the cloud. The electrical circuit diagram for non-volatile memory is shown in Figure 15.

3.2 PROTOTYPE IMPLEMENTATION

The sensor prototype implementation phase is essential for the construction of the vibration and temperature sensor. With the electronic component selection stage completed, and the electronic schematic finalized, the electronic circuit was designed on a printed circuit board (PCB). For this, the EasyEDA software was used (EasyEDA, 2025). Using the layout tools, we strategically arranged the components on both sides of the PCB (top and bottom) to optimize the routing of the electrical connections and ensure a compact and efficient design that facilitates soldering and assembly of the PCB in the sensor mechanical housing. The final sensor PCB design and its dimensions can be seen in Figure 16.

Figure 16 – Developed sensor printed circuit board design, with components positioned and electronic routing completed.

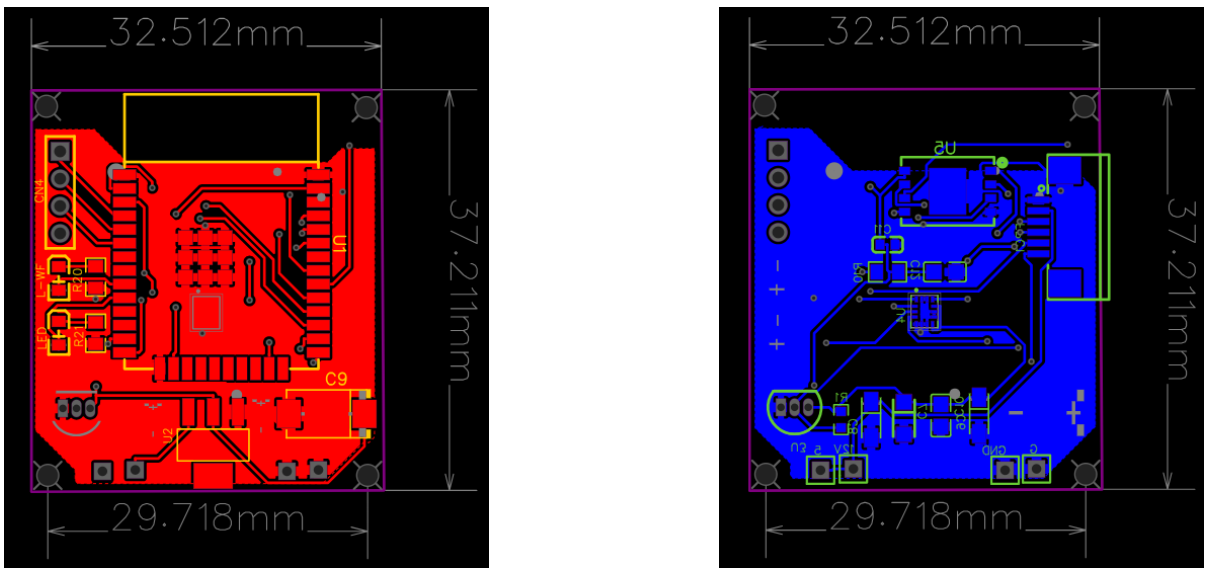

(a) Top View.

(b) Bottom View

After routing the electronic circuit, the printed circuit board was manufactured and the components were soldered. Figure 17 shows the prototype of the processing and acquisition board, which is already properly soldered with all electronic components.

Figure 17 – Implementation of the sensor printed circuit board, with components soldered.

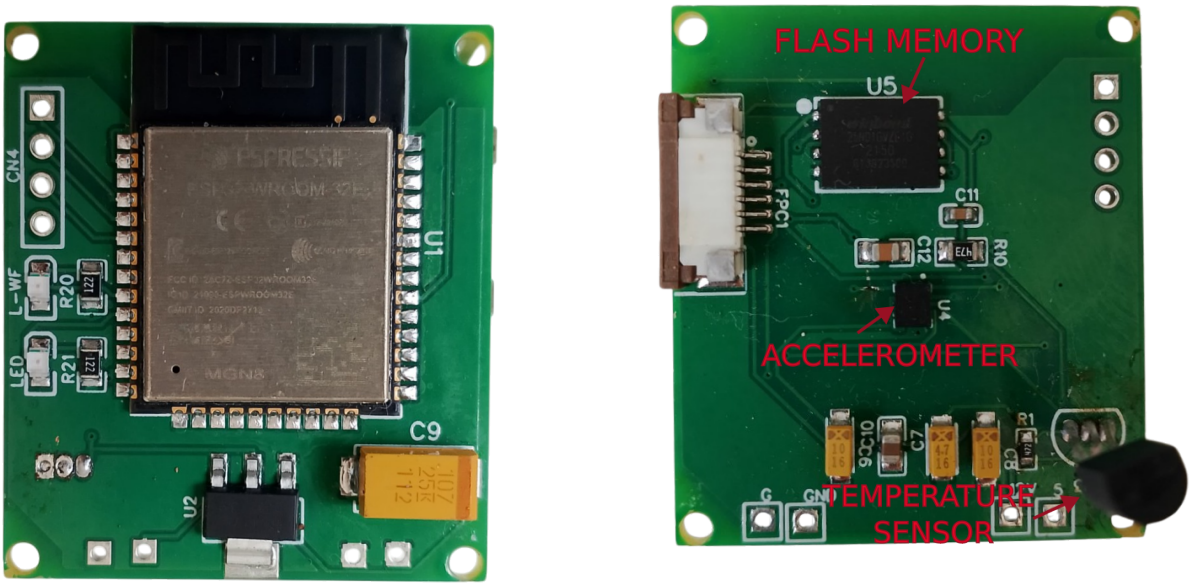

(a) PCB assembled top view.

(b) PCB assembled bottom view

With the PCB design finalized and its dimensions in hand, we began developing the mechanical box responsible for housing the electronic circuit and batteries. This step was performed using the free software FreeCAD (FREECAD,), widely used for 3D modeling of mechanical parts. The main requirement of the mechanical design was to ensure that the sensor had a compact design and, at the same time, was resistant to the ingress of water and dust, allowing its use in industrial and outdoor environments. To this end, the box was designed to allow the assembly of all electronic components (PCB and battery) through a single opening, facilitating both assembly and maintenance.

The final structure of the sensor case consists of only two parts: the main body (case) and the cover, which is fixed by screws with millimeter threads (M2 x 10). The same screws used to fix the cover also hold and secure the PCB, which, in turn, keeps the batteries locked inside the box. This simple design makes it easy to assemble the sensor and contributes to the robustness of the assembly.

Once the design was ready, the case was printed using a 3D printer and the sensor was assembled, as shown in Fig. 18. As the sensor is exposed to harsh industrial environments, we used FRP 193 filament for printing, which consists of a material with good mechanical resistance, classified as flame retardant and is also a good electrical insulator. Figure 19 illustrates an exploded view of the fully assembled sensor prototype, detailing the integration of the electronic board, battery and housing components.

To attach the sensor to the machine, we use a neodymium magnet, which offers several advantages. The use of the magnet allows a firm and stable attachment and at the same time easy removal and repositioning without the need for additional tools. In addition, this approach reduces installation time and avoids drilling or modifications to

Figure 18 – Sensor case printed with a 3D printer.

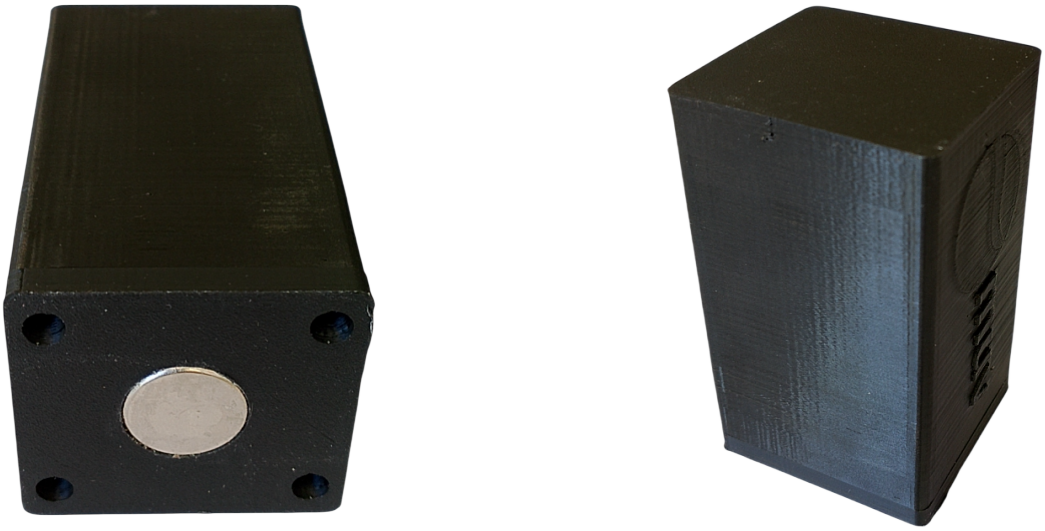

(a) Case assembled bottom view.

(b) Case assembled side view

Figure 19 – Exploded view of the sensor node for vibration and temperature measurement.

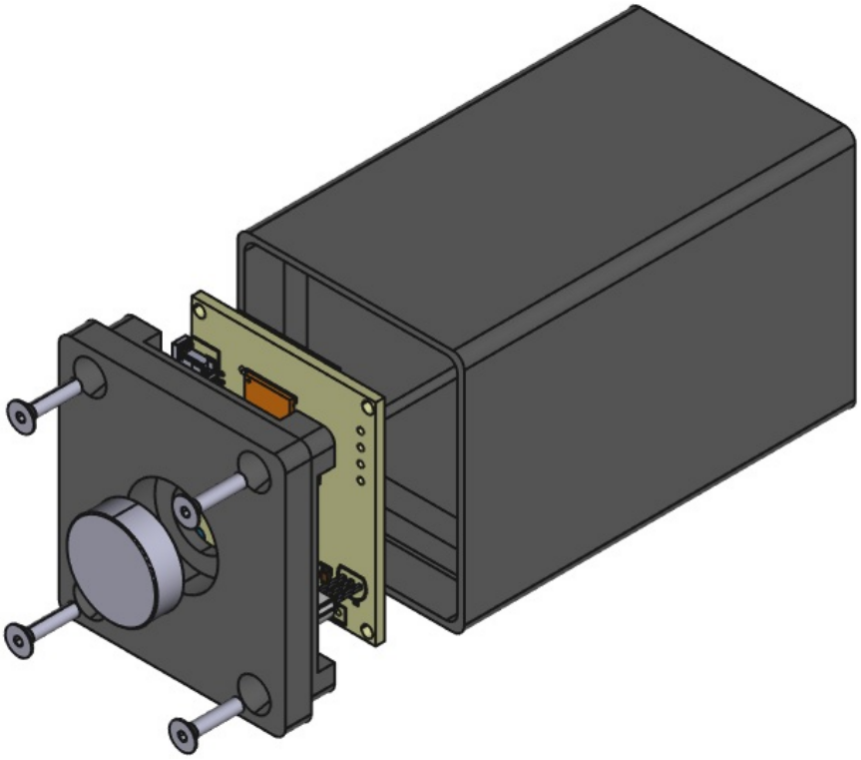

the machine structure, making the sensor more versatile for vibration and temperature measurements at different points on the equipment.

3.3 EMBEDDED SOFTWARE

To manage the reading of the accelerometer and the temperature sensor as well as the processing and transmission of the vibration data to the local server or cloud, a firmware

for the microcontroller was developed, as shown in Figure 20. This flowchart provides a simplified view of how the implemented sensor works and highlights the fundamental steps of the firmware operation.

It is important to remember that the implemented software includes a series of additional processes, such as parallel task execution, filtering and preprocessing of acquired signals, wireless communication management and energy consumption optimization. However, the representation of the sensor operation flow is capable of providing an overview of the main operations of the system, facilitating the analysis of its functioning and the architecture of the implemented sensor.

The sensor designed to measure vibration and temperature is activated as soon as it is connected to the battery. The first step in the firmware is to set the operating time in power saving mode, i.e. the interval during which the device remains in deep sleep before waking up to perform a new data acquisition and check whether the machine is operating or stopped. The longer this time, the longer the battery life will be, on the other hand, the vibration and temperature data sampling will be lower, which may prevent accurate monitoring of the actual operating status of the machine.

After the time the sensor remains in power-saving mode has been set, the acceleration and temperature reading task begins, in other words, we start data acquisition. In the same step, the acquired data is processed and stored in memory. In parallel with the data acquisition task, the system initializes the Wi-Fi and MQTT communication modules so that the information can be sent to the cloud or server.

The sensor then tests the connection to the Wi-Fi network and the MQTT broker. After Wi-Fi initialization, if no connection can be established, all ESP32 modules are turned off to reduce power consumption, and the sensor enters deep sleep mode for 15 minutes before trying again. If the connection is successful, the system checks to see if a new firmware version is available before continuing with normal operation. The firmware check is only performed once every 24 hours, because establishing a connection to the server where the firmware files are hosted is slow.

Once communication with the MQTT broker is established, the sensor waits for the task of reading and processing the acceleration and temperature data to complete. It is important to emphasize that when using the edge computing strategy, that is, when data processing is performed locally on the device, the reading and processing task may take longer to complete due to the computational effort required to process the collected acceleration data and extract the parameters from the vibration signal.

After collecting and processing the variation and temperature data, the implemented sensor checks whether the RMS vibration velocity is greater or less than 0.2 mm/s. This check is important to determine the operational status of the machine, i.e. whether it is running or inactive. If the RMS value of the vibration velocity is less than 0.2 mm/s, it means that the machine is not in operation. Since the machine is stopped, the accelerom-

Figure 20 – Embedded software operating flowchart.

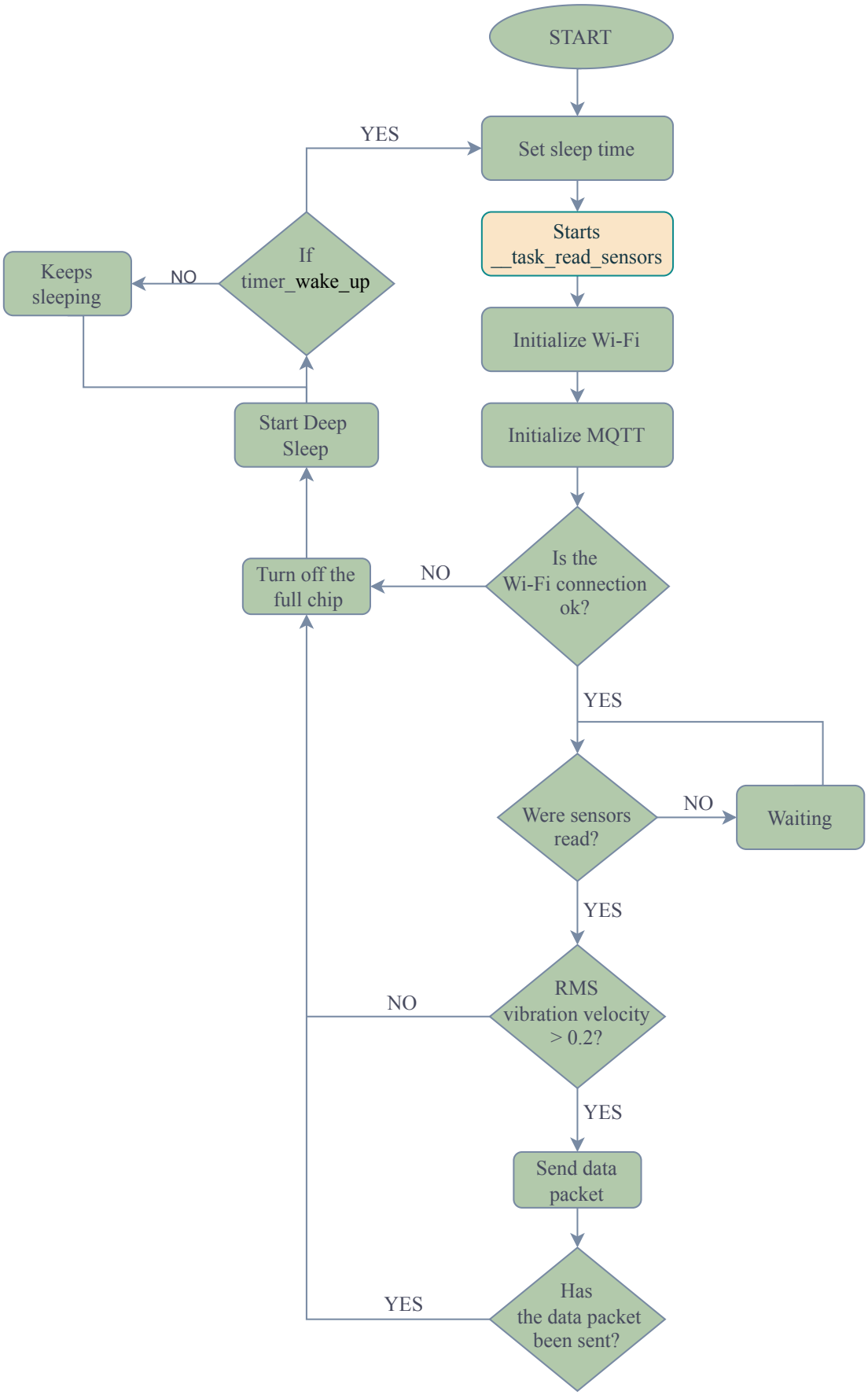

eter as well as all ESP32 modules are turned off to reduce power consumption and the implemented IoT sensor goes into deep sleep for 10 minutes. After this time, it wakes up, repeats all previous steps and performs a new check of the machine status. If the machine is in operation (RMS velocity greater than 0.2 mm/s), the processed vibration and temperature data are sent to the database. To optimize power consumption, all ESP32 modules are turned off again and the sensor goes into deep sleep for 5 minutes before resuming the monitoring cycle.

As a strategy to optimize the battery consumption of the developed sensor, the deep sleep time is configured according to the system conditions. As explained earlier, when the sensor is not connected to Wi-Fi, it enters deep sleep for 15 minutes to reduce power consumption while waiting for a new connection attempt. When the machine is not in operation, the sleep time is 10 minutes to ensure efficient monitoring without wasting energy. When the machine is in operation, the sensor only goes into deep sleep for 5 minutes, allowing a higher frequency of data acquisition and transmission for more accurate monitoring.

An important factor is the approach used for data processing. If the data is processed directly at the sensor (edge computing), the execution time of the sampling and processing task is longer than in an approach where the raw data is sent directly to the cloud (cloud computing). On the other hand, local processing of the data reduces the size of the data packet to be transmitted, so that the transmission is faster.

When processing is performed in the cloud, the data acquisition and processing steps are faster, since the sensor only collects, packages and transmits the values, without performing additional calculations. However, since this approach involves sending the raw data, the packets transmitted to the server or cloud are significantly larger. Consequently, the time required for packaging and transmitting the data also increases.

To summarise, edge computing requires more local processing time, but reduces the time for data transfer due to the lower volume of information. Cloud computing, on the other hand, enables faster data acquisition, but leads to longer transmission times due to the size of the packets sent.

3.3.1 DATA ACQUISITION AND PROCESSING

The main function (*___task_read_sensors*) is responsible for collecting acceleration and temperature data, processing it to extract the main features of the vibration signal, and storing it for later analysis or sending it to the cloud. The data reading and processing process can be divided into three steps: communication, acquisition, and feature extraction, in the case of edge processing. If the processing is performed in the cloud, only the communication and acquisition steps are performed, and the raw data is sent directly. Figure 21 illustrates the main steps involved in reading and processing the data from the implemented sensor.

In the communication stage, the buses are initialized to allow data exchange with the sensors. The SPI protocol is used to communicate with the accelerometer, while the 1-wire protocol is used for the temperature sensor. In addition to the communication buses, the data buffers are also initialized. Also in the communication stage, we configure the IIM-42352 accelerometer with an amplitude of ± 2 g so that it operates with the highest available sensitivity (16,384 LSB/g), as shown in Table 8. In the implemented IoT sensor, the ESP32 microcontroller communicates with the IIM-42352 through an SPI bus, which operates at a clock frequency of 23 MHz, ensuring fast and reliable data transmission.

Once communication has been established and the sensors have been configured, the second phase begins: data acquisition. In this step, a temperature sample and 2048 acceleration points are collected on each of the axes (X, Y and Z), using the sensor's FIFO buffer, with a sampling rate of approximately 2 kHz. For vibration monitoring, this sampling rate and number of samples result in a spectral resolution of 0.98 Hz in the FFT, that this, the FFT bins have a spacing of approximately 0.98 Hz. This allows for more accurate identification of nearby frequencies, improving the analysis of the vibration signal.

With the vibration acceleration data sampled, the third phase begins, which consists of extracting the features of the acquired sample. The main features extracted include: RMS acceleration, peak acceleration, RMS velocity and vibration velocity for each of the axes. These metrics are essential for analyzing the vibration behavior and detecting possible anomalies in the monitored equipment.

To extract the signal properties, we first remove the DC component of the acceleration by subtracting the mean value of the sampled signal. We then apply a Hanning window to minimize unwanted effects in the spectral analysis. With the filtered and prepared data, we calculate and store the RMS value and the peak value of the acceleration. The data is then transformed from the time domain to the frequency domain using a Discrete Fourier Transform (DFT) according to Equation 3.1, where $A[k]$ represents the acceleration in the frequency domain, $a[n]$ is the acceleration in the time domain, N is the total number of samples, k is the sample index in the frequency domain, and n is the sample index in the time domain.

$$A[k] = DFT\{a[n]\} = \sum_{n=0}^{N-1} a[n] \cdot e^{-j\frac{2\pi}{N}kn} \tag{3.1}$$

With the acceleration data in the frequency domain, we obtain the vibration velocity by performing the integration according to Equation 3.2, where $A[k]$ and $V[k]$ represent, respectively, the acceleration and velocity in the frequency domain, and ω is the angular velocity in radians per second, as defined in Equation 3.3, where Δt is the sampling period.

Figure 21 – Data acquisition and processing flowchart.

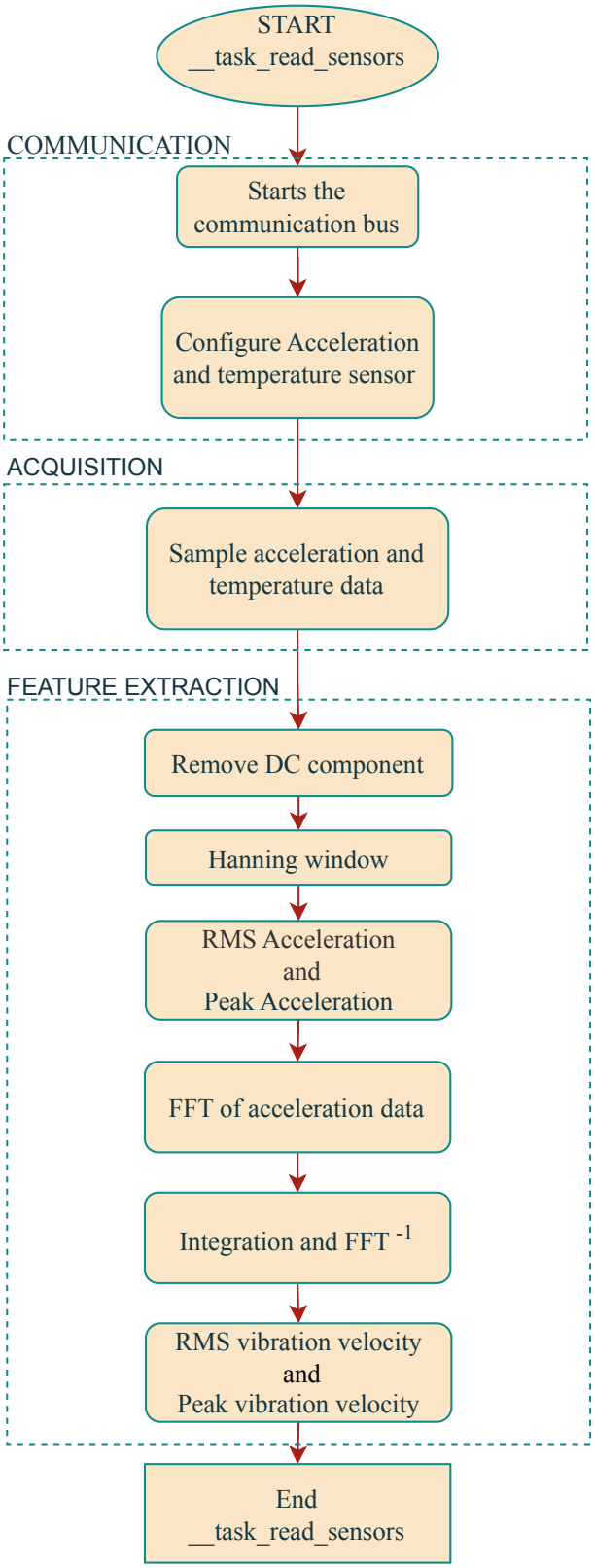

$$V[k] = \frac{A[k]}{j\omega_k} \tag{3.2}$$

$$\omega_k = \frac{2\pi k}{N \cdot \Delta t} \tag{3.3}$$

The vibration velocity could be obtained by integrating the acceleration in the time domain. However, by performing this operation in the frequency domain, low-frequency noise is attenuated, reducing the drift problem caused by small integration errors. In addition, this method makes the process computationally more efficient, since, as can be seen from Equation 3.2, the integration in the frequency domain is simply a division by the frequency (BRANDT; BRINCKER, 2014).

After integration, the Inverse Fourier Transform (IDFT), Equation 3.4, is applied to convert the vibration velocity back to the time domain, remove the DC component of the signal again to eliminate any remaining residuals, and finally calculate and store the RMS and peak values of the vibration velocity. Once all the desired features have been extracted from the signal, the readout and processing function is completed and the data is sent to the cloud.

$$v[n] = IDFT\{V[k]\} \tag{3.4}$$

In the feature extraction phase, the collected data is processed so that only the most important information from the signal is sent to the cloud. This reduces the size of the data packet and shortens the time required for transmission, which is a feature of edge processing. If processing is performed in the cloud, i.e. the data is sent directly to the cloud for subsequent feature extraction, all collected raw data must be sent, which corresponds to 2048 acceleration points per axis and results in a total of 6144 points for the vibration data alone. This amount of data does not include packet headers, timestamp information and temperature information, which can further increase the transmission size. Figure 11 shows the main differences in sensor performance between the edge and cloud processing approaches.

3.4 CONCLUSION

In this chapter, the hardware of the developed IoT sensor was presented in detail, describing the components used and their electrical connections. In addition, the design of the prototype PCB and the mechanical schematic of the assembled sensor were discussed. The operation flow of the firmware was also described in detail, explaining the individual steps and the strategies used to optimize energy consumption, including the use of power-saving modes. Finally, the data acquisition and processing process were examined, highlighting the configuration of the sensors, data acquisition and extraction of vibration signal features as essential elements for the efficient operation of the system.

4 RESULTS AND DISCUSSIONS

To validate the functionality and evaluate the performance of the IoT sensor developed for vibration and temperature monitoring, experimental tests were conducted focusing on three main areas: execution time for data acquisition, processing, and transmission; energy consumption associated with processing and feature extraction at the edge and transmission of raw data to the cloud; and the accuracy of parameters calculated during edge processing compared to those obtained by processing the same data in the cloud. The methodology adopted for these tests, as well as the results obtained, are presented in this chapter.

4.1 EXECUTION TIME

Execution time is defined as the total duration required to complete a full sensor operation cycle, comprising the following steps: sensor activation and configuration; acceleration signal acquisition (2,048 samples per axis: X, Y, and Z); local data processing (in the case of edge processing), which includes the extraction of features such as RMS and peak acceleration and velocity values, as well as average temperature; initialization of Wi-Fi and the MQTT stack; and, finally, data transmission to the remote server.

Measuring execution time is important to evaluate processing efficiency and data transmission performance in the evaluated scenarios. To enable this analysis, the developed sensor PCB was used along with modified firmware capable of measuring the execution time of each processing step individually. Ten iterations (samples S1 to S10) were performed to obtain average results and reduce the impact of random fluctuations.

The ESP32 microcontroller was configured to operate at 80 MHz to reduce power consumption, despite supporting up to 240 MHz. During data acquisition, 2,048 acceleration samples were collected per axis (X, Y, and Z). Two distinct processing strategies were evaluated:

- Cloud Processing: Raw acceleration data (1,024 samples per axis) is sent directly to the cloud, resulting in a payload of approximately 37.5 kB per cycle.

- Edge Processing: The data is processed locally on the microcontroller to extract key features such as RMS, peak values, and average temperature. This reduces the transmitted data to just 356 bytes per cycle.

In both cases, the data packets were formatted as strings and transmitted using the MQTT protocol.

To ensure timing accuracy, the firmware was adapted to record partial durations of each functional block. All tests were conducted with the sensor positioned approximately 3 meters from the Wi-Fi router, with the sensor resting on a flat surface.

Figure 22 – Time consumed at each operation step for edge and cloud processing approaches. Test was repeated 10 times (samples S1 to S10).

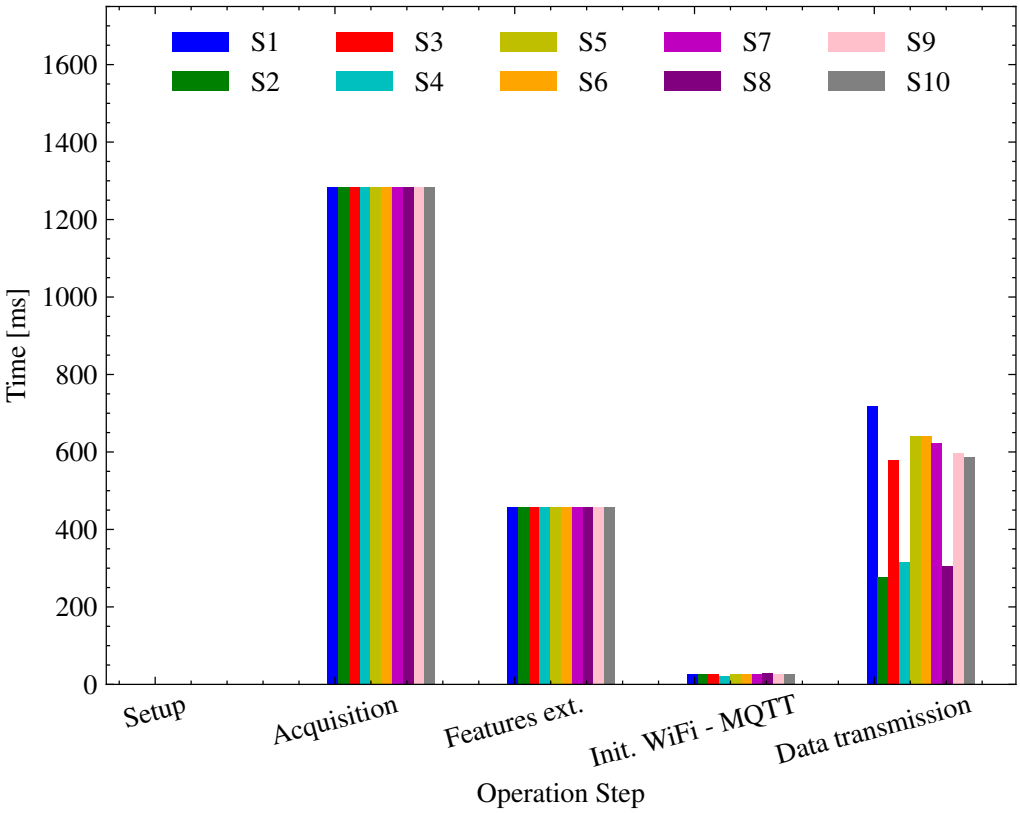

(a) Edge processing.

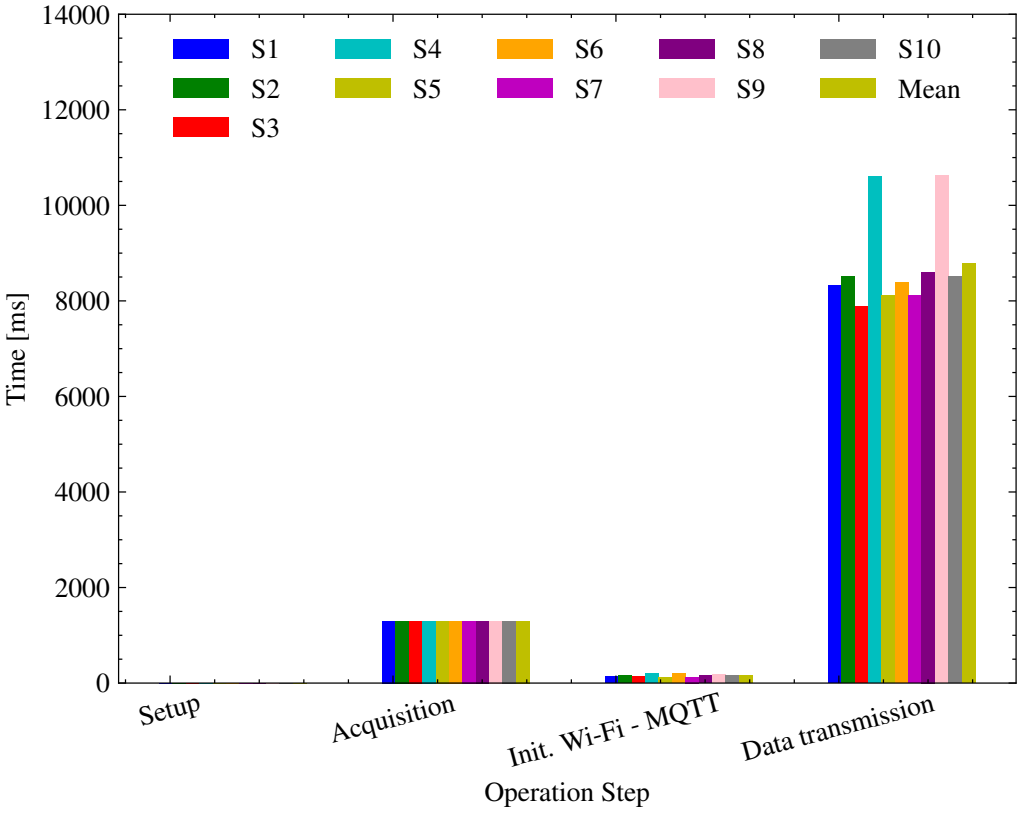

(b) Cloud processing.

Figure 23 – Average time consumed in each step of the operation for edge and cloud processing approach.

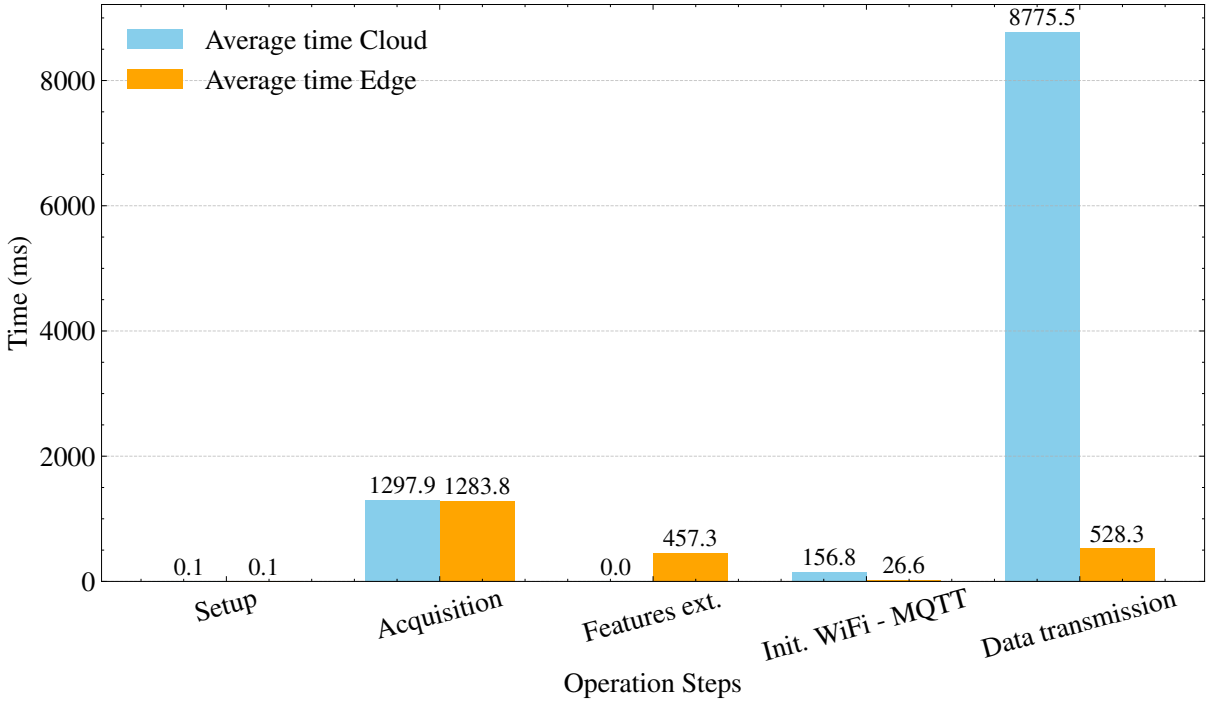

After running the test procedure ten times and collecting the execution times for each step, from microcontroller initialization to data transmission, the results were analyzed using Python. The Figure 22 summarizes the results.

The results indicate that the Wi-Fi configuration and initialization steps are completed quickly in both processing approaches (edge and cloud). Although the edge processing method includes an additional feature extraction step from the acquired signals, the time spent on this step is negligible compared to the time required to transmit the raw data to the cloud.

Figure 23, which presents the average execution times for each step based on the ten test repetitions, highlights the discrepancy between the time to send the raw data and the other steps in the processing cycle. This difference reinforces the advantage of local processing in terms of runtime efficiency, even considering the additional computational effort for feature extraction.

Even when feature extraction time is combined with transmission time in the edge approach, the total duration remains significantly shorter, approximately nine times faster than the time spent solely on data transmission in the cloud processing approach.

Table 9 shows the comparison between the edge and cloud processing approaches, considering the total processing time and the size of the transmitted data packets. It can be seen that the average processing time at the edge is approximately 4.5 times faster than the time required to send raw data directly to the cloud, as occurs in the cloud processing approach. In addition, the size of the data packet sent in the cloud processing approach is

Table 9 – Comparative analysis between edge and cloud processing in terms of total execution time and transmitted data size.

Method	Average Total Time [ms]	Max Deviation from Mean [ms]	Data Packet Size [bytes]
Edge Processing	2296.00	260.54	356
Cloud Processing	10230.20	1848.136	37504

Table 10 – Comparison between edge and cloud approaches regarding transmission rate.

Method	Packet Size [bytes]	Average Transmission Time[ms]	Max Deviation from Mean [ms]	Transmission Rate [bytes/ms]
Edge Processing	356	528.29	242.12	30.67
Cloud Processing	37.504	8775.5	1740.27	4.27

approximately 100 times larger than the edge approach, which directly impacts on the transmission time and network bandwidth consumption.

Table 10 shows the transmission rate observed in each of the approaches. It can be seen that the transmission rate in the cloud-based approach is 6.4 times higher, due to the significantly larger volume of transmitted data. On the other hand, edge computing consumes less bandwidth and is more efficient in scenarios with network restrictions or limitations on data consumption.

Using the same ten runtime samples, we analyzed the time variation for both

Figure 24 – Variation in total time per execution.

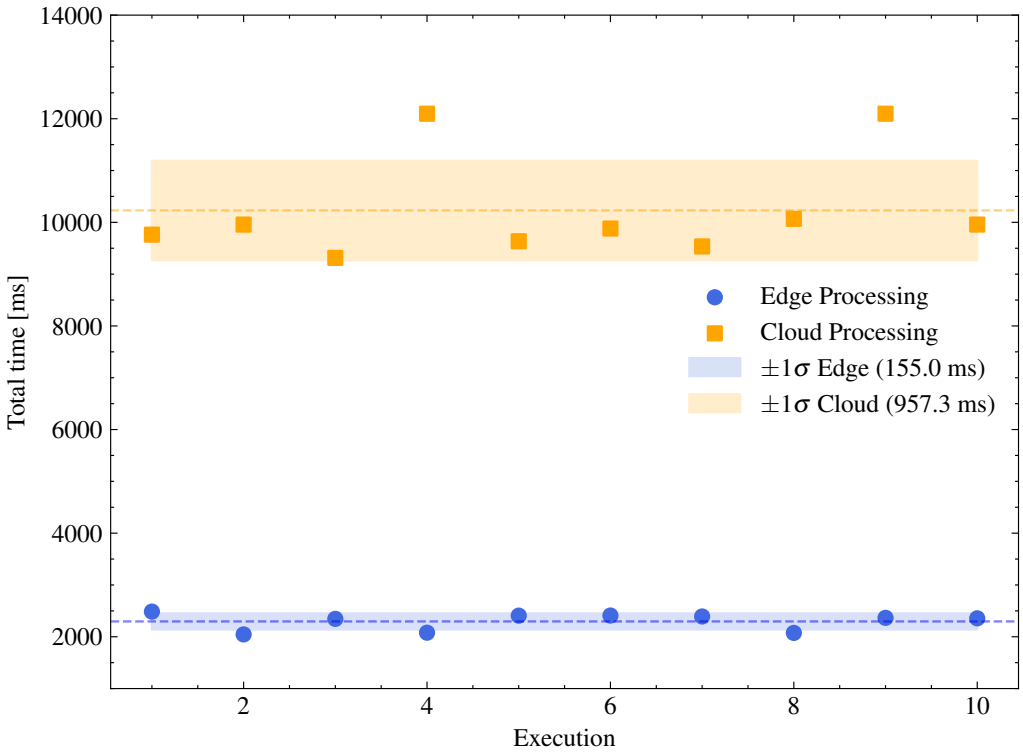

approaches. The diagram in Figure 24 shows the variation in total runtime per sample for both methods. The standard deviation of the runtime for the edge processing approach is approximately 152 ms, while for the cloud processing approach it increases to approximately 973 ms. This data indicates that cloud processing presents almost six times greater variability, making it less predictable and, consequently, less reliable for applications where response time consistency is essential.

Furthermore, analyzing the maximum error values relative to the mean, presented in Table 9, confirms the greater runtime variation for the cloud approach, especially since the sensor needs to send the collected raw data.

Comparing this maximum error with the values in Table 10, which only shows the time spent sending data to the cloud, we conclude that over 90 % of the total variation in execution time (from sensor initialization to data transmission) is related to transmission time. This variation is strongly influenced by the quality of the Wi-Fi connection and the resending of lost packets. The larger the volume of transmitted data, the greater the probability of packet loss and retransmission attempts, resulting in a longer total execution time in the cloud processing approach.

The average execution time of data transmission to the cloud was also analyzed as a function of the packet size, measured in kilobytes, as illustrated in Figure 25. To carry out this study, the size of the transmitted data packet was varied, starting with 64 acceleration points per axis (totaling 2187 kB) and progressively doubling the number

Figure 25 – Time to transmit data versus sample packet size.

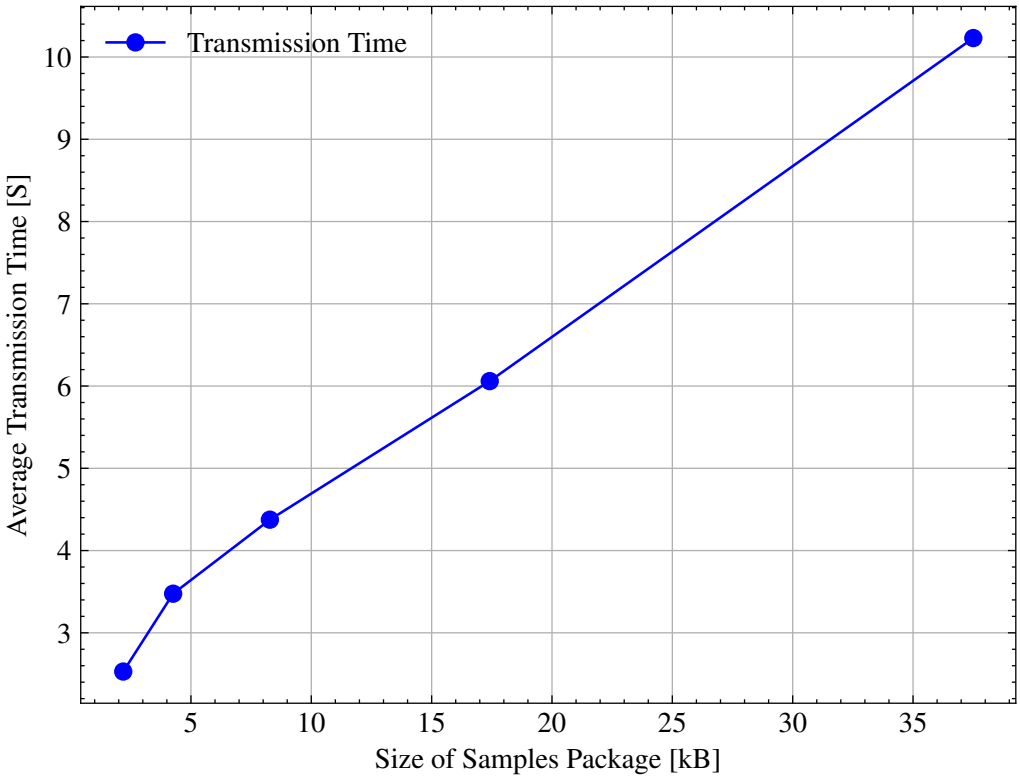

of points until reaching 1024 points per axis (37,504 kB). The fitting equation for this relationship is expressed by Equation 4.1, where E_t represents the execution time and B corresponds to the packet size in kilobytes (kB).

$$E_t = -0.724 \cdot B^2 + 239 \cdot B + 2271 \tag{4.1}$$

This analysis helps us understand the impact that increasing or decreasing the size of data packets has on transmission time, a crucial factor for efficiently scaling IoT systems with energy constraints and response time requirements. For example, doubling the packet size to 75 kB results in approximately 16 seconds of time just to transmit data to the cloud. This is a high value for battery-powered sensors, which have limited available power.

4.2 POWER CONSUMPTION

We measured the power consumption of the IoT sensor for each task in both scenarios: local processing (edge computing) and cloud processing. The test was repeated 5 times (samples S1 to S5) to calculate the average consumption of each operation step for collecting, processing and transmitting data to the cloud. To perform this test, we powered the sensor with 3.7 V using a power bank and connected a 4.9 Ω resistor (resistance measured with the multimeter) in series with the supply source. We then used a differential amplifier with a gain of 50 to amplify the voltage difference across the resistor. This allowed us to accurately monitor the total current flowing through the circuit over time with a

Figure 26 – Testbench for the estimation of instantaneous power consumption.

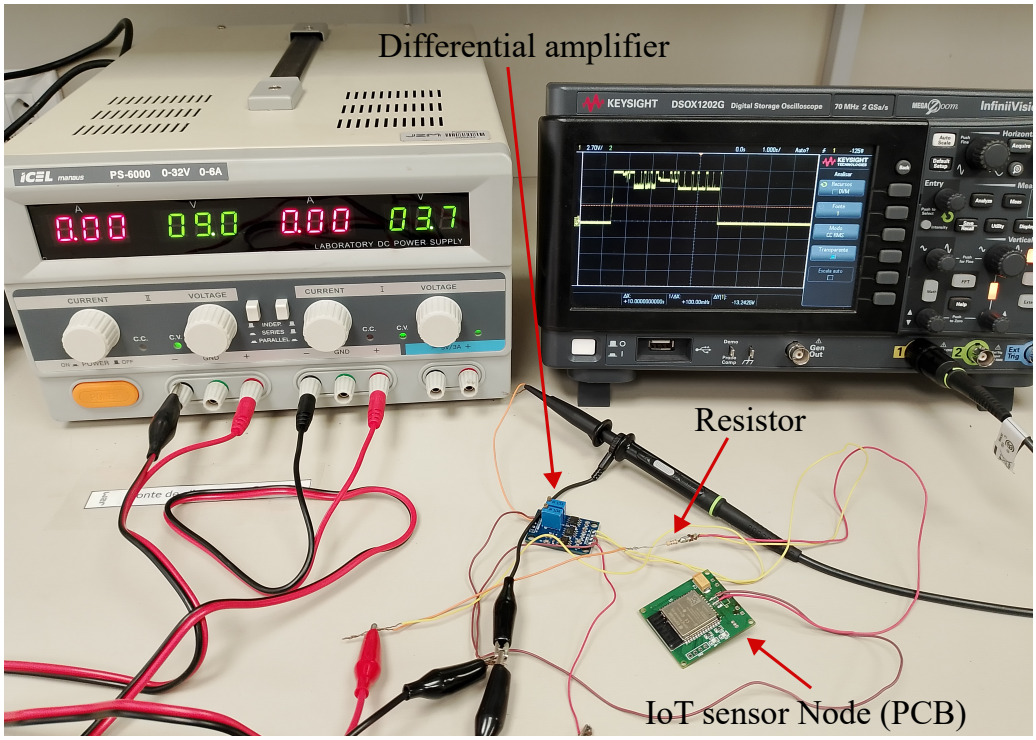

Figure 27 – Energy consumed at each operation step for edge and cloud processing approaches. Test was repeated 5 times (samples S1 to S5).

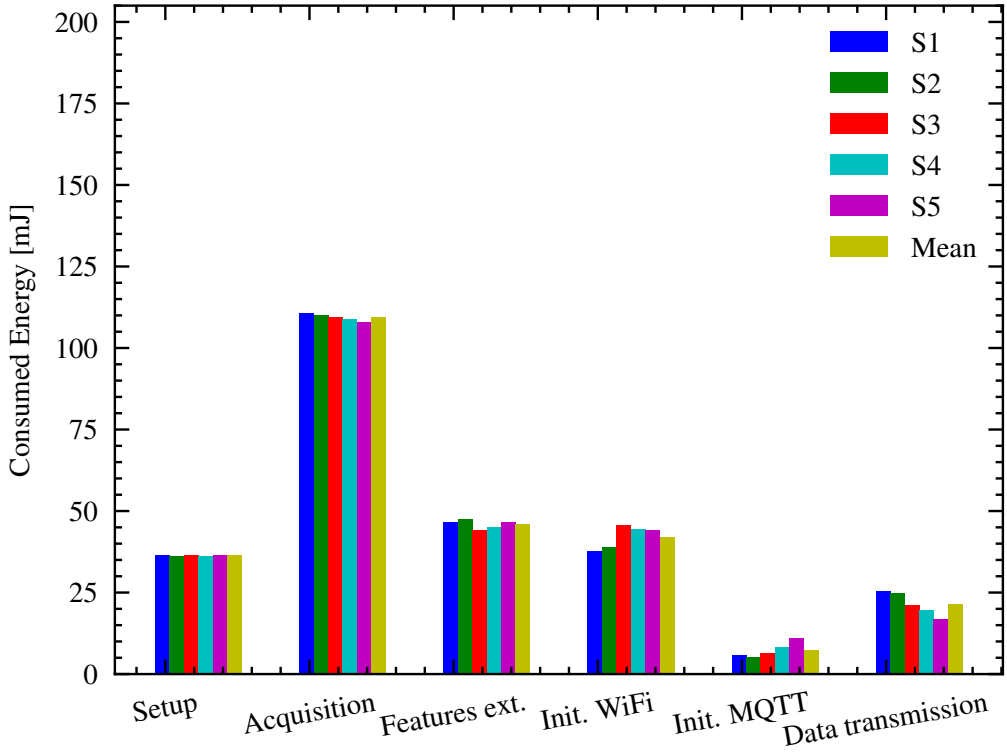

(a) Edge processing.

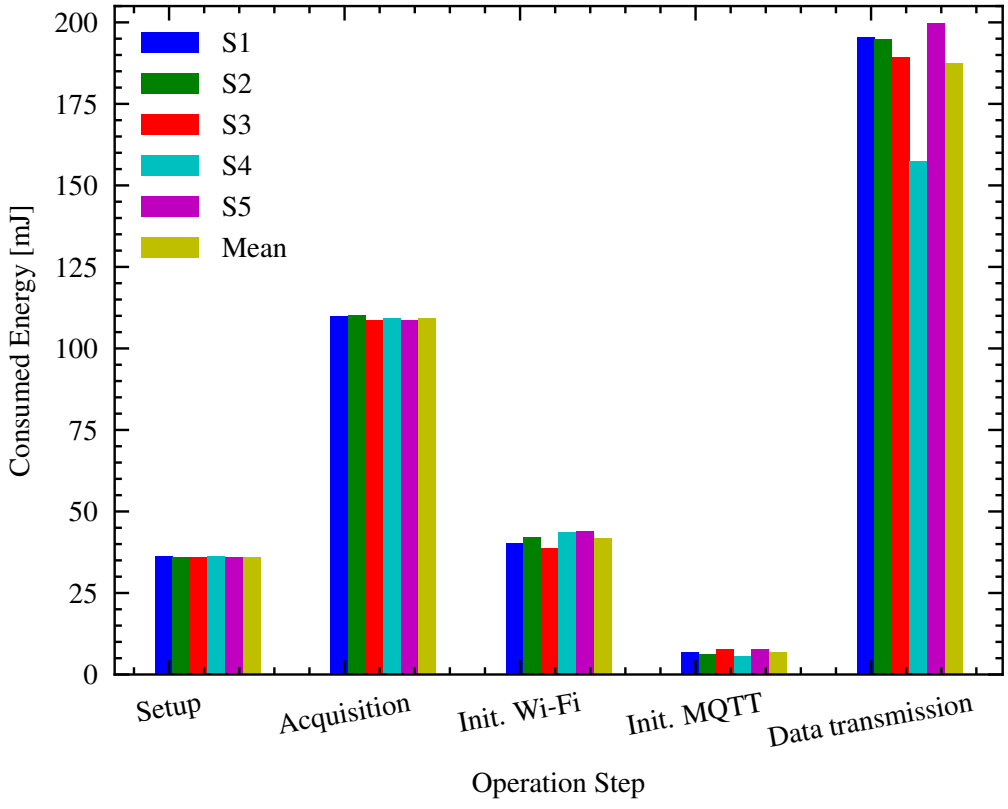

(b) Cloud processing.

Table 11 – Energy consumption statistics (mJ): mean, standard deviation and uncertainty of the mean for Edge and Cloud processing.

Method	**Total Average [mJ]**	**Standard Deviation [mJ]**
Edge Processing	262.29	0.0118
Cloud Processing	381.32	17.46

small IR drop. We connected the output of the differential amplifier to an oscilloscope and recorded several samples of the power consumption during the execution of each function.

The test setup for measuring power consumption is shown in Figure 26. We kept the same microcontroller configuration, data sampling rate, format, and packet size as used in the execution time test. The only exception was in the cloud processing approach, where we chose to transmit only 256 points per axis, which totals a data packet of 8.28 kB. This choice makes the test easier and minimize the influence of possible errors during data transmission to the cloud and additional time spent resending data.

After collecting the data, we used a Python script to process the acquired information. To calculate the energy consumed in each stage of operation and processing, we applied the trapezoidal numerical integration method. The graphs relating to the energy consumption in each phase of the process are shown in Figure 27.

Although edge processing includes an additional computational step involving data processing and feature extraction prior to transmission, the average peak power consumption throughout the process was 109.31 mJ, recorded during the data acquisition phase. In contrast, when sending the raw data directly to the cloud for further processing, the average peak power consumption reached 187 mJ, approximately double.

This increase is directly related to the much larger volume of data transmitted, which requires the microcontroller to remain connected to the Wi-Fi module for significantly longer periods, resulting in higher power consumption. Furthermore, the increased volume of data transmitted correlates with variation in execution time, which in turn impacts power consumption. As seen in the Table 11, the standard deviation of power consumption for cloud processing reaches 17.46 mJ, considering the five samples collected, demonstrating greater variability in power consumption compared to edge processing.

This trend is even more evident in Figures 28a and 28b, which demonstrate the worst-case scenario of the five measured samples. The total energy consumption in the edge processing approach is 34.2 % lower than in the cloud processing approach 262.31 mJ versus 398.78 mJ. Additionally, the results show a significant difference in transmission time between the two approaches (for this test, approximately 1.6 seconds). The Figure 28 also roughly separates each stage from initialization to data transmission. To make this separation, we analyzed the power consumption graph for each stage to understand how each sensor execution stage contributes to power consumption and what the graphical representation of this consumption is.

Figure 28 – Instantaneous power consumption and total energy for executing a task for edge and cloud processing approaches.

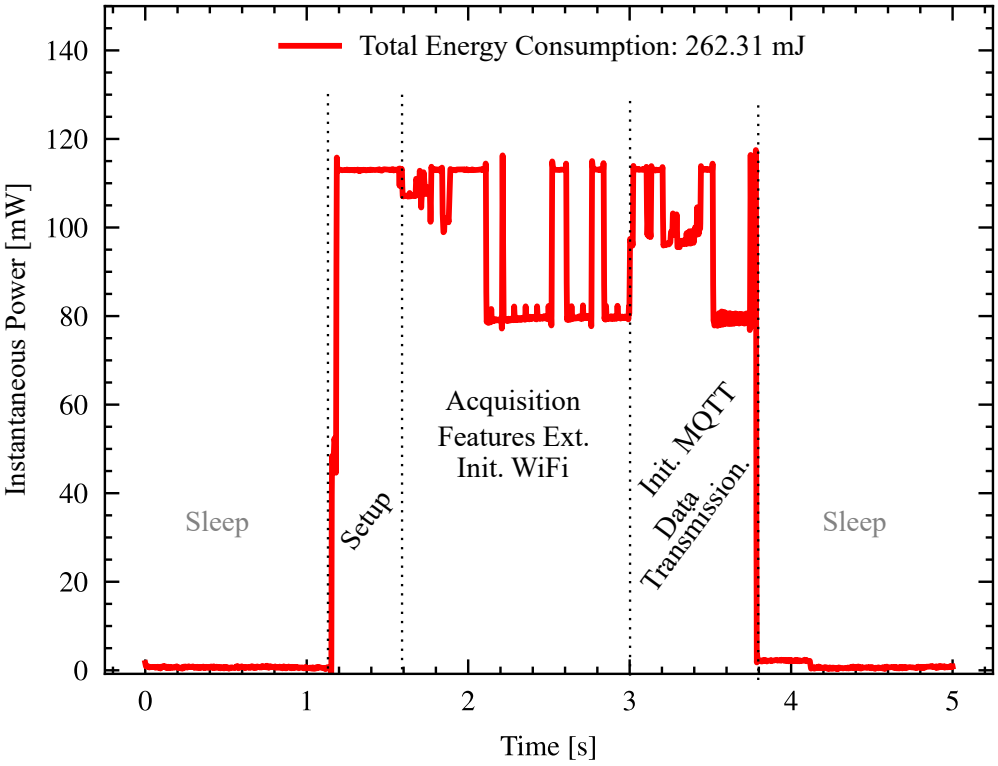

(a) Edge processing.

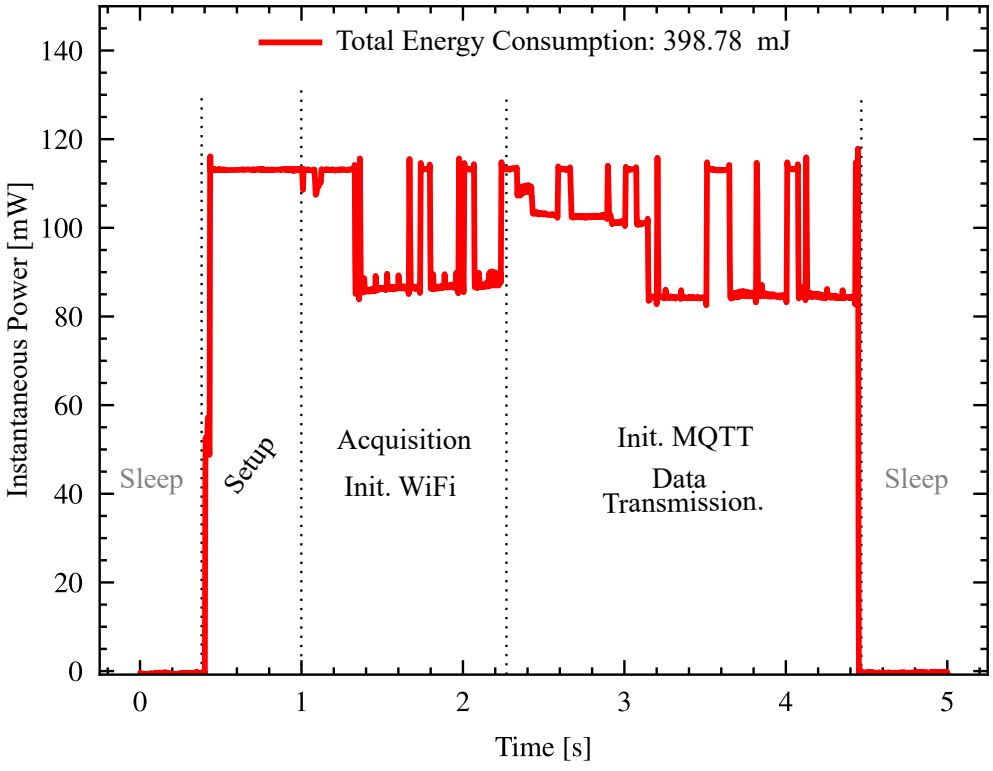

(b) Cloud processing.

When analyzing the relationship between additional execution time and energy consumption, we observe that for each additional second in total processing and transmission time, approximately 85 mJ more energy is consumed. This reinforces the direct impact of the duration of the active connection with the Wi-Fi module on the energy efficiency of the sensor. The reduction in energy consumption obtained by local processing of data (at the edge) is, therefore, very important for battery-powered sensors. This energy saving has a direct impact on the life cycle of the device.

Based on the worst-case power consumption scenarios presented in Figure 28, and considering the Minamoto 18505 battery with a nominal capacity of 4000 mAh and voltage of 3.6 V, we estimated the sensor's lifespan in days for both approaches (cloud and edge processing), using Equations 4.2 and 4.3.

$$B_{\text{cap.}} = \frac{I_N \times V_N \times 3600}{E} \quad [\text{cycles}] \tag{4.2}$$

$$T_{\text{bat}} = \frac{B_{\text{cap.}}}{C_{\text{dia}}} \quad [\text{days}] \tag{4.3}$$

In Equation 4.2, the battery capacity in number of cycles ($B_{\text{cap.}}$) is calculated using the nominal current (I_N, in mAh) and voltage (V_N, in volts). This value is divided by the energy (E, in mWs) consumed per cycle and multiplied by 3600 to ensure proper unit conversion. With the total number of supported cycles estimated, Equation 4.3 is then used to compute the battery lifespan (T_{bat}) in days. This estimation assumes continuous operation, disregards sleep mode consumption, and considers one measurement (or cycle) every 5 minutes.

To estimate the sensor's battery life using the cloud processing approach, we considered the energy consumption shown in Figure 28, which is 398.78 mJ. To this, we added six times 85 mJ to account for the longer transmission time. This adjustment was necessary because the initial consumption test considered only the transmission of 256 acceleration samples per axis (equivalent to 4 seconds of operation). However, according to Table 9, transmitting 1024 samples per axis requires a total execution time of 10.23 seconds.

If each additional second of transmission consumes approximately 85 mJ, the total estimated energy consumption per operation cycle for the cloud approach is 908.7 mJ. By substituting this value into Equation 4.2, the estimated battery life is approximately 198 days.

In contrast, for the edge processing approach, the total energy consumption per cycle was measured at 262.31 mJ. This value already accounts for the acquisition, local processing, and transmission of only the extracted features. Using the same equation, this results in an estimated battery life of approximately 686 days about 3.6 times longer than the cloud approach, where the full raw acceleration data must be transmitted.

4.3 ACCURACY OF EDGE PROCESSING AND SENSOR EVALUATION

To validate the accuracy of the developed sensor, two experimental tests were carried out, one comparing the accuracy of data processing in the cloud and at the edge and a second test comparing the developed sensor with two commercial systems.

The first compared the processed data and parameters extracted locally at the edge (on the IoT sensor itself) with those obtained through cloud processing (on a computer). To enable this analysis, the sensor firmware was adapted to perform the entire acquisition, processing, and feature extraction routine, in addition to transmitting the 2,048 raw acceleration points per axis and the 1,024 FFT points calculated for each axis. To receive and store the data, a Python program was developed as an MQTT client, responsible for listening to topics published by the sensor and recording the data in .csv files, organized by type (raw data, FFT, features extracted) and source (edge or cloud). The test was repeated for ten complete cycles, totaling ten distinct samples used to evaluate the consistency and accuracy of the values obtained in each approach. To perform the tests, we installed the developed IoT sensor on a single-phase bench motor, as shown in Figure 29.

The comparative analysis between edge and cloud data processing focused on four key vibration parameters in the X, Y, and Z axes: RMS acceleration (Ac_{rms}), peak acceleration (Ac_{pk}), RMS velocity (V_{rms}), and peak velocity (V_{pk}). In addition, a comparison was also made between the frequencies spectrum (FFTs) calculated locally at the sensor and remotely in the cloud. The results obtained demonstrated excellent agreement between the values processed in both environments, evidencing the reliability and accuracy of the embedded algorithms implemented in the device.

Figure 29 – Test setup with bench electric motor.

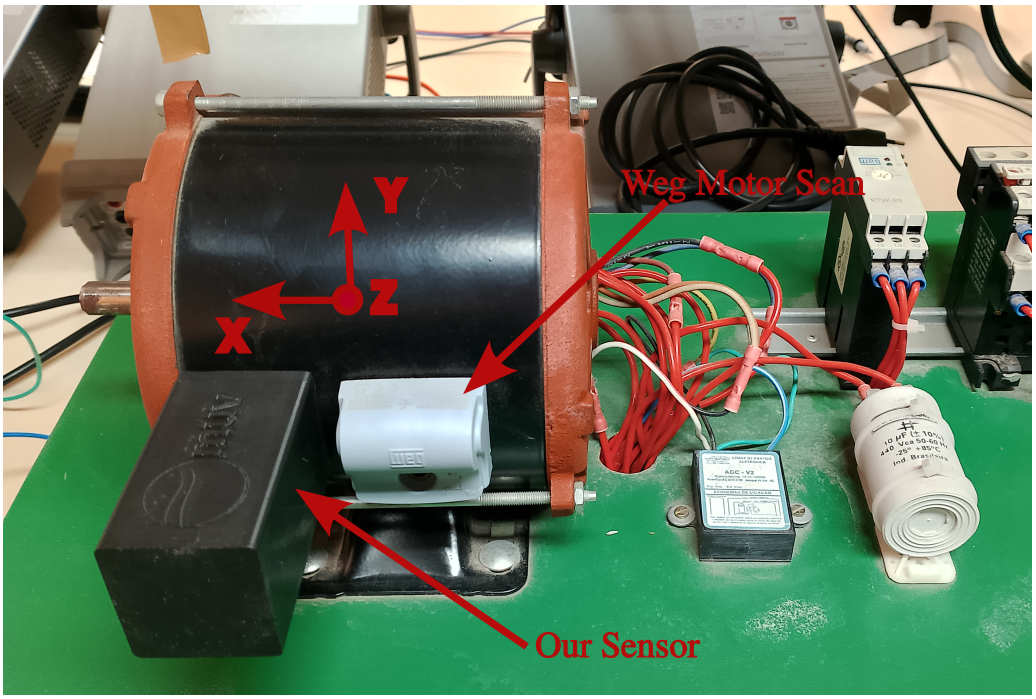

Table 12 – Comparative analysis of RMS vibration acceleration (Ac_{pk}) edge and cloud processing.

$Ac_{\mathbf{rms},X}$			$Ac_{\mathbf{rms},Y}$			$Ac_{\mathbf{rms},Z}$		
Cloud [mm/s²]	Edge [mm/s²]	**Error [%]**	Cloud [mm/s²]	Edge [mm/s²]	**Error [%]**	Cloud [mm/s²]	Edge [mm/s²]	**Error [%]**
0.7832	0.7830	**0.0261**	0.7276	0.7274	**0.0226**	1.4088	1.4084	**0.0272**
0.8465	0.8463	**0.0278**	0.5756	0.5754	**0.0273**	1.3930	1.3927	**0.0205**
0.9326	0.9324	**0.0246**	0.7614	0.7612	**0.0245**	1.9138	1.9131	**0.0373**
0.8921	0.8919	**0.0200**	0.6445	0.6444	**0.0155**	1.7511	1.7505	**0.0355**
1.0865	1.0862	**0.0227**	0.6572	0.6570	**0.0223**	1.6951	1.6948	**0.0183**
0.7425	0.7423	**0.0260**	0.6344	0.6342	**0.0235**	1.4217	1.4215	**0.0136**
0.6861	0.6859	**0.0240**	0.6742	0.6740	**0.0287**	1.3349	1.3347	**0.0155**
0.8069	0.8067	**0.0250**	0.7413	0.7411	**0.0211**	1.4176	1.4171	**0.0317**
0.7273	0.7272	**0.0182**	0.5597	0.5595	**0.0308**	1.5458	1.5454	**0.0245**
1.0148	1.0156	**0.0784**	0.5000	0.4999	**0.0134**	1.3567	1.3563	**0.0291**
Average error		**0.0248**	**Average error**		**0.0230**	**Average error**		**0.0258**

The results for Ac_{rms} are presented in Table 12. It can be seen that the RMS acceleration values obtained for both edge and cloud processing approaches are extremely close. The mean absolute error between the two methods was low, with values of only 0.0248 % on the X-axis, 0.0230 % on the Y-axis, and 0.0258 % on the Z-axis. These minimal differences demonstrate that embedded edge processing, including steps such as signal conditioning, filtering, and RMS calculation, performs equivalently to offline cloud processing.

Similarly, the results for Ac_{pk}, presented in Table 13, demonstrate excellent agreement between the values obtained at the edge and in the cloud. The mean absolute errors remained low: 0.0130 % on the X-axis, 0.0369 % on the Y-axis, and 0.0291 % on the Z-axis. Although slightly higher than the errors observed for RMS acceleration, these

Table 13 – Comparative analysis of peak acceleration (Ac_{pk}) edge and cloud processing.

$Ac_{\mathbf{pk},X}$			$Ac_{\mathbf{pk},Y}$			$Ac_{\mathbf{pk},Z}$		
Cloud [mm/s²]	Edge [mm/s²]	**Error [%]**	Cloud [mm/s²]	Edge [mm/s²]	**Error [%]**	Cloud [mm/s²]	Edge [mm/s²]	**Error [%]**
3.4512	3.4511	**0.0036**	3.1422	3.1403	**0.0591**	5.6562	5.6484	**0.1392**
3.9569	3.9565	**0.0110**	2.9727	2.9739	**0.0405**	5.7044	5.7066	**0.0385**
5.1275	5.1250	**0.0482**	4.8049	4.8034	**0.0298**	11.5179	11.5122	**0.0492**
3.7789	3.7798	**0.0243**	3.3411	3.3419	**0.0214**	7.3561	7.3565	**0.0056**
6.1637	6.1642	**0.0085**	3.6241	3.6244	**0.0092**	11.0311	11.0286	**0.0228**
2.8464	2.8455	**0.0333**	2.6756	2.6751	**0.0169**	5.8302	5.8318	**0.0261**
3.0783	3.0780	**0.0092**	2.7210	2.7199	**0.0415**	6.1697	6.1700	**0.0044**
3.6301	3.6301	**0.0010**	3.3175	3.3190	**0.0459**	8.4475	8.4448	**0.0320**
3.0628	3.0633	**0.0152**	2.2169	2.2162	**0.0332**	6.9053	6.9041	**0.0174**
5.3324	5.3768	**0.8316**	2.2608	2.2598	**0.0428**	5.4754	5.4776	**0.0410**
Average error		**0.0131**	**Average error**		**0.0369**	**Average error**		**0.0291**

Table 14 – Comparative analysis of RMS vibration velocity (V_{rms}) edge and cloud processing.

$V_{\mathbf{rms},X}$			$V_{\mathbf{rms},Y}$			$V_{\mathbf{rms},Z}$		
Cloud [mm/s]	Edge [mm/s]	**Error [%]**	Cloud [mm/s]	Edge [mm/s]	**Error [%]**	Cloud [mm/s]	Edge [mm/s]	**Error [%]**
1.4384	1.4637	**1.7619**	1.9919	2.0309	**1.9547**	1.6913	1.7190	**1.6380**
1.9122	1.9471	**1.8287**	0.9961	1.0159	**1.9894**	1.7409	1.7715	**1.7575**
1.7514	1.7829	**1.7987**	1.5444	1.5732	**1.8665**	1.9870	2.0284	**2.0848**
1.7547	1.7881	**1.9062**	1.4598	1.4899	**2.0578**	1.9338	1.9702	**1.8823**
3.0887	3.1469	**1.8854**	1.5463	1.5752	**1.8721**	2.1247	2.1653	**1.9076**
1.5975	1.6283	**1.9269**	1.8635	1.8982	**1.8608**	1.9527	1.9931	**2.0674**
1.6444	1.6734	**1.7636**	2.0237	2.0613	**1.8552**	2.1457	2.1831	**1.7407**
2.2002	2.2415	**1.8762**	1.5857	1.6138	**1.7720**	2.1737	2.2121	**1.7665**
1.6809	1.7117	**1.8304**	1.7395	1.7719	**1.8644**	2.6527	2.6986	**1.7306**
3.4912	3.5601	**1.9728**	1.5386	1.5684	**1.9354**	2.5844	2.6286	**1.7119**
Average error		**1.8533**	**Average error**		**1.8693**	**Average error**		**1.7620**

values are still extremely low, indicating high accuracy in the embedded calculation. The only noteworthy occurrence is the occurrence of an outlier on the X-axis, which exceeded 0.8 %, possibly due to a specific fluctuation in the signal.

The V_{rms} analysis also produced consistent results, with average errors of 1.85 %, 1.87 %, and 1.76 % for the X, Y, and Z axes, respectively; the data can be seen in Table 14 . Given that velocity is found by integrating the acceleration signal, these slightly larger discrepancies are expected due to the greater sensitivity to low-frequency noise and drift. However, the results corroborate the accuracy of the edge-processed data.

For the (V_{pk}) values, the average errors were higher: 7.04 %, 4.79 %, and 7.54 % for the X, Y, and Z axes, respectively, as shown in Table 15. These deviations may be related to inaccuracies in the peak value detection function, as well as to rounding effects

Table 15 – Comparative analysis of peak vibration velocity (V_{pk}) edge and cloud processing.

$V_{\mathbf{pk},X}$			$V_{\mathbf{pk},Y}$			$V_{\mathbf{pk},Z}$		
PC [mm/s]	Node [mm/s]	**Error [%]**	PC [mm/s]	Node [mm/s]	**Error [%]**	PC [mm/s]	Node [mm/s]	**Error [%]**
5.8546	5.2421	**10.4625**	6.5211	6.4429	**1.1981**	5.9822	6.4109	**7.1662**
7.1307	7.3558	**3.1571**	3.4826	3.2933	**5.4350**	6.5783	6.7914	**3.2409**
6.5513	6.1181	**6.6136**	5.6830	5.1555	**9.2814**	9.6188	10.5369	**9.5447**
6.6824	6.0367	**9.6621**	4.3917	4.5186	**2.8896**	8.3558	7.7665	**7.0519**
9.7210	10.3585	**6.5575**	5.0181	4.7131	**6.0769**	9.5729	8.1093	**15.2892**
5.9954	5.2650	**12.1829**	5.9796	6.1328	**2.5630**	7.8562	7.2337	**7.9234**
6.4060	6.1882	**3.4004**	6.4548	7.0753	**9.6141**	7.5217	9.2597	**23.1073**
7.4967	8.0568	**7.4721**	5.4239	5.6485	**4.1406**	9.2285	7.2228	**21.7337**
5.5540	5.7303	**3.1743**	5.4842	6.1012	**11.2519**	9.6771	9.9014	**2.3181**
11.1288	13.0186	**16.9810**	4.8932	4.7580	**2.7628**	9.0663	9.5886	**5.7608**
Average error		**7.0428**	**Average error**		**4.7878**	**Average error**		**7.5448**

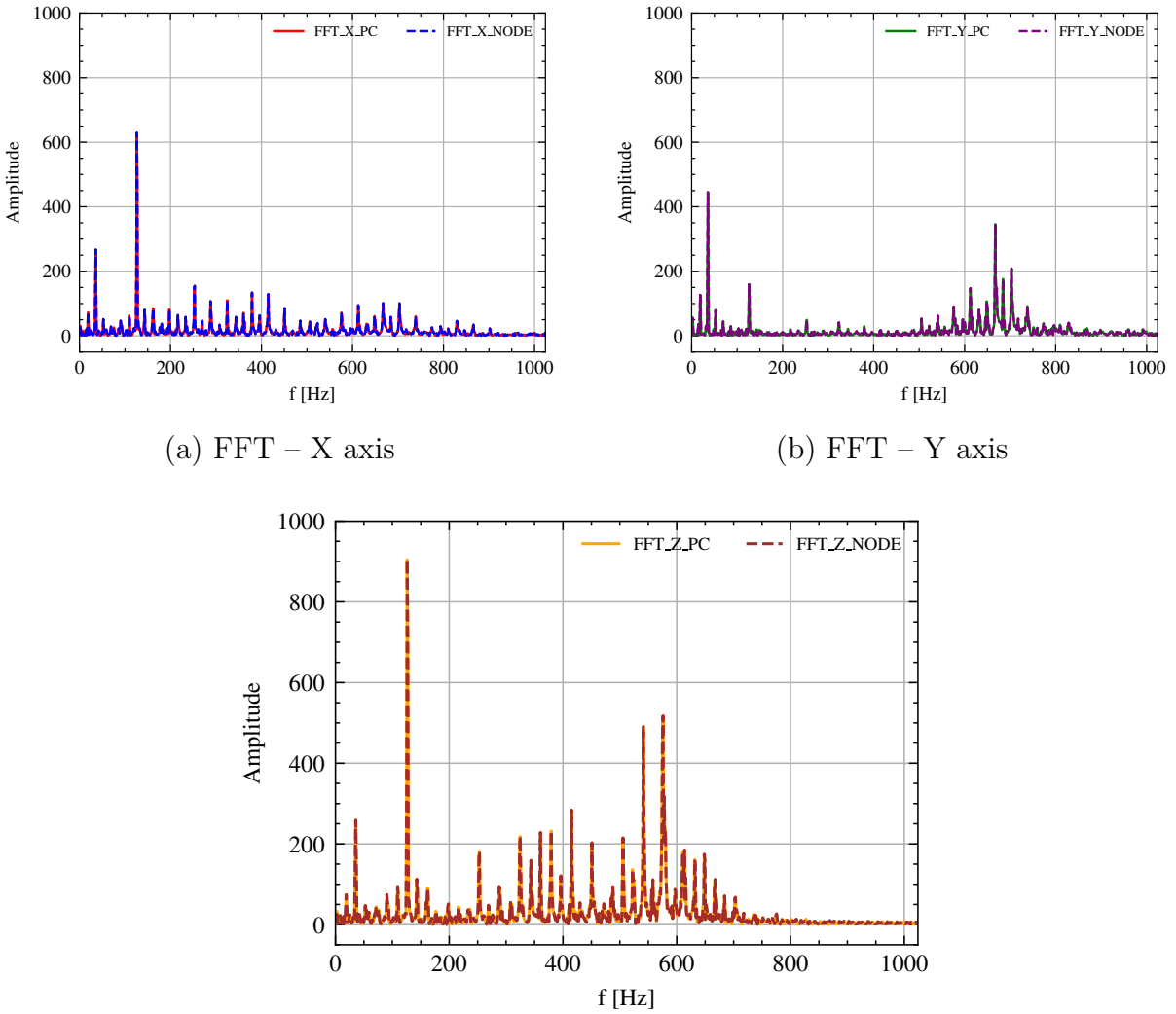

(a) FFT – X axis

(b) FFT – Y axis

(c) FFT – Z axis

Figure 30 – Fast Fourier Transforms (FFT) of acceleration signals along the X, Y, and Z axes, comparing data processed on the cloud and on the edge.

during embedded processing. Although some samples presented a maximum error greater than 20 %, the average error remained below 10 %, which can be considered acceptable considering the computational limitations inherent to embedded systems.

After comparing the processing and feature extraction performed at the edge and in the cloud, the frequency spectrum was also analyzed using the FFTs calculated for each axis. To this end, we plotted the FFTs generated at the sensor (edge) alongside those calculated on the computer (cloud) to verify compatibility. Figure 30 shows the FFTs corresponding to the X, Y, and Z axes. Analyzing the graphs, it can be observed that the frequency spectra obtained with both methods are perfectly compatible, both in terms of frequency and amplitude, confirming the accuracy of the fast Fourier transform algorithm implemented in the embedded sensor.

In summary, the results of the comparison between acceleration data processing for vibration feature extraction indicate that the hardware limitations of the implemented

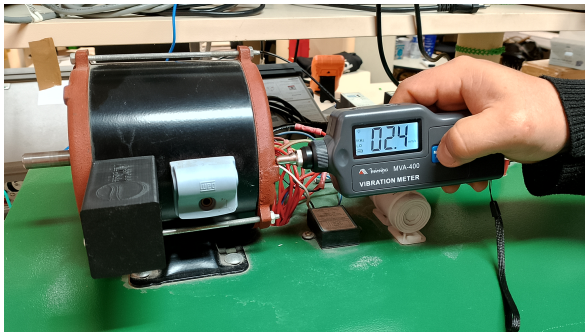

(a) Axial – Trial 1

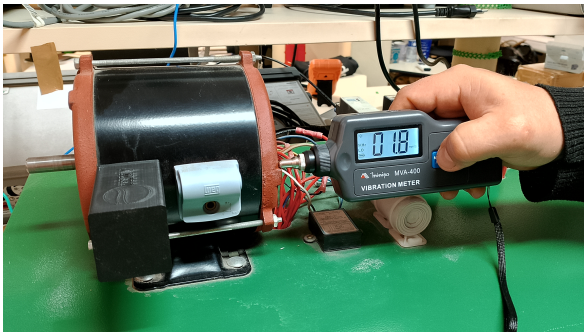

(b) Axial – Trial 2

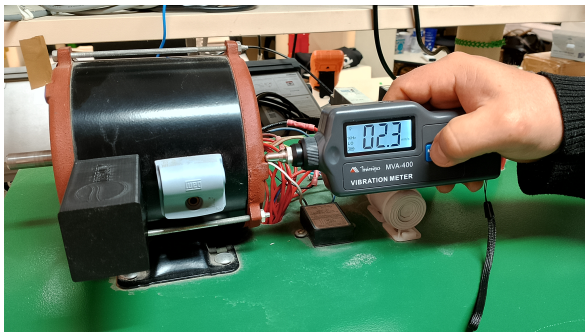

(c) Axial – Trial 3

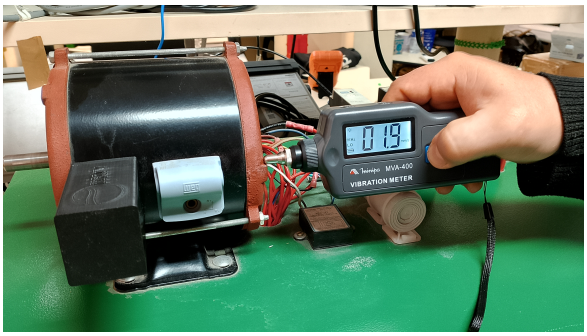

(d) Axial – Trial 4

Figure 31 – RMS Axial vibration measured with Minipa MVA-400 meter.

sensor do not compromise the accuracy of the results when compared to computer-based processing. Thus, the results of the first test demonstrate that the signal processing routines incorporated into the IoT sensor are reliable, producing results consistent with those obtained through cloud-based analysis. The low error rates observed across all metrics analyzed reinforce the feasibility of real-time feature extraction directly at the edge, which is essential for IoT applications that require low power consumption.

In the second test, we compared the developed sensor with two commercial vibration meters: the Minipa MVA-400 and WEG's IoT sensor, the WEG Motor Scan. The Minipa MVA-400 is a portable vibration meter based on a ceramic piezoelectric accelerometer, capable of measuring in the 10 Hz to 1 kHz range (low-frequency "LO" mode) and a declared error of $\pm 5\ \% + 2$ digits (Minipa do Brasil Ltda., 2021). Measurements were taken on the axial and radial axes of the motor, with axial vibration corresponding to the X-axis of the developed sensor and radial vibration to the Z-axis.

The WEG Motor Scan is a smart sensor developed for continuous monitoring of electric motors in industrial environments. It is a device designed for continuous operation under harsh conditions, which integrates triaxial vibration sensors and a temperature sensor. Its main technical features include: a triaxial MEMS vibration sensor with a measuring range of up to ± 16 g and a typical frequency response of up to 1 kHz (WEG Equipamentos Elétricos S.A., 2020).

The developed IoT sensor was installed alongside the WEG Motor Scan on the

(a) Radial – Trial 1

(b) Radial – Trial 2

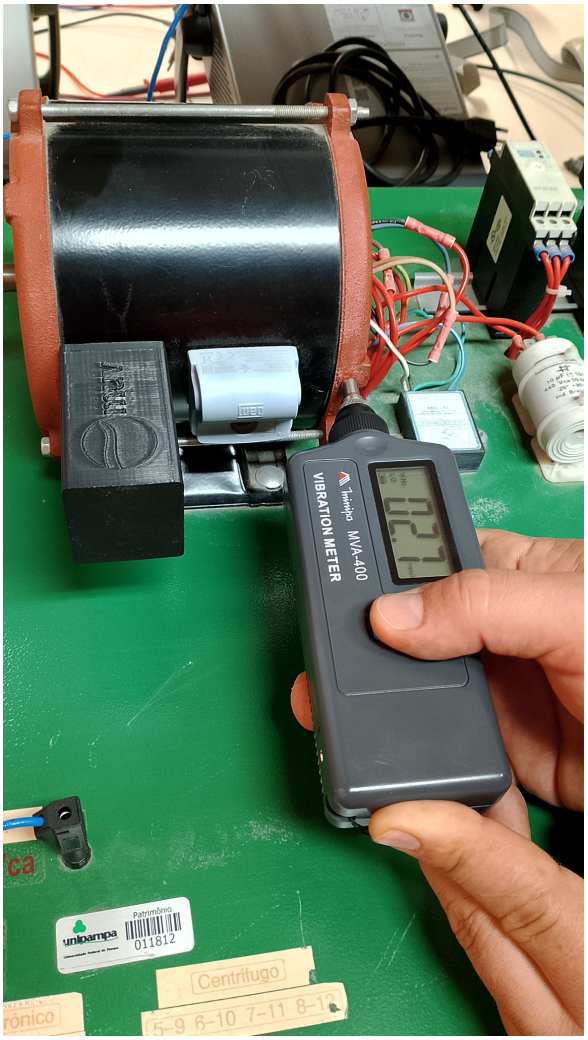

(c) Radial – Trial 3

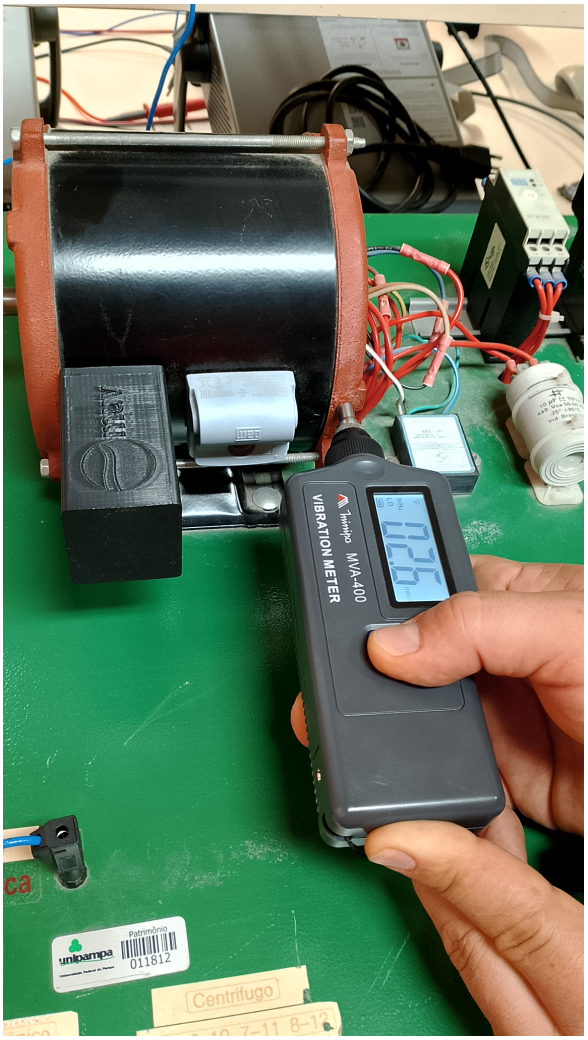

(d) Radial – Trial 4

Figure 32 – RMS Radial vibration measured with Minipa MVA-400 meter.

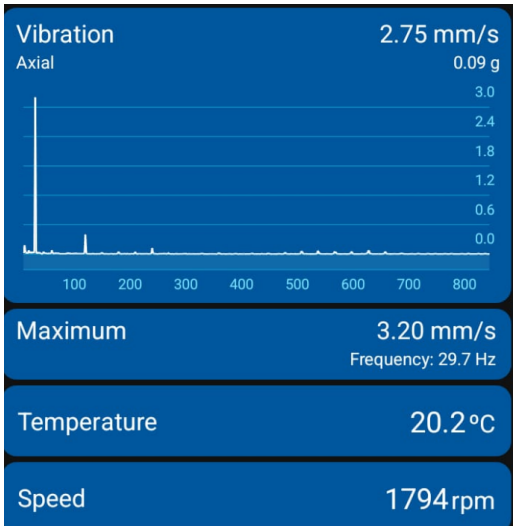

(a) Axial - Trial 1

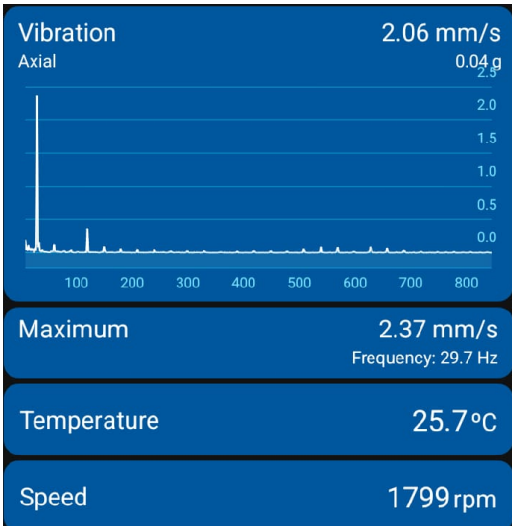

(b) Axial - Trial 2

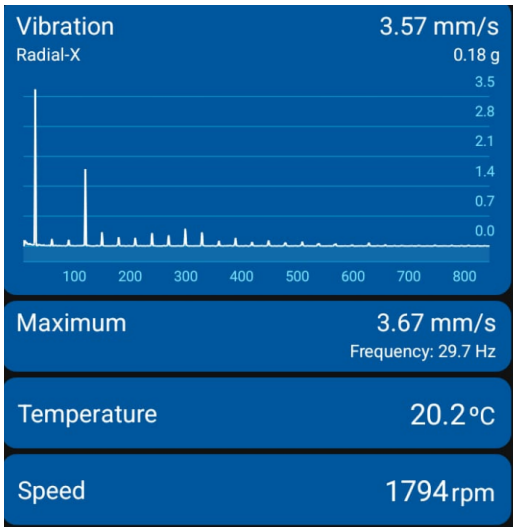

(c) Radial X - Trial 1

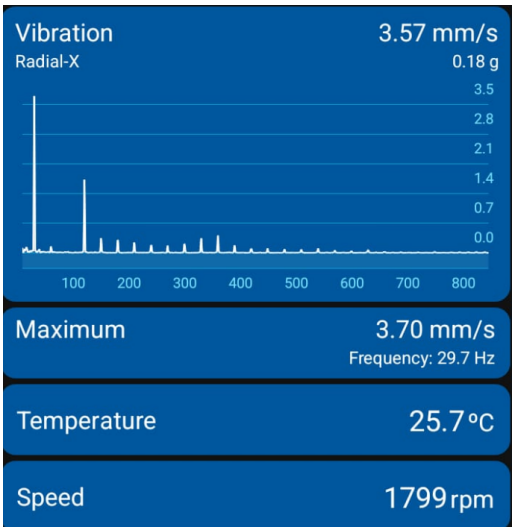

(d) Radial X - Trial 2

(e) Radial Y - Trial 1

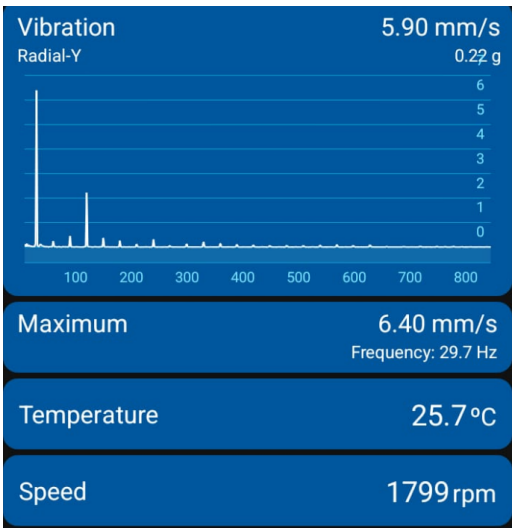

(f) Radial Y - Trial 2

Figure 33 – RMS vibration measured with WEG Motor Scan sensor.

same bench electric motor, operating under the same conditions. This configuration allowed for direct comparison of the vibration values obtained by both devices. The test setup is illustrated in Figure 29.

Using the MVA-400 meter, four measurements of axial and radial vibration were collected. The results are presented in Figures 31 and 32. The average axial vibration (X-axis of the implemented sensor) measured by the Minipa device was 2.1 mm/s, while the average radial vibration (Z-axis) was 2.50 mm/s. In comparison, the developed IoT sensor recorded average values of 2.09 mm/s on the X-axis and 2.14 mm/s on the Z-axis, as shown in Table 14.

To further assess performance, the sensor was also compared to the WEG Motor Scan a commercial solution widely used for continuous monitoring of electric motors in industrial environments. Two RMS vibration measurements were collected for each axis, as illustrated in Figure 33. The WEG device's axial, radial X, and radial Y measurements correspond to the X, Z, and Y axes of the developed sensor, respectively. It reported average values of 2.41 mm/s (axial), 3.57 mm/s (radial X), and 5.77 mm/s (radial Y).

Compared to the developed sensor's measurements 2.09 mm/s (X), 2.14 mm/s (Z), and 1.90 mm/s (Y), the discrepancies were most significant on the radial axes, with deviations exceeding 60 %.

These differences can be attributed to three factors. First, the WEG Motor Scan likely applies proprietary filtering and a broader data window to compute a global RMS value, though these processing details are not publicly disclosed. Second, the measurements were not collected simultaneously, allowing for natural fluctuations in motor vibration. Third, the WEG sensor supports acceleration ranges up to 16 g, while the developed sensor is limited to 2 g making it more sensitive to low-amplitude vibrations but also more susceptible to noise in high-vibration environments.

Overall, the developed sensor showed excellent agreement with the Minipa MVA-400, particularly in the axial direction, with a difference of less than 1 %. Although larger deviations were observed when compared to the WEG device, they are reasonable given the methodological, technological, and contextual differences. Despite this, the sensor effectively tracked real vibration patterns and proves to be a technically viable solution for electric motor monitoring—especially in scenarios where cost-effectiveness and integration flexibility are critical.

4.4 CONCLUSION

In this chapter, we presented the tests carried out to evaluate the implemented sensor in terms of runtime, power consumption, and vibration data accuracy. Three experiments were conducted to this end.

The first experiment assessed the impact of performing data processing on the sensor itself and the influence of data packet size on the runtime required for each step, from

processing to cloud transmission. The second experiment compared the power consumption of two approaches: local processing on the sensor versus direct transmission of raw data to the cloud. The third experiment evaluated the accuracy of feature extraction performed at the edge and in the cloud, and compared the results of the implemented system with those of two commercial solutions.

The results indicate that power consumption is directly proportional to the sensor's operating time, especially when the Wi-Fi module is active—either attempting or executing data transmission. Larger data packets lead to higher energy consumption. Although edge processing adds an additional computation step, this approach significantly reduces overall power consumption compared to transmitting raw data.

With regard to data processing accuracy, the results showed minimal differences between edge and cloud processing, with the worst-case average error remaining below 10%. When compared to commercial devices, the implemented system presented vibration measurements of similar magnitude, confirming its suitability for machine vibration monitoring.

5 FINAL CONCLUSION

This study presents the main causes of failures in rotating electrical machines, such as induction motors, and reviews the main techniques presented in the literature for measuring and analyzing vibrations in rotating machines.

This literature review revealed several sensors for monitoring vibrations in machines, as well as several vibration analysis techniques for detecting failures in their early stages, each with its own advantages and disadvantages. Among the methods and techniques for monitoring and analyzing vibrations, IoT sensors, MEMS accelerometers, and edge processing have gained considerable prominence in recent years due to their cost-effectiveness.

A MEMS accelerometer was selected for the development of a vibration monitoring sensor. The implementation of a battery-powered IoT sensor node mounted on a magnet for monitoring vibration in electric motors was detailed, as well as the evaluation of the trade-offs between sensor data processing, edge computing, and sending data directly to the cloud for further analysis and processing.

Tests demonstrated that the local data processing approach resulted in a significant reduction in transmission time. Edge computing reduced total processing time by 4.5 times and data packet size by 100 times compared to cloud processing.

When testing energy consumption, it was found that processing data in the sensor leads to a 34.2 % reduction, which is particularly important for battery-powered applications. Furthermore, it was found that for each additional second of processing and transmission, there is an increase in energy consumption of approximately 85 mJ, highlighting the impact of prolonged use of the microcontroller's Wi-Fi module in cloud-based approaches. These findings confirm that edge computing is more energy-efficient and also offers greater stability and predictability at runtime.

Overall, the implemented sensor performed as expected, and testing showed that the use of edge computing in IoT devices for industrial condition monitoring significantly improves performance, reduces energy consumption, and enables more scalable, sustainable, and autonomous monitoring solutions for predictive maintenance of electrical rotating machinery.

In addition to the energy and performance benefits, the local processing approach also proved accurate and reliable. The parameters extracted at the edge showed minimal deviation compared to those calculated via cloud processing, with average errors of less than 0.03 % for RMS and peak acceleration, and less than 2 % for RMS and peak velocity. These results demonstrate the feasibility of embedded signal processing algorithms for accurate vibration analysis, eliminating the need for raw data transmission.

Regarding autonomy, power consumption estimates indicated that the system operating with edge processing could achieve a battery life of approximately 686 days, while the cloud-based approach would limit battery life to approximately 198 days—a

reduction of more than 70 %. This confirms that edge processing not only improves energy efficiency but also significantly extends the lifespan of the sensor node, making it more suitable for remote or difficult-to-access industrial facilities.

Finally, when compared to commercial systems such as the Minipa MVA-400 vibration meter and the WEG Motor Scan sensor, the implemented device showed good agreement in the measurements obtained. The average values measured by the developed sensor differed by less than 5 % in the axial direction and presented larger deviations in the radial axes, especially when compared to WEG's global RMS measurements. These differences are likely due to the different internal signal processing methods and reference orientations used by commercial devices. Despite this, the implemented system was able to capture consistent vibration patterns and magnitudes, demonstrating its technical feasibility and competitiveness as a low-cost alternative for predictive maintenance applications.

5.1 FUTURE WORK

The topic of vibration analysis for predictive maintenance still has several open research opportunities, which leaves room for the continuation of this work, especially for the improvement of sensors to measure vibrations and detect machine failures for predictive maintenance. Some suggestions for future work are:

- Technology - Implement data compression algorithms and techniques to reduce the payload to be transmitted to the cloud;
- Tests - Analyze sensor performance on machines in different operating states, such as operating normally without faults, operating with imbalance and misalignment;
- Software - Implement AI analysis for classifying faults in rotating machinery.

BIBLIOGRAPHY

ABBOUD, D. et al. Envelope analysis of rotating machine vibrations in variable speed conditions: A comprehensive treatment. *Mechanical Systems and Signal Processing*, Elsevier, v. 84, p. 200–226, 2017. Citado na página 40.

AL-BADOUR, F.; SUNAR, M.; CHEDED, L. Vibration analysis of rotating machinery using time–frequency analysis and wavelet techniques. *Mechanical Systems and Signal Processing*, Elsevier, v. 25, n. 6, p. 2083–2101, 2011. Citado na página 42.

ALTHUBAITI, A.; ELASHA, F.; TEIXEIRA, J. A. Fault diagnosis and health management of bearings in rotating equipment based on vibration analysis – a review. *Journal of Vibroengineering*, EXTRICA, v. 24, p. 46–74, 2 2022. ISSN 13928716. Citado na página 20.

AMEZQUITA-SANCHEZ, J. P.; ADELI, H. Signal processing techniques for vibration-based health monitoring of smart structures. *Archives of Computational Methods in Engineering*, Springer, v. 23, p. 1–15, 2016. Citado na página 28.

AN, K. et al. Edge solution for real-time motor fault diagnosis based on efficient convolutional neural network. *IEEE Transactions on Instrumentation and Measurement*, IEEE, v. 72, p. 1–12, 2023. Citado na página 19.

BAL, M. Industrial applications of collaborative wireless sensor networks: A survey. In: IEEE. *2014 IEEE 23rd international symposium on industrial electronics (ISIE)*. [S.l.], 2014. p. 1463–1468. Citado na página 34.

BIN, G. et al. Early fault diagnosis of rotating machinery based on wavelet packets—empirical mode decomposition feature extraction and neural network. *Mechanical Systems and Signal Processing*, Elsevier, v. 27, p. 696–711, 2012. Citado na página 44.

BRANDT, A.; BRINCKER, R. Integrating time signals in frequency domain – comparison with time domain integration. *Measurement*, v. 58, p. 511–519, 2014. ISSN 0263-2241. Disponível em: <https://www.sciencedirect.com/science/article/pii/S0263224114003832>. Citado na página 63.

BRIGHAM, E. O.; MORROW, R. E. The fast fourier transform. *IEEE Spectrum*, v. 4, n. 12, p. 63–70, 1967. Citado na página 39.

BRUNO, R.; CONTI, M.; GREGORI, E. Mesh networks: commodity multihop ad hoc networks. *IEEE communications magazine*, IEEE, v. 43, n. 3, p. 123–131, 2005. Citado na página 35.

CARVALHO, D. F. de; MIERS, C. C. Process automation and monitoring systems based on iiot using private lorawan networks: A case study of arcelormittal vega facilities. In: *IoTBDS*. [S.l.: s.n.], 2023. p. 243–254. Citado na página 36.

CHANG, K.-H. Bluetooth: a viable solution for iot?[industry perspectives]. *IEEE Wireless Communications*, IEEE, v. 21, n. 6, p. 6–7, 2014. Citado na página 34.

CHEIKH, I. et al. Multi-layered energy efficiency in lora-wan networks: A tutorial. *IEEE Access*, IEEE, v. 10, p. 9198–9231, 2022. Citado na página 34.

CHEN, B. et al. Igigram: An improved gini index-based envelope analysis for rolling bearing fault diagnosis. *Journal of Dynamics, Monitoring and Diagnostics*, p. 111–124, 2022. Citado na página 40.

CHENG, F. et al. Fault diagnosis of wind turbine gearboxes based on dfig stator current envelope analysis. *IEEE Transactions on Sustainable Energy*, IEEE, v. 10, n. 3, p. 1044–1053, 2018. Citado na página 40.

CHENG, Y. et al. Intelligent fault diagnosis of rotating machinery based on continuous wavelet transform-local binary convolutional neural network. *Knowledge-Based Systems*, Elsevier, v. 216, p. 106796, 2021. Citado na página 20.

CIPRIANI, G. et al. Automatic detection of thermal anomalies in induction motors. In: IEEE. *2021 IEEE International Conference on Environment and Electrical Engineering and 2021 IEEE Industrial and Commercial Power Systems Europe (EEEIC/I&CPS Europe)*. [S.l.], 2021. p. 1–6. Citado 2 vezes nas páginas 25 and 26.

CORREA, J. C. A. J.; GUZMAN, A. A. L. *Mechanical vibrations and condition monitoring*. [S.l.]: Academic Press, 2020. Citado 4 vezes nas páginas 28, 29, 30, and 31.

DEREVIANCKINE, G. H. et al. Opportunities and challenges of lora 2.4 ghz. *IEEE Communications Magazine*, p. 1–7, 2023. Citado na página 36.

DINEVA, A. et al. Fault diagnosis of rotating electrical machines using multi-label classification. *Applied Sciences*, Multidisciplinary Digital Publishing Institute, v. 9, n. 23, p. 5086, 2019. Citado na página 25.

DING, C. et al. Kernel ridge regression-based chirplet transform for non-stationary signal analysis and its application in machine fault detection under varying speed conditions. *Measurement*, Elsevier, v. 192, p. 110871, 2022. Citado na página 43.

DOWELL, M.; SYLVESTER, G. Turbomachinery prognostics and health management via eddy current sensing: current developments. In: *1999 IEEE Aerospace Conference. Proceedings (Cat. No.99TH8403)*. [S.l.: s.n.], 1999. v. 3, p. 1–9 vol.3. Citado na página 29.

DZHUDZHEV, B. et al. Vibration measurement with piezoelectric transducer. In: *XLVIII International Scientific Conference on Information, Communication and Energy Systems and Technologies ICEST 2013*. [S.l.: s.n.], 2013. Citado na página 31.

EasyEDA. *EasyEDA - Online PCB Design & Circuit Simulator*. 2025. Acesso em: 10 mar. 2025. Disponível em: <https://easyeda.com/>. Citado na página 55.

Electric Motor Engineering. *Electric motor in disassembled state: 3D illustration on a white*. 2025. Acesso em: 14 jun. 2025. Disponível em: <https://www.electricmotorengineering.com/electric-motors-and-their-impact-on-mechanics/electric-motor-in-disassembled-state-3d-illustration-on-a-white/>. Citado na página 26.

ERTÜRK, M. A. et al. A survey on lorawan architecture, protocol and technologies. *Future Internet*, MDPI, v. 11, n. 10, p. 216, 2019. Citado na página 35.

FELLAN, A. et al. Enabling communication technologies for automated unmanned vehicles in industry 4.0. In: IEEE. *2018 International Conference on Information and Communication Technology Convergence (ICTC)*. [S.l.], 2018. p. 171–176. Citado na página 35.

FREECAD. <https://www.freecad.org/>. Accessed: 2024-09-10. Citado na página 56.

FU, L. et al. Edgecog: a real-time bearing fault diagnosis system based on lightweight edge computing. *IEEE Transactions on Instrumentation and Measurement*, IEEE, 2023. Citado na página 19.

GAEID, K. S.; PING, H. W. Wavelet fault diagnosis and tolerant of induction motor: A review. *International Journal of the Physical Sciences*, v. 6, n. 3, p. 358–376, 2011. Citado na página 25.

GANGSAR, P.; TIWARI, R. Multiclass fault taxonomy in rolling bearings at interpolated and extrapolated speeds based on time domain vibration data by svm algorithms. *Journal of Failure Analysis and Prevention*, Springer, v. 14, p. 826–837, 2014. Citado na página 37.

GHAZALI, M. H. M.; RAHIMAN, W. Vibration analysis for machine monitoring and diagnosis: a systematic review. *Shock and Vibration*, Hindawi Limited, v. 2021, p. 1–25, 2021. Citado 9 vezes nas páginas 29, 30, 32, 33, 39, 41, 42, 43, and 44.

GOYAL, D.; PABLA, B. The vibration monitoring methods and signal processing techniques for structural health monitoring: a review. *Archives of Computational Methods in Engineering*, Springer, v. 23, p. 585–594, 2016. Citado 5 vezes nas páginas 29, 39, 40, 41, and 44.

Guru Manikandan, K. et al. Investigations on suitability of mems based accelerometer for vibration measurements. *Materials Today: Proceedings*, v. 45, p. 6183–6192, 2021. ISSN 2214-7853. International Conference on Mechanical, Electronics and Computer Engineering 2020: Materials Science. Disponível em: <https://www.sciencedirect.com/science/article/pii/S221478532038127X>. Citado 2 vezes nas páginas 20 and 31.

HE, C. et al. Real-time fault diagnosis of motor bearing via improved cyclostationary analysis implemented onto edge computing system. *IEEE Transactions on Instrumentation and Measurement*, IEEE, 2023. Citado na página 21.

HOU, L.; BERGMANN, N. W. Novel industrial wireless sensor networks for machine condition monitoring and fault diagnosis. *IEEE Transactions on Instrumentation and Measurement*, v. 61, n. 10, p. 2787–2798, 2012. Citado na página 34.

HOWARD, I. *A Review of rolling element bearing vibration detection, diagnosis and prognosis*. [S.l.]: Defence Science And Technology Organization Canberra (Australia), 1994. Citado na página 37.

HUANG, Z. et al. Tool wear monitoring with vibration signals based on short-time fourier transform and deep convolutional neural network in milling. *Mathematical Problems in Engineering*, Hindawi Limited, v. 2021, p. 1–14, 2021. Citado na página 42.

IKPEHAI, A. et al. Low-power wide area network technologies for internet-of-things: A comparative review. *IEEE Internet of Things Journal*, v. 6, n. 2, p. 2225–2240, 2019. Citado na página 35.

INVENSENSE, T. *IIM-42352 Datasheet*. [S.l.], 2022. Disponível em: <https://invensense.tdk.com/wp-content/uploads/2021/01/DS-000442-IIM-42352-TYP_v1.4.pdf>. Citado na página 53.

JABER, A. A.; BICKER, R. Design of a wireless sensor node for vibration monitoring of industrial machinery. *International Journal of Electrical & Computer Engineering (2088-8708)*, v. 6, n. 2, 2016. Citado na página 35.

JAIN, P. H.; BHOSLE, S. P. Analysis of vibration signals caused by ball bearing defects using time-domain statistical indicators. *International Journal of Advanced Technology and Engineering Exploration*, Accent Social and Welfare Society, v. 9, n. 90, p. 700, 2022. Citado 2 vezes nas páginas 37 and 38.

JOSHITHA, C. et al. Lorawan based cattle monitoring smart system. In: IEEE. *2021 7th International Conference on Electrical Energy Systems (ICEES)*. [S.l.], 2021. p. 548–552. Citado na página 35.

JUNIOR, R. F. R. et al. Fault detection and diagnosis in electric motors using convolution neural network and short-time fourier transform. *Journal of Vibration Engineering & Technologies*, Springer, p. 1–12, 2022. Citado na página 42.

KHADERSAB, A.; SHIVAKUMAR, S. Vibration analysis techniques for rotating machinery and its effect on bearing faults. *Procedia Manufacturing*, Elsevier, v. 20, p. 247–252, 2018. Citado na página 39.

KUMAR, A.; SATHUJODA, P.; BHALLA, N. A. Vibration signal analysis of a rotor-bearing system through wavelet transform and empirical mode decomposition. *IOP Conference Series: Materials Science and Engineering*, IOP Publishing, v. 1248, p. 012027, 7 2022. ISSN 1757-8981. Citado 2 vezes nas páginas 19 and 37.

KUMAR, B. K.; DIWAKAR, G.; SATYNARAYANA, M. Determination of unbalance in rotating machine using vibration signature analysis. *International Journal of Modern Engineering Research (IJMER)*, Citeseer, v. 2, n. 5, p. 3415–3421, 2012. Citado na página 39.

KÜNAS, C. A. et al. Edge computing versus cloud computing: Impact on retinal image pre-processing. In: IEEE. *2022 International Symposium on Computer Architecture and High Performance Computing Workshops (SBAC-PADW)*. [S.l.], 2022. p. 51–56. Citado na página 45.

LAKIS, A. Rotating machinery fault diagnosis using time-frequency methods. In: CITESEER. *Proceedings of the 7th WSEAS International Conference on Electric Power Systems, High Voltages, Electric Machines*. [S.l.], 2007. Citado 4 vezes nas páginas 39, 41, 42, and 43.

LEE, J.-S.; SU, Y.-W.; SHEN, C.-C. A comparative study of wireless protocols: Bluetooth, uwb, zigbee, and wi-fi. In: *IECON 2007 - 33rd Annual Conference of the IEEE Industrial Electronics Society*. [S.l.: s.n.], 2007. p. 46–51. Citado na página 36.

LEE, S. B. et al. Condition monitoring of industrial electric machines: State of the art and future challenges. *IEEE Industrial Electronics Magazine*, IEEE, v. 14, n. 4, p. 158–167, 2020. Citado na página 19.

LEIBER, M. et al. Differentiable adaptive short-time fourier transform with respect to the window length. In: IEEE. *ICASSP 2023-2023 IEEE International Conference on Acoustics, Speech and Signal Processing (ICASSP)*. [S.l.], 2023. p. 1–5. Citado na página 42.

LEONARDI, L. et al. Industrial lora: A novel medium access strategy for lora in industry 4.0 applications. In: IEEE. *IECON 2018-44th Annual Conference of the IEEE Industrial Electronics Society*. [S.l.], 2018. p. 4141–4146. Citado na página 34.

LI, H.; AI, S. Application of order bi-cepstrum to gearbox fault detection. In: *2008 7th World Congress on Intelligent Control and Automation*. [S.l.: s.n.], 2008. p. 1781–1785. Citado 2 vezes nas páginas 39 and 40.

LI, Q. et al. Fault diagnosis of wind turbine gearbox based on improved elm algorithm and multimodal sensor fusion. *Measurement*, Elsevier, v. 180, p. 109598, 2021. Citado na página 20.

LI, S. et al. A review on the signal processing methods of rotating machinery fault diagnosis. In: IEEE. *2019 IEEE 8th Joint International Information Technology and Artificial Intelligence Conference (ITAIC)*. [S.l.], 2019. p. 1559–1565. Citado na página 42.

LI, X. et al. Intelligent Machinery Fault Diagnosis With Event-Based Camera. *IEEE Transactions on Industrial Informatics*, IEEE, PP, p. 1–10, 2023. ISSN 19410050. Disponível em: <http://journals.sagepub.com/doi/10.1177/14759217211029201>. Citado na página 28.

LI, Y. et al. A new rolling bearing fault diagnosis method based on multiscale permutation entropy and improved support vector machine based binary tree. *Measurement*, Elsevier, v. 77, p. 80–94, 2016. Citado na página 42.

LI, Y. et al. Early fault diagnosis of rolling bearings based on hierarchical symbol dynamic entropy and binary tree support vector machine. *Journal of Sound and Vibration*, v. 428, p. 72–86, 2018. ISSN 0022-460X. Disponível em: <https://www.sciencedirect.com/science/article/pii/S0022460X1830261X>. Citado na página 26.

LIAO, Y. et al. Manufacturing process monitoring using time-frequency representation and transfer learning of deep neural networks. *Journal of Manufacturing Processes*, Elsevier, v. 68, p. 231–248, 2021. Citado na página 43.

LIN, H.-C. et al. Bearing vibration detection and analysis using enhanced fast fourier transform algorithm. *Advances in Mechanical Engineering*, SAGE Publications Sage UK: London, England, v. 8, n. 10, p. 1687814016675080, 2016. Citado na página 39.

LIPUS, J. et al. Vibration and related diagnostics of motors and generators. *MM Science Journal*, p. 1639–1642, 2016. Citado na página 26.

LIU, R. et al. Artificial intelligence for fault diagnosis of rotating machinery: A review. *Mechanical Systems and Signal Processing*, Elsevier, v. 108, p. 33–47, 2018. Citado na página 44.

LIU, X. et al. Fault diagnosis of rotor broken bar in induction motor based on successive variational mode decomposition. *Energies*, MDPI, v. 15, n. 3, p. 1196, 2022. Citado na página 43.

LIU, Y. et al. Asymmetric penalty sparse model based cepstrum analysis for bearing fault detections. *Applied Acoustics*, Elsevier, v. 165, p. 107288, 2020. Citado 2 vezes nas páginas 39 and 40.

LOPARO, K. A. et al. Fault detection and diagnosis of rotating machinery. *IEEE Transactions on Industrial Electronics*, IEEE, v. 47, n. 5, p. 1005–1014, 2000. Citado na página 42.

LU, S. et al. Edge computing on iot for machine signal processing and fault diagnosis: A review. *IEEE Internet of Things Journal*, IEEE, v. 10, n. 13, p. 11093–11116, 2023. Citado 4 vezes nas páginas 20, 21, 44, and 45.

LU, Z. J. *The elements of statistical learning: data mining, inference, and prediction.* [S.l.]: Oxford University Press, 2010. Citado na página 28.

LYCZKOWSKI, E. et al. Wireless communication in industrial applications. In: *2019 24th IEEE International Conference on Emerging Technologies and Factory Automation (ETFA)*. [S.l.: s.n.], 2019. p. 1392–1395. Citado na página 36.

MADHUKAR, G. et al. A machine learning based methodology for fault diagnosis in rotating machine. In: *2023 IEEE International Conference on Integrated Circuits and Communication Systems (ICICACS)*. [S.l.: s.n.], 2023. p. 1–5. Citado na página 19.

MALLA, C.; PANIGRAHI, I. Review of condition monitoring of rolling element bearing using vibration analysis and other techniques. *Journal of Vibration Engineering & Technologies*, Springer, v. 7, p. 407–414, 2019. Citado na página 26.

MARTÍNEZ, C.; ERAS, L.; DOMÍNGUEZ, F. The smart doorbell: A proof-of-concept implementation of a bluetooth mesh network. In: *2018 IEEE Third Ecuador Technical Chapters Meeting (ETCM)*. [S.l.: s.n.], 2018. p. 1–5. Citado na página 35.

MARTINS, D. H. C. de S. S. et al. Diagnostic and severity analysis of combined failures composed by imbalance and misalignment in rotating machines. *The International Journal of Advanced Manufacturing Technology*, Springer, v. 114, n. 9-10, p. 3077–3092, 2021. Citado na página 39.

MEHRJOU, M. R. et al. Rotor fault condition monitoring techniques for squirrel-cage induction machine—a review. *Mechanical Systems and Signal Processing*, Elsevier, v. 25, n. 8, p. 2827–2848, 2011. Citado na página 41.

MIKHAYLOV, K. et al. Lora wan for wind turbine monitoring: Prototype and practical deployment. In: IEEE. *2018 10th International Congress on Ultra Modern Telecommunications and Control Systems and Workshops (ICUMT)*. [S.l.], 2018. p. 1–6. Citado na página 35.

Minipa do Brasil Ltda. *Manual do Medidor de Vibração MVA-400*. 2021. <https://www.minipa.com.br/images/Manual/MVA-400-1101-BR_manual.pdf>. Acesso em: 25 jul. 2025. Citado na página 79.

NASCIMENTO, E. G. S. et al. T4pdm: a deep neural network based on the transformer architecture for fault diagnosis of rotating machinery. *arXiv preprint arXiv:2204.03725*, 2022. Citado na página 20.

PAI, P. F. et al. Time-frequency method for nonlinear system identification and damage detection. *Structural Health Monitoring*, SAGE Publications Sage UK: London, England, v. 7, n. 2, p. 103–127, 2008. Citado na página 44.

PATIL, S. S.; GAIKWAD, J. A. Vibration analysis of electrical rotating machines using fft: A method of predictive maintenance. In: *2013 Fourth International Conference on Computing, Communications and Networking Technologies (ICCCNT)*. [S.l.: s.n.], 2013. p. 1–6. Citado na página 39.

PEDOTTI, L. A. d. S. et al. Dispositivo iot de baixo custo para diagnóstico de falhas em máquinas rotativas. [sn], 2019. Citado na página 27.

PEDOTTI, L. A. D. S.; ZAGO, R. M.; FRUETT, F. Fault diagnostics in rotary machines through spectral vibration analysis using low-cost mems devices. *IEEE Instrumentation & Measurement Magazine*, IEEE, v. 20, n. 6, p. 39–44, 2017. Citado 2 vezes nas páginas 28 and 31.

PEDOTTI, L. A. S.; ZAGO, R. M.; FRUETT, F. Instrument based on mems accelerometer for vibration and unbalance analysis in rotating machines. In: IEEE. *2016 1st International Symposium on Instrumentation Systems, Circuits and Transducers (INSCIT)*. [S.l.], 2016. p. 25–30. Citado na página 20.

POPESCU, T. D.; AIORDACHIOAIE, D.; CULEA-FLORESCU, A. Basic tools for vibration analysis with applications to predictive maintenance of rotating machines: an overview. *The International Journal of Advanced Manufacturing Technology*, Springer, p. 1–17, 2021. Citado na página 20.

PREETHI, I.; SURYAPRAKASH, S.; MATHANKUMAR, M. A state-of-art approach on fault detection in three phase induction motor using ai techniques. In: *2021 5th International Conference on Computing Methodologies and Communication (ICCMC)*. [S.l.: s.n.], 2021. p. 567–573. Citado na página 26.

QIAN, G. et al. Edge computing: A promising framework for real-time fault diagnosis and dynamic control of rotating machines using multi-sensor data. *IEEE Sensors Journal*, IEEE, v. 19, n. 11, p. 4211–4220, 2019. Citado 5 vezes nas páginas 19, 20, 21, 44, and 45.

RADI, A.; AL. et. A multisignal wavelet variance-based framework for inertial sensor stochastic error modeling. *IEEE Transactions on Instrumentation and Measurement*, IEEE, v. 68, n. 12, p. 4924–4936, 2019. Citado na página 41.

RANDALL, R.; SMITH, W. New cepstral methods for the diagnosis of gear and bearing faults under variable speed conditions. In: *ICSV23 conference, Athens*. [S.l.: s.n.], 2016. Citado 2 vezes nas páginas 39 and 40.

RANDALL, R. B. A history of cepstrum analysis and its application to mechanical problems. *Mechanical Systems and Signal Processing*, Elsevier, v. 97, p. 3–19, 2017. Citado 2 vezes nas páginas 39 and 40.

RANDALL, R. B.; ANTONI, J. Rolling element bearing diagnostics—a tutorial. *Mechanical systems and signal processing*, Elsevier, v. 25, n. 2, p. 485–520, 2011. Citado na página 40.

RANGEL-MAGDALENO, J. et al. Hilbert spectrum analysis of induction motors for the detection of incipient broken rotor bars. *Measurement*, Elsevier, v. 109, p. 247–255, 2017. Citado na página 40.

RANJAN, R.; GHOSH, S. K.; KUMAR, M. Fault diagnosis of journal bearing in a hydropower plant using wear debris, vibration and temperature analysis: A case study. *Proceedings of the Institution of Mechanical Engineers, Part E: Journal of Process Mechanical Engineering*, v. 234, n. 3, p. 235–242, 2020. Disponível em: <https://doi.org/10.1177/0954408920910290>. Citado na página 20.

RIZZI, M. et al. Using lora for industrial wireless networks. In: IEEE. *2017 IEEE 13th international workshop on factory communication systems (WFCS)*. [S.l.], 2017. p. 1–4. Citado na página 34.

ROMANSSINI, M. et al. A review on vibration monitoring techniques for predictive maintenance of rotating machinery. *Eng*, MDPI, v. 4, n. 3, p. 1797–1817, 2023. Citado na página 19.

ROMANSSINI, M.; AGUIRRE, P. C. C. de; GIRARDI, A. G. Iot sensor node with edge computing for efficient vibration monitoring of industrial motors. *IEEE CASS Latin American Symposium on Circuits and Systems*, IEEE, v. 16th, n. 188, 2025. Citado na página 44.

RONDÓN, R. et al. Understanding the performance of bluetooth mesh: Reliability, delay, and scalability analysis. *IEEE Internet of things journal*, IEEE, v. 7, n. 3, p. 2089–2101, 2019. Citado na página 34.

ROSSI, A. et al. Accuracy characterization of a mems accelerometer for vibration monitoring in a rotating framework. *Applied Sciences*, MDPI, v. 13, n. 8, p. 5070, 2023. Citado 3 vezes nas páginas 20, 31, and 32.

SALEEM, M. A.; DIWAKAR, G.; SATYANARAYANA, M. Detection of unbalance in rotating machines using shaft deflection measurement during its operation. *IOSR J. Mech. Civ. Eng*, v. 3, n. 3, p. 08–20, 2012. Citado na página 39.

SANGEETHA, V. et al. Anomaly detection in rotary equipment using hybrid model with hgso optimization. In: IEEE. *2024 IEEE International Conference on Electronics, Computing and Communication Technologies (CONECCT)*. [S.l.], 2024. p. 1–6. Citado 2 vezes nas páginas 26 and 27.

SANTHOSHI, M. S. et al. An investigation on rolling element bearing fault and real-time spectrum analysis by using short-time fourier transform. In: SPRINGER. *Proceedings of International Conference on Recent Trends in Machine Learning, IoT, Smart Cities and Applications: ICMISC 2020*. [S.l.], 2021. p. 561–567. Citado na página 42.

SATYAM, M.; RAO, V. S.; DEVY, C. Cepstrum analysis: An advanced technique in vibration analysis of defects in rotating machinery. *Defence Science Journal*, Defence Scientific Information & Documentation Centre, v. 44, n. 1, p. 53, 1994. Citado 2 vezes nas páginas 39 and 40.

SATYANARAYANAN, M. The emergence of edge computing. *Computer*, IEEE, v. 50, n. 1, p. 30–39, 2017. Citado 2 vezes nas páginas 21 and 45.

SCHEFFER, C.; GIRDHAR, P. *Practical machinery vibration analysis and predictive maintenance*. [S.l.]: Elsevier, 2004. Citado 7 vezes nas páginas 28, 29, 30, 31, 32, 33, and 41.

SEFERAGIĆ, A. et al. Survey on wireless technology trade-offs for the industrial internet of things. *Sensors*, MDPI, v. 20, n. 2, p. 488, 2020. Citado na página 34.

SHUKLA, K.; NEFTI-MEZIANI, S.; DAVIS, S. A heuristic approach on predictive maintenance techniques: Limitations and scope. *Advances in Mechanical Engineering*, SAGE Publications Sage UK: London, England, v. 14, n. 6, p. 16878132221101009, 2022. Citado 2 vezes nas páginas 19 and 20.

SICARD, B. et al. Predictive maintenance and condition monitoring in machine tools: An iot approach. In: IEEE. *2022 IEEE International IOT, Electronics and Mechatronics Conference (IEMTRONICS)*. [S.l.], 2022. p. 1–9. Citado 3 vezes nas páginas 34, 35, and 36.

SILVESTRE, J. d. S. F. *Diagnóstico de Máquinas Elétricas Pela Análise de Vibração Mestrado em Engenharia Eletrotécnica Sistemas Elétricos de Energia Novembro de 2012*. Dissertação (Dissertação de mestrado) — Instituto Superior de Engenharia do Porto, 2012. Disponível em: <https://core.ac.uk/download/pdf/47138270.pdf>. Citado na página 27.

SINHA, J. K. *Vibration analysis, instruments, and signal processing*. [S.l.]: CRC press, 2014. Citado na página 34.

SOFI, A. et al. Structural health monitoring using wireless smart sensor network–an overview. *Mechanical Systems and Signal Processing*, Elsevier, v. 163, p. 108113, 2022. Citado na página 34.

SUN, K.; JIN, T.; YANG, D. A new reassigned spectrogram method in interference detection for gnss receivers. *Sensors*, MDPI, v. 15, n. 9, p. 22167–22191, 2015. Citado na página 43.

SUSANTO, A. et al. Application of hilbert–huang transform for vibration signal analysis in end-milling. *Precision Engineering*, Elsevier, v. 53, p. 263–277, 2018. Citado na página 44.

SWAMY, S. N.; KOTA, S. R. An empirical study on system level aspects of internet of things (iot). *IEEE Access*, v. 8, p. 188082–188134, 2020. Citado na página 34.

TENG, W. et al. Compound faults diagnosis and analysis for a wind turbine gearbox via a novel vibration model and empirical wavelet transform. *Renewable energy*, Elsevier, v. 136, p. 393–402, 2019. Citado na página 42.

TEZ, S.; AKIN, T. Fabrication of a sandwich type three axis capacitive mems accelerometer. In: IEEE. *SENSORS, 2013 IEEE*. [S.l.], 2013. p. 1–4. Citado na página 31.

TIBONI, M. et al. A review on vibration-based condition monitoring of rotating machinery. *Applied Sciences*, MDPI, v. 12, n. 3, p. 972. Citado na página 20.

VARANIS, M. et al. Mems accelerometers for mechanical vibrations analysis: A comprehensive review with applications. *Journal of the Brazilian Society of Mechanical Sciences and Engineering*, Springer, v. 40, p. 1–18, 2018. Citado na página 31.

VILLARROEL, A.; ZURITA, G.; VELARDE, R. Development of a low-cost vibration measurement system for industrial applications. *Machines*, Multidisciplinary Digital Publishing Institute, v. 7, n. 1, p. 12, 2019. Citado na página 19.

VISHWAKARMA, M. et al. Vibration analysis & condition monitoring for rotating machines: a review. *Materials Today: Proceedings*, Elsevier, v. 4, n. 2, p. 2659–2664, 2017. Citado na página 39.

WANG, J. et al. Edge cloud offloading algorithms: Issues, methods, and perspectives. *ACM Computing Surveys (CSUR)*, ACM New York, NY, USA, v. 52, n. 1, p. 1–23, 2019. Citado na página 46.

WANG, L.-H. et al. Motor fault diagnosis based on short-time fourier transform and convolutional neural network. *Chinese Journal of Mechanical Engineering*, SpringerOpen, v. 30, n. 6, p. 1357–1368, 2017. Citado na página 42.

WANG, X. et al. Efficient data reduction at the edge of industrial internet of things for pmsm bearing fault diagnosis. *IEEE Transactions on Instrumentation and Measurement*, IEEE, v. 70, p. 1–12, 2021. Citado na página 19.

WEG Equipamentos Elétricos S.A. *Catálogo Técnico - WEG Motor Scan*. 2020. <https://static.weg.net/medias/downloadcenter/h9d/h28/WEG-Motor-Scan-50078032-catalogo-pt.pdf>. Acesso em: 25 jul. 2025. Citado na página 79.

WIXTED, A. J. et al. Evaluation of lora and lorawan for wireless sensor networks. In: IEEE. *2016 IEEE SENSORS*. [S.l.], 2016. p. 1–3. Citado na página 35.

WU, D. et al. A fog computing-based framework for process monitoring and prognosis in cyber-manufacturing. *Journal of Manufacturing Systems*, Elsevier, v. 43, p. 25–34, 2017. Citado na página 34.

YADAV, O. P.; PAHUJA, G. Bearing health assessment using time domain analysis of vibration signal. *International Journal of Image, Graphics and Signal Processing*, Modern Education and Computer Science Press, v. 10, n. 3, p. 27, 2020. Citado 2 vezes nas páginas 37 and 38.

YU, W. et al. A survey on the edge computing for the internet of things. *IEEE Access*, v. 6, p. 6900–6919, 2018. Citado 2 vezes nas páginas 45 and 46.

ZHANG, D.; FENG, Z. Enhancement of time-frequency post-processing readability for nonstationary signal analysis of rotating machinery: Principle and validation. *Mechanical Systems and Signal Processing*, Elsevier, v. 163, p. 108145, 2022. Citado na página 44.

ZHANG, F. et al. Fault diagnosis of a wind turbine gearbox based on improved variational mode algorithm and information entropy. *Entropy*, MDPI, v. 23, n. 7, p. 794, 2021. Citado na página 35.

ZHAO, Z. et al. Challenges and opportunities of ai-enabled monitoring, diagnosis & prognosis: a review. *Chinese Journal of Mechanical Engineering*, SpringerOpen, v. 34, n. 1, p. 1–29, 2021. Citado na página 28.

ZHOU, W. et al. Lora-hybrid: A lorawan based multihop solution for regional microgrid. In: IEEE. *2019 IEEE 4th International Conference on Computer and Communication Systems (ICCCS)*. [S.l.], 2019. p. 650–654. Citado na página 35.